CHARACTERIZATION OF POLARONS AND EXCITONS IN MONODISPERSE PLATINUM ACETYLIDE MATERIALS

By

JULIA MARIE KELLER

A DISSERTATION PRESENTED TO THE GRADUATE SCHOOL
OF THE UNIVERSITY OF FLORIDA IN PARTIAL FULFILLMENT
OF THE REQUIREMENTS FOR THE DEGREE OF
DOCTOR OF PHILOSOPHY

UNIVERSITY OF FLORIDA

2010

To my beautiful babies

ACKNOWLEDGMENTS

I must first acknowledge my mentor, Professor Kirk Schanze for his invaluable encouragement, guidance and patience; he has taught me much beyond the science presented herein, both how to be an individual thinker as well as a team player. I also owe much gratitude to my committee members for their continued assistance, advice and support, as well as John R. Miller for his time spent in collaboration with us. My time with the entire Schanze group has been rewarding, but I want to thank Dr. Yongjun Li especially; we shared a hood together, learned alongside each other, and we had a load of laughs along the way. In him I have found a colleague and friend for life.

I ultimately thank my Lord and Savior Jesus Christ for carrying me through this journey. I have been blessed with a wonderful, strong and selfless husband, Jonathan; we share in this accomplishment. We have been blessed with a beautiful son, Joshua, that has brought joy to every aspect of our lives, and we are very shortly expecting our baby girl as we begin a new chapter. This is for them. My parents have also been on this adventure with me, as well as my best friend in life, my twin sister Stephanie. Their love, prayers and support have meant everything to me.

Finally, if it were not for all of my friends here I would not have survived. I must particularly thank Phillip Shelton, Seth Dumbris, Dr. Kye Young Kim, Dr. John Peak, Abby Shelton and Dr. Jarrett Vella for always providing me with a smile when I needed it most. I also thank my close friends at Westside, especially the Robinsons, for being my home away from home and for loving my family so well. I am blessed. I close this chapter of my life with the words that I came in upon: “Enter to think God’s thoughts after Him. Go forth to apply His thoughts in service”.

TABLE OF CONTENTS

page

LIST OF TABLES

LIST OF FIGURES

Abstract of Dissertation Presented to the Graduate School
of the University of Florida in Partial Fulfillment of the
Requirements for the Degree of Doctor of Philosophy

CHARACTERIZATION OF POLARONS AND EXCITONS IN MONODISPERSE PLATINUM ACETYLIDE MATERIALS

By

Julia Marie Keller

May 2010

Chair: Kirk S. Schanze
Major: Chemistry

The overall goal of this work was to design, synthesize and characterize various series of platinum-acetylide oligomers in order to better understand the structure-property relationships in these types of materials. Specifically, this research sought to further define the photophysical properties of both triplet excitons and negative polarons in these molecules by means of both steady-state and time-resolved methods. The results of this work not only provide insight into the synthesis of monodisperse organometallic oligomers, but they also provide a more in-depth understanding of both the structure and dynamics of excited and charged states within conjugated systems that feature organometallic or metal-organic moieties.

First, we report the synthesis and characterization of a series of monodisperse platinum-acetylide oligomers Pt_nNDI_2, where NDI is an easily reducible end group. The oligomers were synthesized via an iterative-convergent approach utilizing organometallic synthons that feature orthogonally protected terminal acetylene units. The oligomers were characterized by electrochemistry, UV-visible absorption and photoluminescence spectroscopy. The emission spectra reveal that the triplet exciton is

efficiently quenched in the NDI end-capped oligomers, and the quenching is thought to arise due to exciton migration followed by photoinduced charge separation.

Variable temperature steady-state emission studies, pulse radiolysis measurements and ultrafast transient absorption measurements were applied to examine the transport dynamics of negative polaron and triplet exciton states in the Pt_nNDI_2 series. Ultrafast single shot experiments, compared to simulated random-walk data, reveal trapping of the anion radical for $Pt_{10}NDI_2$ in short times with the lifetime for polaron diffusion estimated to be ~27 ps. Low temperature emission studies reveal that the rate-limiting step for exciton quenching is exciton diffusion. Femtosecond transient absorption data was coupled with simulation data to extract a triplet exciton hopping rate of ~27.2 ps.

Another series of platinum-acetylide oligomers Ph_nPt_2 were also synthesized, consisting of a phenylene ethynylene core of varying length capped by platinum end groups. The study was meant to examine the effects on excited state properties between two platinum moieties of increasing organic spacer distances. Optical data conclude that the singlet exciton remains highly delocalized throughout the series, but approaching its limit. The extent of delocalization in triplet exciton seems to have been reached by Ph_4Pt_2, and phosphorescence yields at ambient temperatures decreased with increasing spacer length until emission was almost elusive in the n=9 oligomer.

CHAPTER 1
INTRODUCTION TO PLATINUM ACETYLIDE MATERIALS

Platinum acetylide materials have attracted much attention over the last decade, owing to both the unique photophysical properties they exhibit as well as their application to optical and electronic fields. To gain a better understanding of these materials, this chapter has been divided into two major sections. The first section provides an overview of the basic concepts of photophysics such as light absorption, emission, and photoinduced electron and energy transfer. The second section broadly introduces platinum acetylide materials including synthetic methods and photophysical properties.

Introduction to Photophysics

The Nature of Light and Matter

Light emission is generated as a result of energy changes of the valence electrons in atoms and molecules. Because of the direct relationship between light and matter, theories of both atomic structure and the nature of light have developed simultaneously.[1-3] The scientific understanding of the nature of light began with Sir Isaac Newton's particle theory, introduced in his *Opticks*, published in 1704.[4] According to Newton, "Light is composed of tiny particles, or corpuscles, emitted by luminous bodies." Around the same time, Huygens introduced his wave theory of light; however this concept was not widely accepted until the 19th century when Maxwell developed the classical electromagnetic theory. With the addition of a single term to existing laws, the Maxwell equations converged the theories of electricity, magnetism and optics into one single concept: the electromagnetic field. Maxwell had also discovered a fundamental constant of nature, the speed of light (3×10^8 m s^{-1}). Concurrently, our

understanding of atomic theory was of the classical sense, describing electrons as particles that obey Newton's laws of classical mechanics.

The conflicting models of the wave nature of light and the particle nature of electrons were altered in the 1900s after Planck carried out his now famous blackbody experiment. He suggested that the distribution of energy emitted by a blackbody was not continuous but rather emitted in discrete packets called "quanta". Inspired by his findings, Einstein developed the modern theory of wave-particle duality of photons (incorporating his observations of the photoelectric effect), concluding that energy of a photon is proportional to its frequency. Following Einstein's lead, de Broglie revolutionized the concept that electrons, and all matter, behave with dual wave-particle nature. His formula, relating wavelength and momentum, was confirmed for electrons by electron diffraction experiments. Schrödinger developed the proper mathematical formulation describing the wavefunction of electrons. Now known as quantum theory, this model has defined our current understanding of atomic structure. Today we describe the nature of light and electrons as both waves and particles.[5]

Absorption of Light

The interaction of light with matter can provide useful information about molecular electronic structure. When an atom or molecule absorbs light, electromagnetic radiation is taken up by matter, typically via a valence shell electron, promoting it to a higher energy level. Because the energy levels of the electrons in a molecule are not continuous but discrete, the frequency of the incident light must equal the molecular resonant frequency for absorption to occur. The energy of light absorbed therefore provides the energy difference of the two molecular orbitals involved in the transition.

The relationship between the frequency of light absorbed and its energy is described in Equation 1-1 below:

$$E = h\nu = (hc/\lambda) \quad (1\text{-}1)$$

where h is Planck's constant (6.63×10^{-34} J·s), ν is the frequency of light absorbed (sec^{-1}), *c* is the speed of light (3.0×10^{8} $m \cdot s^{-1}$) and λ is the wavelength of light (m).

Another important feature of light absorption is the intensity of the light that is absorbed by a molecule at a particular frequency, the absorbance. The relationship between molecular absorbance and light intensity is described by the Beer-Lambert Law (Equation 1-2):

$$A = -\log (I/I_o) = -\log T = \varepsilon bc \quad (1\text{-}2)$$

in which A is the absorbance at a particular frequency of light, I_0 is the intensity of incident light, I is the intensity of exiting light, T is the transmittance, ε is the molar absorptivity of the molecule ($L \cdot mol^{-1} \cdot cm^{-1}$), b is the pathlength of the light (cm) and c is the concentration of the absorbing species ($mol \cdot L^{-1}$). The molar absorptivity is a measure of the probability of the electronic transition; this property is proportional to the transition dipole moment between the two electronic states.

While an electronic transition absorbs at a discrete energy by definition (Equation 1-1), molecular absorption spectra typically consist of broad absorption bands rather than sharp lines. This phenomenon originates from the collective electronic transitions that accompany the various vibrational states of the molecular bonds. These vibronic transitions are explained by the Franck-Condon Principle;[6,7] electronic transitions occur very rapidly (10^{-15} s) compared to nuclear motions (10^{-13} s).

From a classical perspective, the principle approximates all electronic transitions as originating from an instantaneous, motionless state of the molecule; nuclear motions resume after the electronic transition has taken place. This is depicted in Figure 1-1. Here, the Morse potentials of both the ground and excited states are shown with their respective equilibrium geometries. Vertical transitions occur from the lowest vibrational level of the ground state to vibrational levels of the excited electronic state. From a quantum mechanical perspective, the probability of each vibronic transition occurring (defining the intensity of the absorption) is proportional to the square of the vertical overlap of the vibrational wavefunctions of the ground and excited state. In solution, particularly in solvents of high dielectric constants, vibronic bands are not well resolved due to solvation effects with the excited state chromophore.

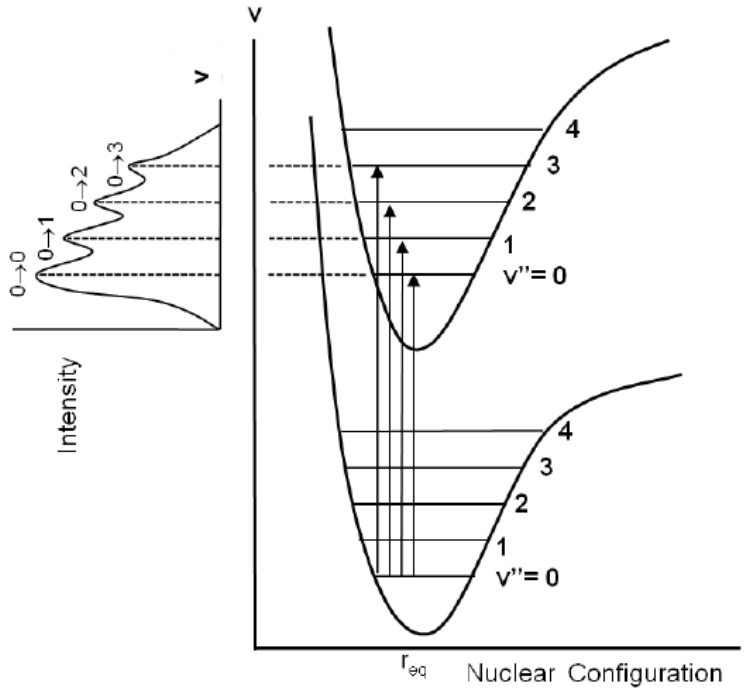

Figure 1-1. The Franck-Condon principle. The figure was adopted from Atkins.[1]

Excited State Properties

From initial excitation to the first ('hot') electronic excited state, the molecule quickly relaxes to the lowest vibrational level of that state via either thermal or collisional relaxation (Kasha's Rule). For solvated molecules, the rate of relaxation is dependent on the viscosity of the solvent. Generally, solvent relaxation is short compared to the lifetime of the excited state (10^{-13}-10^{-12} s), allowing full relaxation of the excited state. In the case of highly viscous solvents or short-lived excited states, however, other processes may occur prior to complete equilibration of the excited molecule.

When the initial electronic state of the molecule is neutral, the electrons are generally paired and of opposite spin states, according to Hund's Rule. Upon excitation the electron does not change spin states, in keeping with spin restriction rules imposed by quantum mechanics, and the initial excited state formed is termed a singlet excited state (S_1). In some instances, however, the spin of the promoted electron can flip, changing the overall spin momentum of the excited molecule to three. This process is referred to as intersystem crossing (ISC). The resulting state, a triplet state (T_1), is characterized by an excited state with electrons with parallel spins. Similar to initial formation of the singlet excited state, the triplet excited state is initially formed in a 'hot' state via coupling of equal energy singlet and triplet vibrational levels before relaxation to the lowest vibrational level.

Intersystem crossing is "forbidden" by quantum rules (due to conservation of momentum), and in organic molecules it typically occurs at a slow rate and therefore generates low yields of triplet. When strong spin-orbit coupling is present, however, the rate and yield of ISC are greatly increased. Spin-orbit coupling is facilitated by the heavy atom effect: this occurs when the spin angular momentum and orbital angular

momentum can interact in such a way that the total orbital momentum is conserved. For this reason, ISC yields are typically higher in organometallic and inorganic molecules—including platinum acetylides, the focus of this study.

The energy of the first triplet excited state is always lower in energy than that of the first singlet excited state. Coulombic repulsion is higher for the singlet as the electron spins are paired and are not forbidden to occupy the same space; for the triplet, the spins are parallel and therefore forbidden to occupy the same region. The singlet-triplet energy splitting (E_{S-T}) is then larger for small molecules than for larger molecules, typically.[8]

Upon equilibration of either metastable excited state, an electron will eventually return to ground state configuration by one of two mechanisms: radiative or nonradiative decay. For radiative decay processes, the excited electron deactivates by emission of a photon equaling the energy difference from the equilibrated excited state to some vibronic level of the ground state (similar to the absorption of a photon). Emission from the singlet excited state is termed fluorescence (F); emission from the triplet excited state is termed phosphorescence (P). Fluorescence is a quantum mechanically allowed process as it involves a transition from states with the same spin, and it is therefore a fast process (10^8 s^{-1}).[9] Phosphorescence is a forbidden process, and although facilitated by spin-orbit coupling it is much slower (10^5-10^2 s^{-1}). A third type of radiative decay is called delayed fluorescence. The lifetime of this process is somewhat longer as S_1 is populated via an indirect route, namely via a thermally assisted $T_1 \rightarrow S_1$ mechanism or via bimolecular triplet-triplet $T_1+T_1 \rightarrow S_0+S_1$ annihilation mechanism. Another phenomenon of radiative decay that is commonly seen is the Stokes shift;

recall that vibrational relaxation to the lowest excited state, v=0, is typically fast, therefore the energy of the radiative decay will be smaller than that of absorption. This results in fluorescence emission of a longer wavelength than absorption, and the extent of the Stokes shift correlates to the structural differences between the ground and singlet excited states.

Nonradiative decay is the other deactivation mechanism involved in excited state relaxation. Here, the energy difference between two states of the same spin is dissipated as heat. Both nonradiative decay and vibrational relaxation processes are referred to as internal conversion (IC). The relative rate of this process is defined by the energy gap law which relates a decrease in excited state energy with an exponential increase in the rate of nonradiative decay. The energy gap law has been applied to aromatic hydrocarbons, rare earth ions and more recently Pt-containing conjugated polymers and monomers—the focus of the present study.[10]

All of the above mentioned processes are depicted in the Jablonski diagram shown in Figure 1-2. From these transitions, two additional characteristics of the excited state need defining, as they will be frequently discussed herein: the photoluminescence quantum yield, Φ_{PL}, and the lifetime, τ, of an excited state process. The photoluminescence (PL) quantum yield defines the efficiency of a PL process; it is calculated as a ratio of the number of photons emitted to the number of photons absorbed. It is also defined as the ratio of the rate PL decay from a particular excited state to the sum of the rates of all processes of decay from that excited state, given as:

$$\Phi_{PL} = k_{PL} / (\Sigma k_{decays}) \quad (1\text{-}3)$$

where Φ_{PL} is the quantum yield for a particular photoluminescence process, k_{PL} is rate constant of the emission process and k_{decays} includes all other rate constants for decay pathways from that excited state. Experimentally, the fluorescence or phosphorescence quantum yields can be found by measuring the photoluminescence of a known fluorophore with the same experimental parameters as the molecule being characterized.[11]

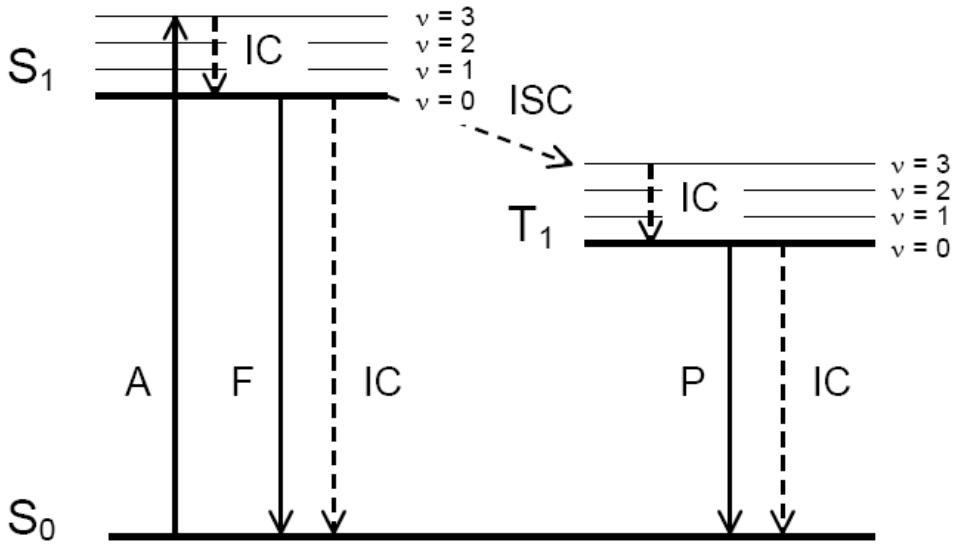

Figure 1-2. Jabloski diagram illustrating possible transitions.

The photoluminescence lifetime, τ_{PL}, is defined as the time for the luminescence signal to decay to 1/*e* of its initial value. This value is equal to the inverse of the sum of all decay processes, both radiative and nonradiative, from the excited state being studied:

$$\tau = 1 / (\Sigma k_r + \Sigma k_{nr}) \quad (1\text{-}4)$$

where k_r defines all radiative pathways and k_{nr} defines all nonradiative pathways.

Energy Transfer

As well as the self-relaxation pathways from the excited state previously discussed, an excited state may also return to the ground state via an energy transfer mechanism. In the presence of an acceptor moiety, deactivation of the excited state could occur by the bimolecular process given:

$$D^* + A \rightarrow D + A^* \quad (1\text{-}5)$$

where D is the donor, A is the acceptor and * denotes the excited state. For this process to occur, it is necessary that (1) the energy of D* is higher than the energy of A* for the exchange to be thermodynamically favorable, and (2) the rate of energy transfer must be within the lifetime of D*. Several different mechanisms of energy transfer exists, but they can be broadly classified as either radiative transfer or radiationless transfer processes.

Radiative energy transfer involves emission of D* followed by reabsorption of that energy by the acceptor A, as shown below.

$$D + h\nu \rightarrow D^*$$

$$D^* \rightarrow D + h\nu'$$

$$A + h\nu' \rightarrow A^* \quad (1\text{-}6)$$

It is necessary in this process that the absorption energies of A and the emission energies of D* overlap to some extent. The solvent viscosity does not affect the rate of energy transfer, and energy transfer is effective even from longer distances. Also notable, the lifetime of D* is unaffected by the energy transfer process.

There are two main mechanisms of radiationless energy transfer: the dipole-dipole (Coulombic) process and the electron exchange process. The Coulombic (Förster) mechanism is a long-range (up to 100 Å) energy transfer process that involves

the coupling of both the ground and excited state oscillating dipoles.[12] This interaction causes perturbation of the electronic structures in both the donor and acceptor, leading to excitation of the electron on the acceptor and deactivation of the donor electron. No contact between the donor and acceptor is required, but the mechanism does necessitate sufficient overlap of the absorption of A and the emission of D*, and only singlet-singlet transfer is allowed. This mechanism is represented in Figure 1-3. The probability for this mechanism is proportional to $1/R^6$ (where R is the distance between the donor and the acceptor). The rate of energy transfer is independent of the solvent viscosity, however the lifetime of the donor will be shortened by the process.

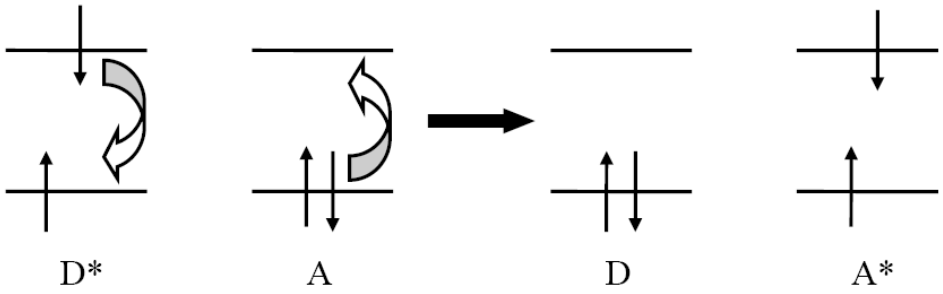

Figure 1-3. Coulombic (Förster) mechanism for long-range energy transfer.

The electron exchange (Dexter), or collisional, mechanism involves overlap of the orbitals between the donor and acceptor involved in the transfer.[13] Therefore, this process occurs for molecules that are in close proximity to one another (~10-15 Å). The rate of energy transfer is limited by molecular diffusion of D* and A, and it is therefore dependent on both the temperature and viscosity of the solvent. Both S-S and T-T transfer mechanisms are allowed by this process, and this is the dominant mechanism in triplet-triplet energy transfer. A schematic of this process is given in Figure 1-4.

Triplet-triplet energy transfer is forbidden by the dipole-dipole mechanism, but it is allowed by the electron exchange mechanism. Because the lifetimes of triplet excited

states are relatively long, they are often used to facilitate the energy transfer process as donors with acceptor molecules that possess a low quantum yield of generated triplet. This is a way of effectively enhancing the triplet yield of the acceptor, in a process referred to as triplet sensitization. The triplet-triplet transfer rate is dependent on the difference in the donor and acceptor triplet energies ($\Delta E_{T\text{-}T}$).

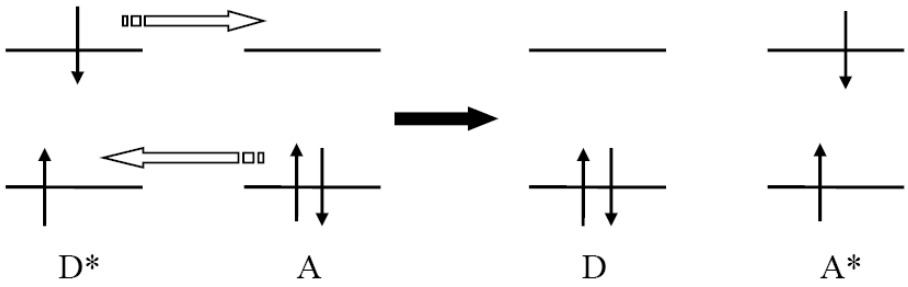

Figure 1-4. Electron exchange (Dexter) mechanism for short-range energy transfer.

Electron Transfer

Photoinduced electron transfer (PET) is one of the most fundamental mechanisms in natural systems. All processes of respiration and photosynthesis (from which energy is stored or released) rely totally on electron transfer reactions of cofactors in proteins. Scientists continually endeavor to gain a better understanding of such processes in attempts to exploit the development of new technology.[14] However, controlling these reactions remains a challenge at the forefront of scientific research, applied to areas such as electrical energy storage, chemical sensing, memory devices, etc.

Upon excitation of a chromophore, systems with donor-acceptor characteristics may facilitate a PET as another form of molecular deactivation. PET is characterized by transfer of an electron either from an excited donor molecule (D*) to a ground state acceptor (A) or from an excited state acceptor (A*) to a donor (D).

$D^* + A \rightarrow D^+ + A^-$

$D + A^* \rightarrow D^+ + A^-$ (1-7)

The electron transfer process would be highly endothermic without photoexcitation, but the process is more favorable with promotion of an electron to a higher energy level (Figure 1-5). The products of such a process are a reactive radical cation/anion (contact) pair. The decay pathways of the PET intermediate are outlined in Figure 1-6. While the individual spins of either the cation or anion radical formed, after initial PET from the singlet excited state, is a doublet, the overall spin of the contact pair is either a singlet or a triplet. The ion pair can decay either by recombination—returning to the ground state, separation to form a isolated ion pair, or formation of an excited state triplet; however, should no other deactivation process occur, recombination of charge is inevitable.[15,16]

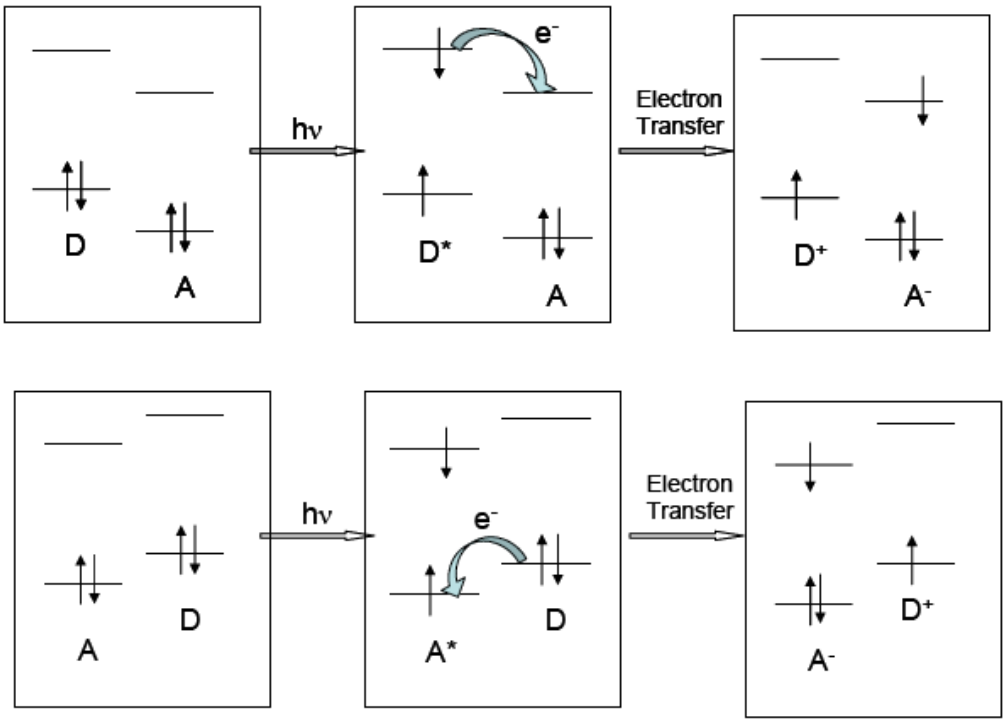

Figure 1-5. A schematic presentation of a photoinduced electron transfer process.

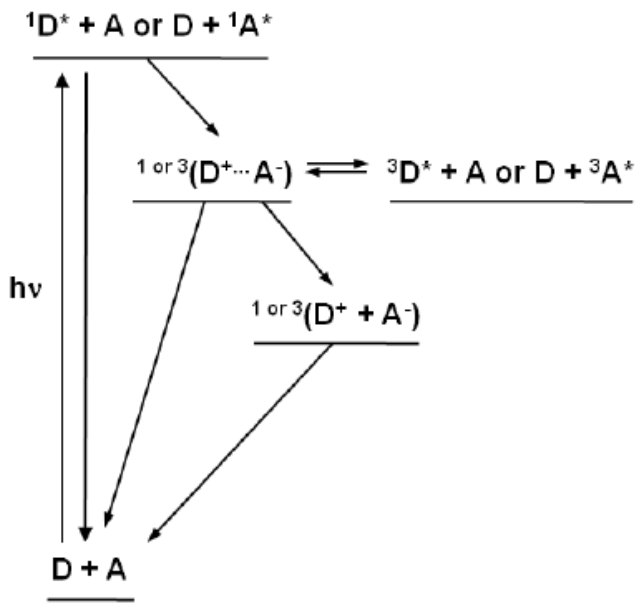

Figure 1-6. Decay pathways of photoinduced electron transfer.[15,16]

Marcus theory.

A theoretical description of electron transfer was developed by Marcus in the 1960s, and the Nobel Prize was awarded for his advances in 1992.[17] For electron transfer processes, no chemical bonds are broken, only structural changes occur in reactants and the neighboring solvent molecules. Therefore, a description of electron transfer may be presented by using reaction coordinates based on the potential energy surfaces of the reactants and products. Electron transfer is then defined as the crossing from the well of the reactants' potential energy surface to the well of the products' potential energy. Marcus developed an equation that relates the rate of electron transfer within D/A systems with the free energy of reaction and the electronic interaction between the donor and the acceptor:

$$\kappa_{ET} = \frac{2\pi}{\hbar} V_{DA}^2 \left(\frac{1}{(4\pi\lambda T)^{\frac{1}{2}}} \right) e^{-\frac{(\Delta G^0 + \lambda)^2}{4\lambda\kappa T}} \quad (1\text{-}8)$$

where ΔG^0 is the free energy of reaction, V_{DA} is the electronic coupling between the donor and acceptor, and λ is the total reorganizational energy for the donor, acceptor and solvent involved in electron transfer.[18]

This expression describes a nonlinear behavior of the electron transfer rate on the reaction free energy. This is quite different from the typical thinking of a linear free energy relationship between the rate of a reaction and its equilibrium constant, which predicts the rate of electron transfer should increase with the free energy for the reaction $-\Delta G^0$. Rather, the Marcus equation demonstrates how the rate of electron transfer will increase with $-\Delta G^0$ until a maximum rate is observed for $-\Delta G^0 = \lambda$, followed by a decrease in rate, a phenomenon known as the "Marcus inverted region" which has been observed experimentally.[19,20] In other words, the Marcus theory predicts that the rate for electron transfer will decrease if the driving force is high, that is, if the process is highly exothermic.

Solution phase electron transfer.

There are two types of reorganizational energy involved in electron transfer. λ_{in} refers to the free energy change associated with nuclear bond length changes within the reactant molecules. λ_{out} refers to the free energy change associated with the slow changes in the polarization of the surrounding solvent molecules preceding ET; this term is dependent on solvent polarity, separation of the redox sites and the shape of the reacting molecules.[21] Most PET studies are performed in solution phase. In solution, when a reactant is photoexcited, a series of short-lived ion-pair intermediates is created due to the interaction between an excited state and the ground state. Solvation and electrostatics can determine the extent of stability of the created ion pairs. An ion-pair

that is separated by several solvent molecules results in a pair of geminate ions is called a solvent-separated ion pair (SSIP); the driving force of ET in this type is given by Rehm-Weller equation (Equation 1-9):

$$\Delta G_{SSIP} = E^0(D^+/D) - E^0(A/A^-) - \Delta G^* + w_p - w_R \quad (1\text{-}9)$$

in which $E^0(D^+/D)$ is the oxidation potential of the donor, $E^0(A/A^-)$ is the reduction potential of the acceptor, ΔG^* is the free-energy of the equilibrated excited-state, and w_P and w_R are the work terms for electrostatic interaction in the product (P) and in the reactant (R) states. The work terms describe the influences of the donor and acceptor charges (Z_{D^-} and Z_A) and their center-to-center distances from one another (d_{CC}) in relation to the static dielectric constant (ε_S) of the solvent as shown (Equation 1-10).

$$w = Z_D Z_A e^2 / d_{cc}\, \varepsilon_S \quad (1\text{-}10)$$

This relationship describes a greater influence of electrostatics in nonpolar solvents and predicts the greater feasibility for ion dissociation in more polar solvents.

The collision of neutral reactants within the solvent cage is said to form either a contact ion pair (CIP) or an intimate CT complex, an exciplex. Solvent polarity and reactant structures heavily influence the production of either; nonpolar solvents are typically favored for exciplex formation, however, and this intermediate is generally distinguished by the emission of light observed in the emission spectrum.

Spin dynamics of PET.

As PET can occur from either the singlet or triplet state, spin restriction rules dictate that electron spin is usually conserved. However, there are some examples of systems in which singlet-triplet intersystem crossing of an ion pair has been observed; major factors that contribute to this conversion are hyperfine coupling, Zeeman splitting,

and spin-orbit coupling.[22] When a force whose energy is stronger than the exchange interaction, or charge separation energy (J), operates during electron transfer process, electron spin multiplicity changes and ISC occurs.

Hyperfine coupling involves the interaction between the spin magnetic moment of an unpaired electron and the nuclear spin magnetic moment. When J, between the singlet and triplet, becomes smaller than this energy ($\Delta E_{hf} > J$), a spin flip takes place by hyperfine coupling. For a solvent-separated ion pair or free ion, ISC is operated by the hyperfine coupling mechanism because J becomes negligible at such large distances; for a contact ion pair or exciplex, J becomes large due to small distance. The Zeeman Effect describes splitting of degenerate electronic energies upon exposure to a magnetic field; with increasing applied strength of the external field, Zeeman splitting breaks up the T_0 degeneracy into T_+ and T_- sublevels and may induce a spin flip via a S-T transition. Spin-orbit coupling is generally not a common mechanism for ionic intersystem crossing, as it usually involves the interaction of electrons about a single atomic nucleus.

PET in metal-organic dyads.

A dyad is a supramolecular assembly consisting of a light-absorbing chromophore and an electron donor or acceptor moiety. Much early work in the PET field has focused on organic donor-acceptor systems (which most recently has encompassed C_{60}, porphyrins and phthalocyanines moieties),[23-28] but research quickly began to incorporate transition metals. While initial systems focused on bimolecular PET dynamics, the development of unimolecular, covalently linked chromophore-quencher systems grew increasingly popular concurrently with advancements in instrumentation as well as synthetic methodologies. These systems provide the benefit of negating

diffusion dynamics by controlling the length and orientation of the spacer while also allowing control or variation of the spacer between the donor and acceptor moieties; they are generally characterized by long lifetimes of the charge separated (CS) state which allows the possibility to collect the charges at corresponding electrodes in photovoltaic devices, thus generating photocurrent. Because the field of PET is extremely diverse, only metal-organic dyads will be mentioned.

Metal-organic dyads consist of a transition metal complex that serves as the light absorbing chromophore, as well as an organic electron donor or acceptor. More commonly, these systems contain a metal with a d^6 electronic configuration; the lowest excited state arises from a metal to ligand charge transfer (MLCT) transition that involves promotion of a metal centered d electron into a ligand based π^* level. Two modes of decay from this state are possible, separating metal-organic dyads into two categories (Types 1 and 2), as shown in Figure 1-7.

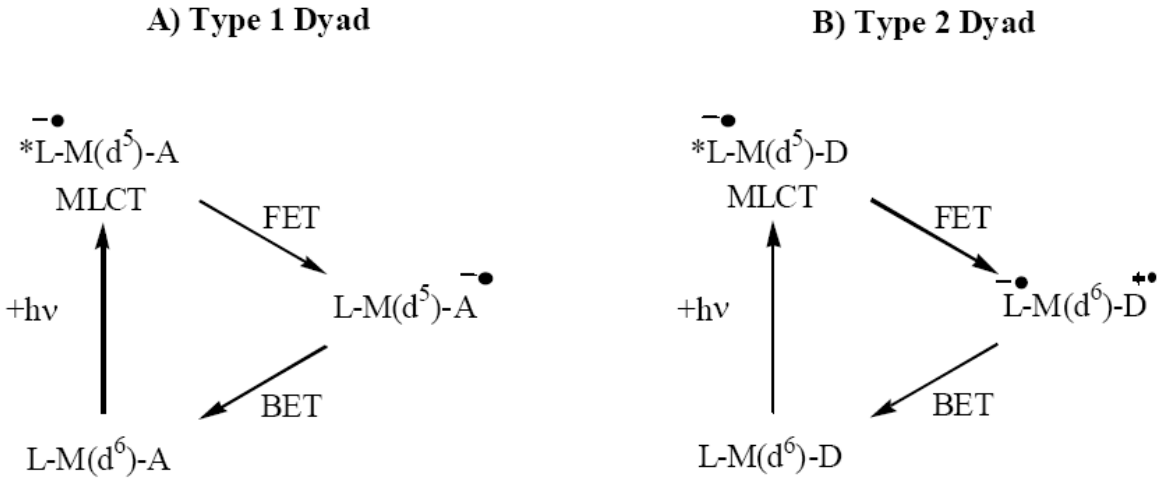

Figure 1-7. Type 1 and 2 metal-organic dyads.

A Type 1 metal-organic dyad consists of an electron acceptor covalently linked to the d^6 metal chromophore. Forward electron transfer (FET) occurs via donation of the

promoted MLCT electron to the empty π^* orbital of the organic acceptor. Back electron transfer (BET) then occurs via electron transfer from the π^* orbital of the organic acceptor back to the d-shell of the transition metal (Figure 1-7a). A Type 2 metal-organic dyad consists of an electron donor covalently linked to the d^6 metal chromophore. FET occurs via electron transfer from a π orbital of the organic donor to the hole left in the d-shell of the transition metal from MLCT. BET then occurs via charge recombination between the organic radical anion radical cations. (Figure 1-7b). Several examples of these types exist in the literature, far too many to mention within.

Photophysical Properties of Conjugated Materials

Conjugated materials are unsaturated, meaning the entire molecule consists of atoms with a continuous π orbital system. The first report concerning the conductivity in these types of materials described the redox properties of polyacetylene.[29] Shirakawa, Heeger,and MacDiarmid were more recently acknowledged in 2000 with the Nobel Prize in Chemistry for their insights, as conjugated polymers have since been found useful for a wide variety of applications, mainly in devices. Research has seen success with these types of materials in light emitting diodes, light emitting electrochemical cells, plastic lasers, and thin-film transistors.[30] A wide variety of conjugated polymer structures have been reported, a few of which are depicted in Figure 1-8. These organic conjugated polymers, other than polyacetylene, generally feature aromatic or heteroaromatic rings that are either directly connected or connected by conjugated vinyl or ethynyl linkers.

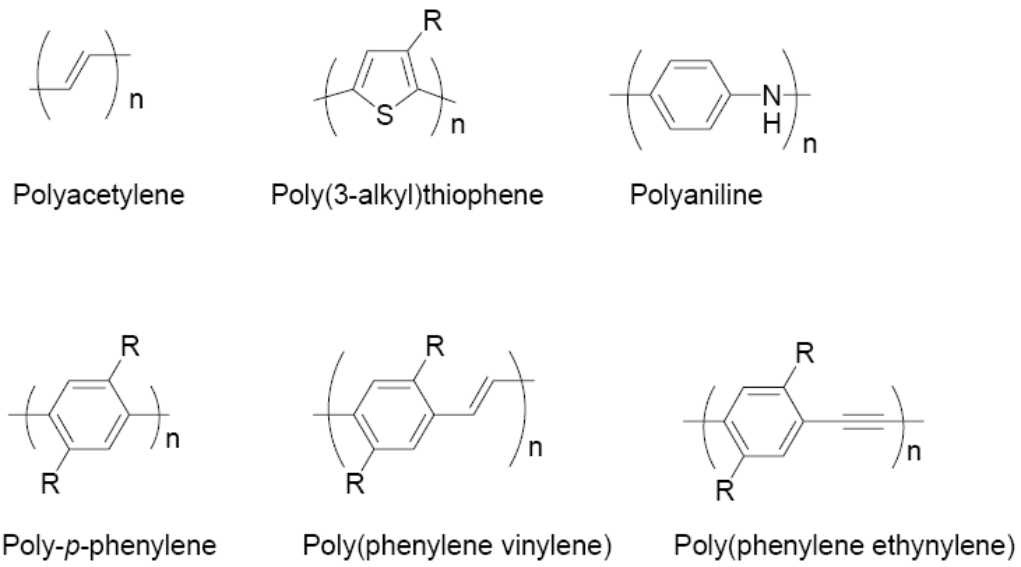

Figure 1-8. Examples of organic conjugated polymer structures.

Molecular wires in conjugated organic systems

One major reason why conjugated polymers make excellent candidates for electronic, electro-optical and optical applications is that they provide exceptional transport properties for charges and excitons. Much research has focused on understanding carrier transport properties in these materials, especially in understanding bulk properties of polymers in films.[31-35] However, another area in the field remains focused on the transport properties of these materials as single-chain "molecular wires", or single molecules acting as one-dimensional carriers.

For a molecule to exhibit "molecular wire" properties, the appropriate molecular geometry is required, as well as the molecule's ability to adopt a predictable conformation. In addition, the material must be an excellent charge carrier and must display similar energetics over a long distance of the molecule.[36] Several examples of conjugated organic materials used as molecular wires are known.[37,38] The concept of an organic molecular electronics device was first proposed by Aviram and Ratner[39], but

it was not until the measurement of electrical conduction through a single benzene-1,4-dithiol molecule that molecular-scale electronics attracted serious attention.[40] In a more recent example, a linear terphenyl molecule was spanned across two gold electrodes via thiol substituents.[41] Upon application of a potential across the electrodes, the terphenyl moiety undergoes a conformational change and completes the circuit between the electrodes with a measurable conductivity and resistivity (Figure 1-9).

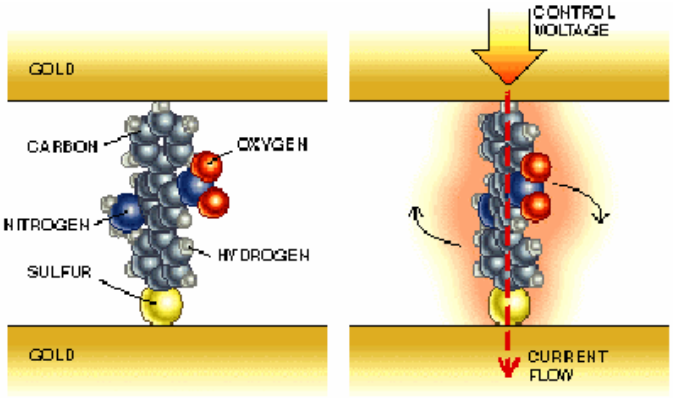

Figure 1-9. A conjugated oligomer in use as a molecular wire.[41]

Charge in organic conjugated systems

Electronically conducting polymers are believed to possess a spatially delocalized band-like electronic structure much like that of a solid-state semiconductor, stemming from the splitting of interacting molecular orbitals of the constituent monomer units.[30,42] The mechanism of conductivity for these materials that is generally accepted is based on the motion of charged defects within the conjugated framework. The charge carriers, either positive (p-type) or negative (n-type), are produced via oxidation or reduction of the polymer, respectively.[42,43]

Oxidation of a conjugated material initially generates a positive polaron with both spin and charge (Figure 1-10). A positive polaron, generally referred to as a radical cation, consists of both the hole site and the structural distortion which accompanies it.

(However, radical cations by strict definition are slightly different in that the term particularly refers to self-trapped polarons). The cation and radical moieties form bound species. Calculations have shown that the combination of nearby polarons would produce a lower energy bipolaron (of the singlet spin pattern).[44,45] Analogously, reduction of a conjugated material would generate a radical anion species, or a negative polaron. Lattice polarization (deformation about the charge carrier moiety) acts as a potential well that hinders the movements of the charge, thus decreasing its mobility. Assuming the charge defect is located between the same conjugated moieties, the same energy barrier to migration exists in either direction of movement, meaning the charge defect can migrate along the conjugated backbone of the material in either direction without changing the energy of the backbone. This property is referred to as the charge mobility of the polymer.

Charge transport, or electron transport (ET), on the intramolecular scale is viewed as an interaction between an electron donor (D) linked to an electron acceptor (A) through some bridging species (B). In general, there are two mechanisms for ET in these D-B-A systems: superexchange and hopping mechanisms. Superexchange occurs via a tunneling process; the electron never occupies the bridging unit during ET.[46] Transport via a hopping mechanism involves reduction (or oxidation) of the bridge by the donor, then to the acceptor.[47] The two processes may occur concurrently in the same system, where the overall rate of electron transfer is equal to the additive rates of each process.

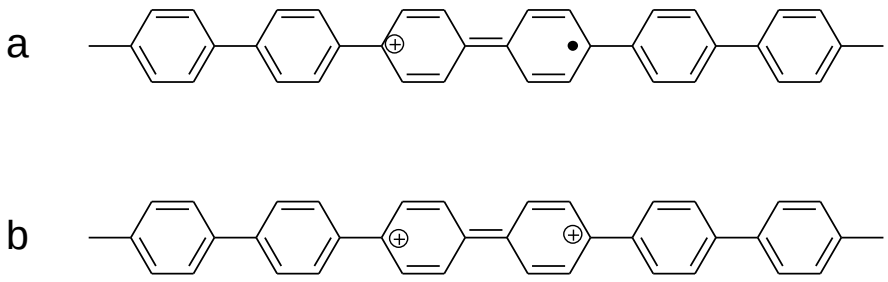

Figure 1-10. Depiction of a polaron (a) and a bipolaron (b) in a poly(phenylene) material.

Excited states of organic conjugated systems

Much of the interest in conjugated polymers has been on the optical properties of phenyl-based light emitting systems, including both linear and nonlinear optical transitions. The valence electrons of conjugated organic molecules absorb in the UV-Vis region of the electromagnetic spectrum; for strong dipole coupling between the ground state and singlet excited state, a singlet excited state is typically produced in high quantum yields. It is found that the lowest excited state of this type has exciton character (the hole and the electron are bound). The singlet exciton is defined as a highly delocalized excited state, typically spanning 10-20 repeat units of the material. In terms of luminescence properties, the $S_1 \rightarrow S_0$ transition, if highly polarized, generally relaxes back to the ground state via fluorescence.

ISC is generally slow in these materials (as discussed previously), thus generating triplet excitons in low quantum yields. Nevertheless, triplet excited state properties are of interest in these materials, as applications in optical properties of these materials is becoming more prevalent: areas of interest include organic light emitting diodes (OLEDs), field-effect transistors, electronic semiconducting materials, light harvesters, photosensitizing and nonlinear applications.[48-52] Understanding more about the triplet state is of particular interest pertaining to OLEDs where electroluminescence is

generated via the recombination of electrons and holes. Emission yields are limited by spin statistics for the recombination events, a large portion of which populate the non-emissive triplet states of these materials.

Burrows and coworkers have measured the quantum yields of ISC in various conjugated polymers using photoacoustic calorimetry.[53] Polythiophenes generally measured higher triplet yields (0.5-0.8) than poly(p-phenylene vinylene)s (0.01-0.04) due to efficient spin-orbit coupling induced by the sulfur atom.

Singlet and triplet energies of various conjugated polymers were measured by Burrows and Monkman using pulse radiolysis and energy transfer techniques.[54] They found a linear correlation between the triplet and singlet energy gaps for the polymers studied. They also found that while planarity of the materials enhanced singlet state delocalization and torsional angles localized the state, both had little effect on the triplet state properties, concluding that the triplet exciton is much more localized than the singlet exciton.

There has been a great deal of interest in studying the transport of excitons along single chain conjugated materials. These investigations are typically performed in dilute solutions, minimizing the probability of interchain interactions.[55] One method of investigating exciton transport in conjugated molecules involves the incorporation of low energy trap sites within the molecule.[56-59] Another method of investigation involves the binding of small molecule quenchers to the conjugated material.[60-62] In either scenario, after photoexcitation of the conjugated material, exciton transfer is confirmed by the quenching of the emission via either a PET process or emission from the lower energy trap.

Platinum Acetylide Materials

Platinum acetylides are a class of organometallic compounds which exhibit useful photophysical properties that lend to potential applications in areas such as optical limiting[63] or electroluminescent devices.[64] These compounds are air-stable, π-conjugated organometallic materials. The structure of platinum acetylides (Figure 1-11) consists of a typical repeat unit of [-C≡C-Pt(PR_3)$_2$-C≡C-Ar-] in which the aryl moiety (such as a phenyl, thiophenyl, pyridinyl, or other group) is bonded to the platinum via an acetylide bridge. The alkyl groups of the neutral phosphine ligands (commonly 1-8 carbons) facilitate in solubilizing the materials in common organic solvents. The Pt(II) center typically adopts a *trans*-square planar geometry.

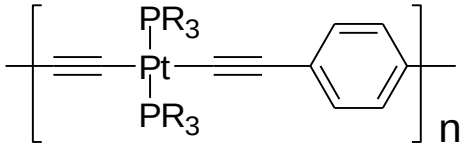

Figure 1-11. The general structural unit of a platinum acetylide.

Synthesis

Hagihara and coworkers first prepared platinum acetylide materials in 1977.[65] Shortly after, they further described the synthesis of *cis* and *trans*-dialkynyl compounds of Pt(II) complexes.[66] The coupling of a platinum chloride complex with an acetylene was best accomplished in the presence of an alkylamine base and catalyzed by copper(I) iodide. The addition of base facilitates the deprotonation of the acetylide ligand, while copper(I) activates the coupling reaction via coordination to the acetylide bond. Inert conditions are necessary to prevent oxidation of the copper catalyst. The same reaction conditions have been applied to polymer synthesis,[67] however higher

molecular weights are afforded with the reaction of trimethyltin-protected acetylides and platinum chloride under conditions of heat.[68]

It was more recently found that either the *cis* or *trans*-$Pt(PR_3)Cl_2$ starting complex could be used to yield a *trans*-platinum acetylide product, as *cis-trans* isomerization is known to occur in the presence of tertiary amines. Either isomer can be distinguished by ^{31}P NMR,[69-71] observing the coupling between phosphorus and an NMR active isotope; J_{Pt-P} (^{195}Pt, I=1/2, 33.8% natural abundance), is generally below 2500 Hz for *trans* isomers and above 2500 Hz for *cis* isomers.

Photophysics

On a more fundamental level, platinum acetylide materials provide a platform for investigation of π conjugation mediated by metal $d\pi$/carbon $p\pi$ interactions.[72] Introduction of a heavy metal such as platinum into the conjugated backbone of organic structures provides insight into the triplet excited state that had been elusive in strictly organic systems. The strong spin-orbit coupling induced by heavy metals provide an increase both the rate of ISC and radiative decay from the triplet; direct measurement of phosphorescence readily provides information as to the energy, vibrational structure and lifetime of the T_1 state.[73]

In general, isoenergetic d-orbitals of transition metals lose degeneracy when in the electronic environment of the ligands (ligand field theory). For the d^8 metal Pt(II), a square planar complex, the d orbitals ($d_{x^2-y^2}$) that align with the four ligands are destabilized, and the orbitals out of the plane (d_{xy}, d_{yz}, d_{xz} and d_{z^2}) are less destabilized by this interaction.[74] This leads to the energy splitting of the d orbitals (Figure 1-12) in

which electronic transitions involving Pt(II) would involve the d_{xy} (HOMO) and $d_{x^2-y^2}$ (LUMO) energy levels.

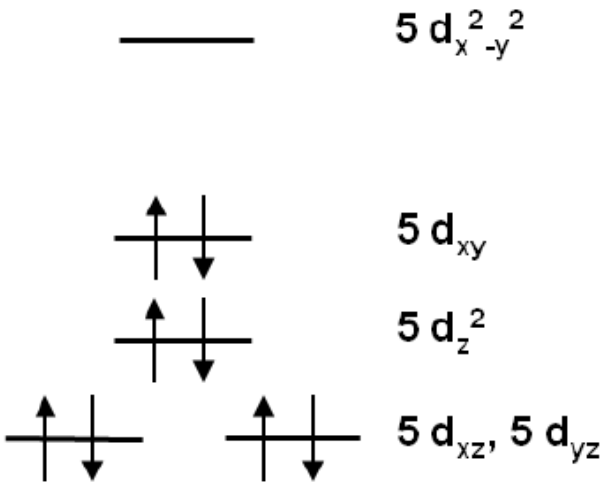

Figure 1-12. Ligand field splitting of the d orbitals of a square planar Pt(II) complex.

In platinum acetylide compounds, optical transitions involve both the platinum d and ligand p_z/π orbitals due to mixing.[72,75] The extent of hybridization between the metal and ligands varies depending on the spacer used. For acetylene or phenylacetylene ligands, mixing with the d orbitals in Pt(II) is also exhibited in the photophysics of the compounds. Chawdhury *et al*.[76] have demonstrated the preservation of conjugation through the platinum centers in a series of thienyl-platinum acetylide dimers and polymers, noting the lowering of the $S_0 \rightarrow S_1$ transition energy with the introduction of platinum. In general, the emission bands of platinum acetylides generally show significant vibronic progressions; this feature is common for MLCT or π-π^* transition states, but not common for d-d transitions which are usually sharp and structureless. The phosphorescent lifetimes are also intermediate between common $^3\pi$-π^* and ^{3}MLCT lifetimes, indicating again the hybridization of the orbitals. In general,

studies find that the fundamental optical transitions in these materials originates from mainly π-π^* transitions in ligand with some contributions from Pt(II) d-orbitals.[77]

Much of the initial photochemical characterization of platinum acetylides was carried out by Lewis, Friend and coworkers.[10,68,71,76,78-86] Polymers and monomers containing phenylene-ethynylene spacers generally absorb around 300-400 nm (Figure 1-13).[73] Polymeric structures typically absorbed at lower energies than the respective monomers, indication a higher extent of delocalization in the ground state geometry.

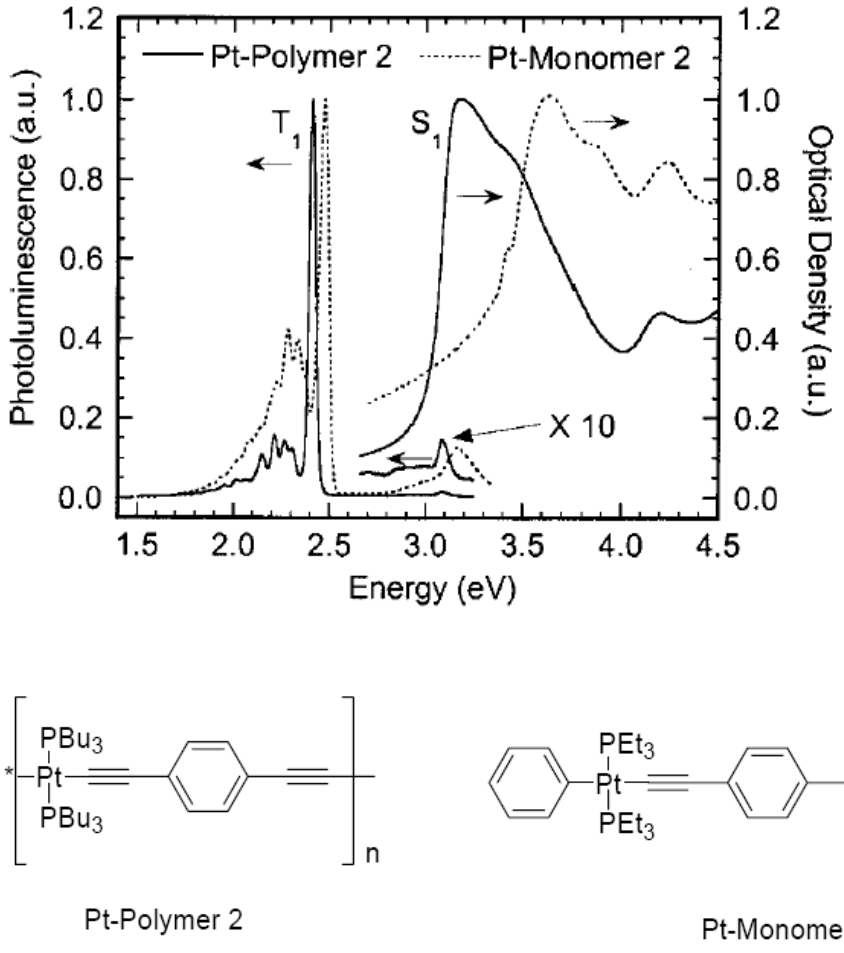

Figure 1-13. Absorption and emission spectra of Pt-phenylethynyl monomer and polymer films. The figure was adopted from Kohler.[73]

Fluorescence emission spectra (between 400-450 nm) were also red-shifted in polymers compared to the monomers, suggesting the S_1 state was also more highly delocalized in the polymers. No differences, however, between the polymers and monomers were seen in the phosphorescence spectra (500-600 nm), indicating a highly localized T_1 state that is confined between two Pt centers. T_1-T_n absorption of the compounds was between 600-800 nm with the polymers absorbing at lower energies than the analogous monomers. This also suggests that the T_n states of the polymers are more highly delocalized than the monomer units.[87]

A more thorough study of exciton delocalization within phenylene-ethynylene-linked Pt-acetylides was reported by Lui and coworkers.[88] Absorption and emission data were reported for a series of monomers ranging from 1 to 7 repeat units (Figure 1-14). Results again indicate a higher degree of delocalization in both the ground and singlet excited states, while the triplet excited state remains highly confined between two platinum moieties. More insightful in this study, however, is the decrease in the extent of red-shifting in both ground state absorptions and fluorescence emissions between n=5 and n=7 units; results conclude that the effective conjugation length of the S_1 state is about 6 repeat units. The S_1-T_1 energy gap was not constant in this oligomer series, varying from 0.91 to 0.78 eV as the oligomers lengthened.

Wilson and coworkers systematically varied the aryl group of the platinum acetylide spacers in the polymer materials (Figure 1-15) to study the effect of excited state energies on triplet state evolution.[86] The onset of singlet absorption varied from 1.7 to 3.0 eV within the series, depending on the spacer used. Photophysical results revealed a decrease in both the lifetimes and emission intensities from the triplet state

as the energy of the triplet state also decreased as non-radiative decay rates increased. Later results concluded that the exponential increase in non-radiative decay rates with decreasing triplet energy levels correlated well with the energy gap law.[10] Results of this series also revealed a constant singlet-triplet energy splitting (~0.7 eV) reguardless of spacer used.

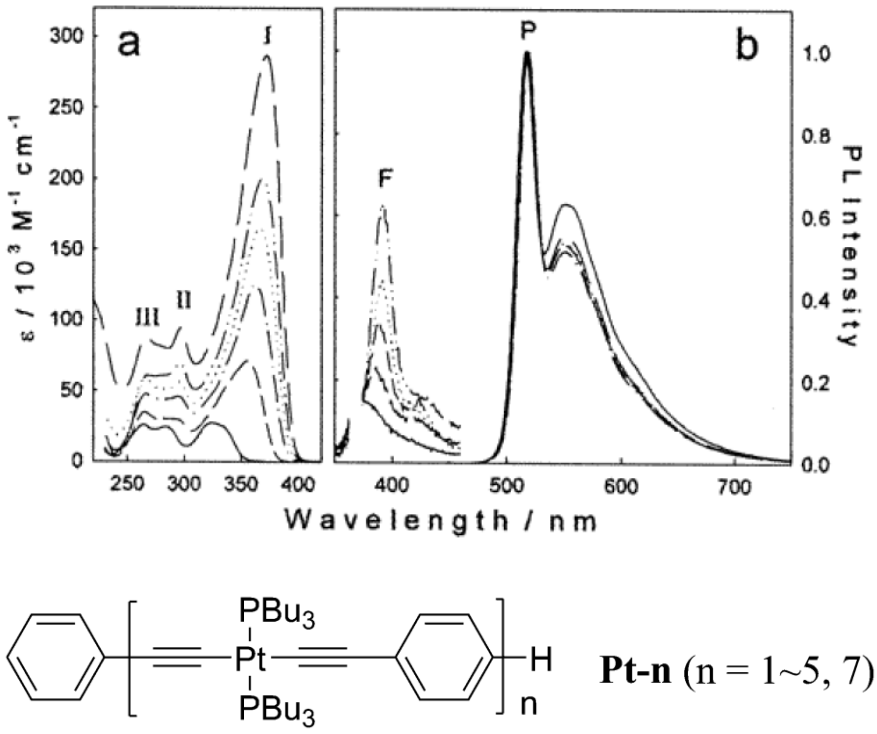

Figure 1-14. Series of platinum acetylide oligomers studied by Liu.[88]

The study was further extended with a more extensive investigation of aryl spacers (Figure 1-16).[73] In all cases, the singlet state was lower in energy for the polymers than the representative monomer materials; the triplet energies between polymer and monomers remained fairly constant throughout the series, however. It was concluded that the singlet state was highly delocalized, reguardless of aryl spacer used, and the triplet state was highly confined across the series. Again, the singlet-triplet splitting

energies remained constant at ~0.7 eV (Figure 1-17). These results are useful in predicting the singlet-triplet energy gap for analogous platinum acetylides.

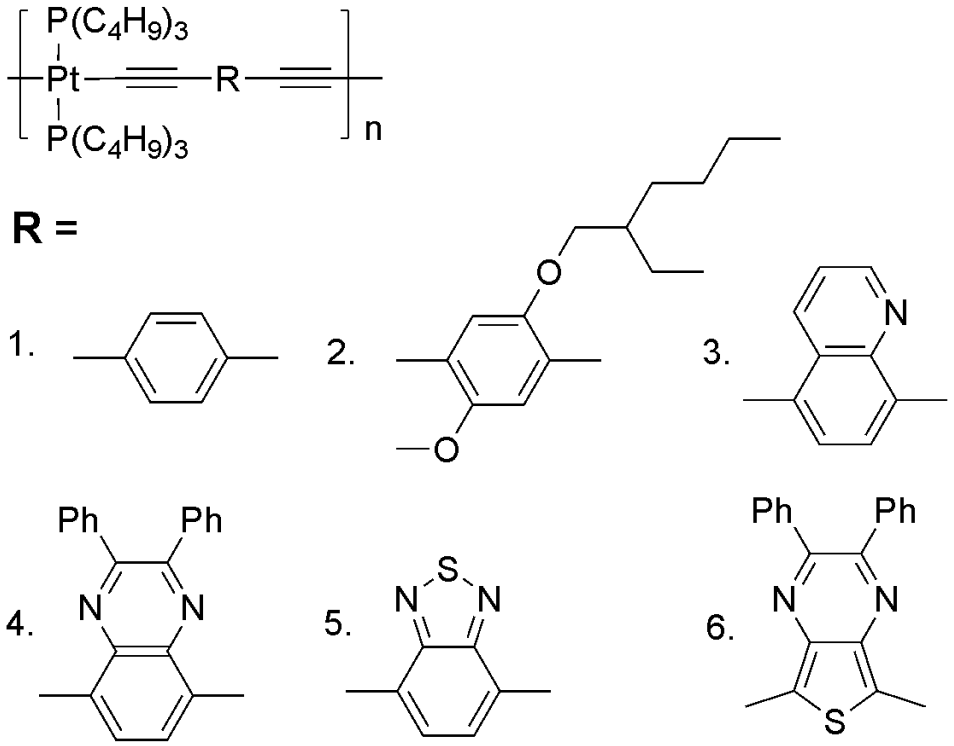

Figure 1-15. Platinum acetylide polymer series studied by Wilson and coworkers.[86]

Rogers and coworkers[87] have studied the relationship between ligand conjugation length and photophysical properties in platinum acetylide oligomers (Figure 1-18). Results of the work concluded that the effect of the heavy metal to induce strong spin-orbit coupling was reduced as the length of the conjugated organic ligand increased within the series; both ground state (S_0-S_1) and triplet state (T_1-T_n) absorption red-shifted with increasing conjugation. The effect on the triplet excited state properties in molecules with increasing conjugation of the organic spacer between two platinum atoms was studied by Farley and coworkers (Figure 1 -19).[89] Triplet emission was assigned to mainly $^3\pi,\pi^*$ character in the diplatinum polyynediyl oligomer series.

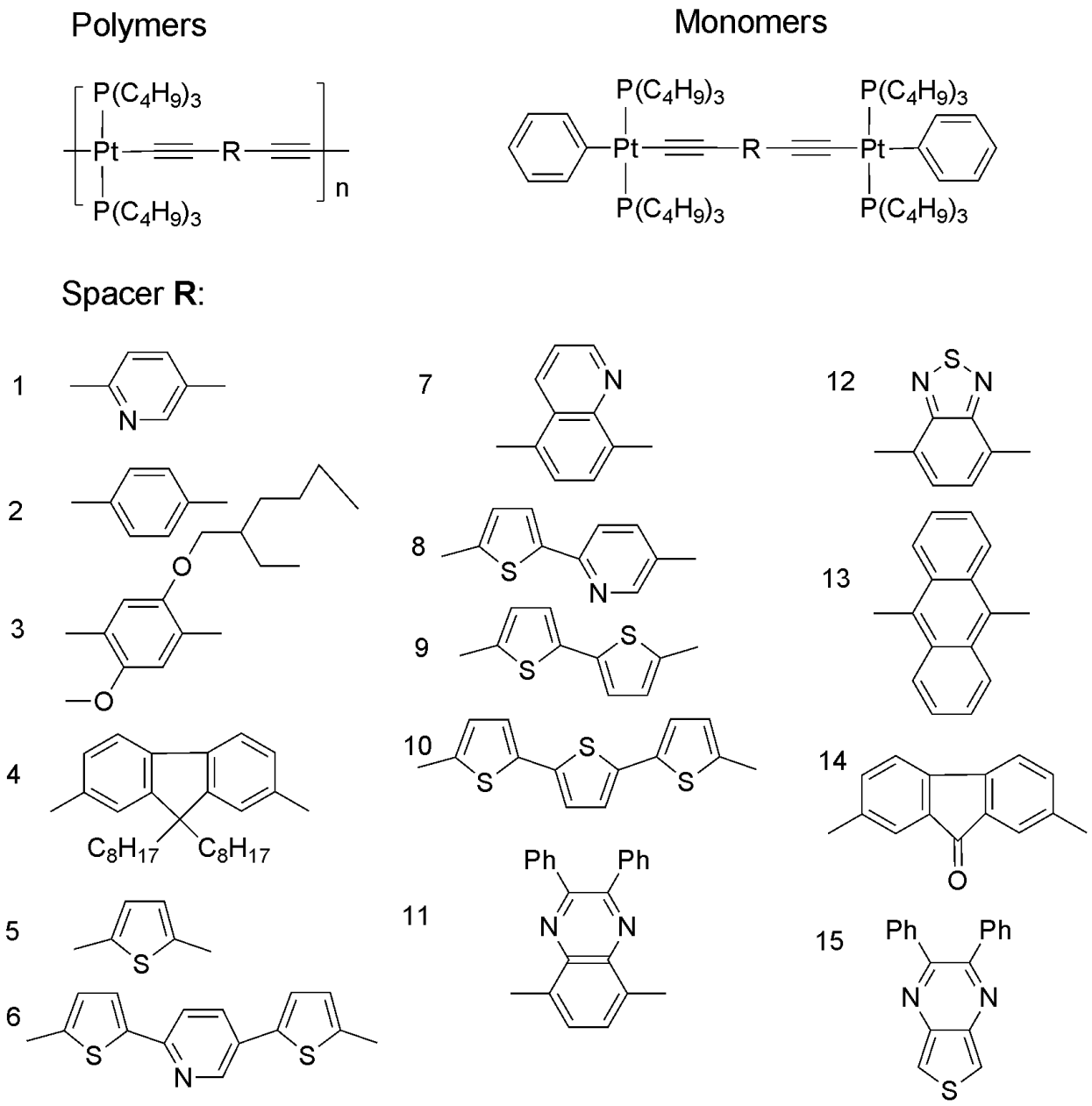

Figure 1-16. More extensive series of platinum acetylides studied by Köhler.[10,73]

Phosphorescence at low temperature was noted to red-shift with increasing acetylene spacer length, and emission lifetimes were noted to decrease with decreasing triplet energy. Triplet-triplet absorption was evident at ambient temperatures and also revealed mainly $^3\pi,\pi^*$ character. The results also revealed non-radiative decay trends that were quantitative with the energy gap law.

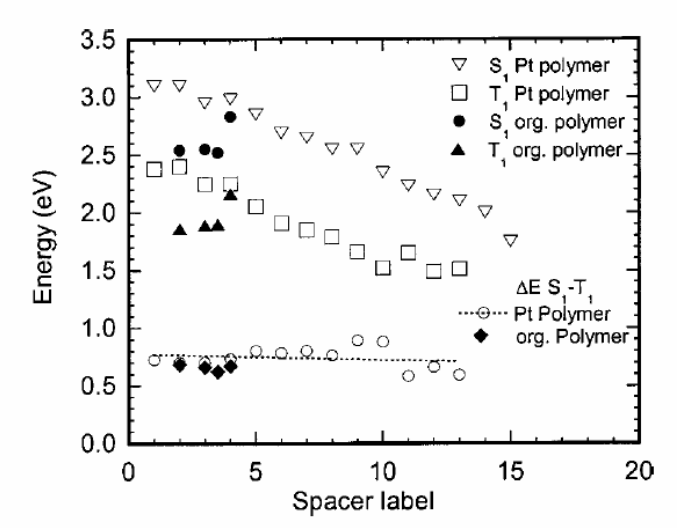

Figure 1-17. Singlet, triplet, and single-triplet splitting energies for a series of polymers and monomers studied by Köhler.[73]

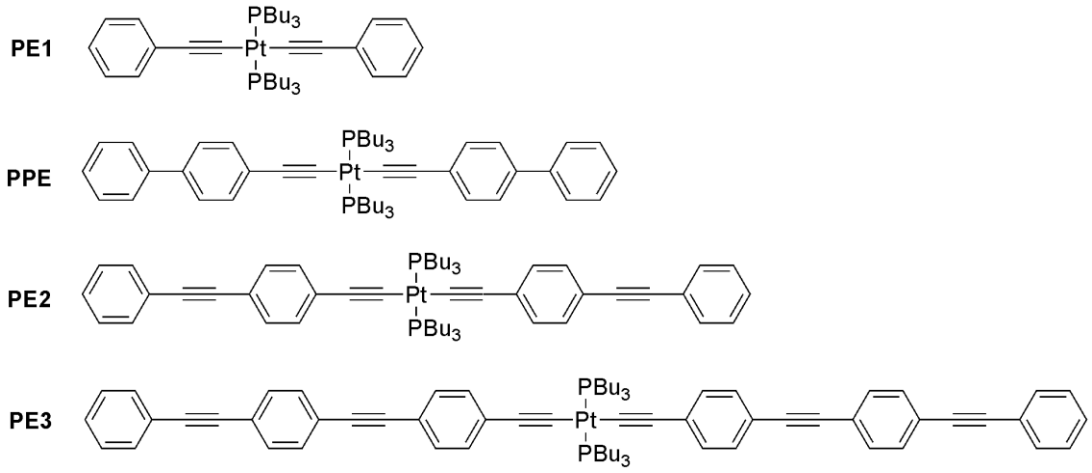

Figure 1-18. A series of platinum acetylide oligomers studied by Rogers.[87]

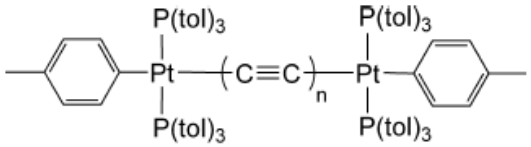

PtC_xPt x = 6, 8, 10, 12
x = 2n
tol = p-tolyl-

Figure 1-19. The series of diplatinum polyynediyl oligomers studied by Farley and coworkers.[89]

Objectives of the Current Study

From previous studies, our group has concluded that both the triplet excited state and the charged ion states of platinum acetylide materials are more spatially confined--restricted within one or two repeat units. In continuation of our investigation into these systems, we seek to further define the properties of these states via both thermodynamic and kinetic experimentation. Herein, we have designed various platinum acetylide oligomer structures to study the properties of both charged and excited states.

In view of these more recent results, it is logical to ask two questions: (1) How rapidly does the triplet exciton or charge (a polaron) migrate along a Pt-acetylide chain? (2) To what extent is the triplet state localized between two platinum atoms in platinum acetylides as the spacer chromophore, phenylene ethynylene, is lengthened? While these questions are of a fundamental nature, the answers apply directly to the application of conjugated materials in molecular electronic devices.

We have investigated the dynamics of both triplet exciton and charge migration along single chains of platinum acetylides through the study of suitably designed platinum acetylide oligomers. First, a series of mono-disperse platinum acetylide oligomers of varying chain lengths were synthesized with low energy, easily reducible naphthalene diimide end-caps to act as triplet energy or electron traps. Ultrafast laser flash photolysis and pulse radiolysis experiments were used to study the dynamics of exciton and charge transport along the chain to the trap sites in the mono-disperse oligomers. To increase the chance of success in measuring the dynamics (which were believed to be relatively fast), oligomers with ultimately relatively long chains were

needed. An iterative-convergent approach was used to successfully synthesize the series in a minimal amount of steps with ease in purification.

The effect of platinum on the triplet state in oligoynes was mentioned earlier. Rigid rod systems such as these are interesting in their potential application toward molecular wire transport of excitons or polarons. The incorporation of platinum into phenylene-ethynylene materials is expected to promote the formation of the triplet excited state, just as in typical platinum acetylide materials. The incorporation of platinum into these organic oligomers is also useful for further study the effective conjugation length and properties of the triplet states in platinum acetylide materials. A series of phenylene-ethynylene spacers of varying length were end-capped with platinum atoms. Photophysical characterization of the properties (absorption, emission, lifetime, etc.) of the ground and excited states of these oligomers has provided insight into the influence of platinum in these systems.

CHAPTER 2
SYNTHESIS OF MONODISPERSE PLATINUM-ACETYLIDE OLIGOMERS END-CAPPED WITH NAPHTHALENE DIIMIDE UNITS

Introduction

There has been much research in the field of conjugated polymers toward the advancement of new optical and electronic applications.[30,90-93] For over two decades, most of the research has focused on the use of purely organic materials, however investigations of organometallic and metal-organic frameworks are becoming increasingly popular.[94-97] Interest in the incorporation of heavy metals into conjugated materials includes both studies of fundamental photophysical properties of these compounds as well as their application in areas of non-linear optics and optoelectronics.[63,98-102]

One promising field that our group has focused on has been the study of platinum (Pt)-acetylide materials of the type [-Pt(PR_3)$_2$-C≡C-Ar-C≡C-], where Ar is an organic arene and the stereochemistry at the square planar Pt(II) center is *trans*-.[88,103-105] Studies have provided considerable insight into the effect of the platinum center within a π-conjugated electronic system. These polymers have demonstrated useful application in organic solar cells and as non-linear absorption materials.[63,99-102,106] The addition of the platinum center most significantly effects the π-framework via a strong spin-orbit coupling, effectively mixing the singlet and triplet excited states which leads to efficient production of long-lived triplet excitons.[72,75,77]

Our group as previously described the results of spectroscopic studies designed toward characterizing the properties of triplet excitons in Pt-acetylide oligomers and polymers.[88,103,104] More recently, we have performed pulse radiolysis[107] experiments to

characterize the spectroscopy and spatial extent of negative ion-radicals (polarons) produced by reduction of the platinum acetylide oligomers.[108] The conclusions of the spectroscopic and pulse radiolysis studies reveal that triplet excitons and negative polarons are spatially confined on the Pt-acetylide chain, delocalized to an extent corresponded to approximately a single repeat unit, e.g., [-Pt-C≡C-Ph-C≡C-Pt-], where Ph = 1,4-phenylene.[104,108] As a continuation of these findings, we have developed a series of Pt-acetylide oligomers that are end-capped with molecular units that can act as "traps" for triplet excitons or negative polarons produced on the chains. Time-resolved spectroscopic studies of such end-capped oligomers carried out using laser flash photolysis and pulse radiolysis have provided considerable insight into the kinetics of triplet exciton and negative polaron diffusion rates in Pt-acetylide materials.

This chapter reports the synthetic work accomplished towards the objective of synthesizing a series of mono-disperse Pt-acetylide oligomers that are end-capped with naphthalene diimide units, Pt_nNDI_2, Figure 2-1. The goal of the synthetic work was to prepare relatively long oligomer chains in order to more successfully measure the dynamics of exciton and polaron hopping along the chains as well as intrinsically increasing the relative concentration of the Pt-acetylide units vs. end-cap units.[58,109-112] The synthetic approach used to construct these oligomers is based on an iterative-convergent method; this approach involves application of organometallic synthons with orthogonally protected terminal acetylenes. There has been considerable research focused on the synthesis of mono-disperse, organic π-conjugated oligomers,[90,113-120] however relatively few studies have been reported describing the preparation of oligomers that contain regular repeats of metal centers in the π-conjugated

sequence.[88,121] The synthetic work described herein is useful, as the protecting group approach that is developed is general and could be used towards the synthesis of a variety of Pt-acetylide based oligomers and dendrimers.

Results and Discussion

Molecular Synthesis and Design

The structures of the end-capped Pt-acetylide oligomers synthesized, Pt_nNDI_2 (n = 2, 3, 6 and 10), are shown in Figure 2-1 below. Each of these oligomers features a Pt-acetylide chain with the repeat unit structure [-Pt(PBu_3)$_2$-C≡C-Ph-C≡C-] (Ph = 1,4-phenylene) in the core of the molecule, as well as 1,4,5,8-naphthalenediimide (NDI) units as end-caps. The NDI unit was chosen as an end-cap because this moiety is reduced at a relatively low potential, therefore it is a lower energy electron acceptor for trapping negative polarons or triplet excitons produced on the chains by pulse radiolysis or optical excitation, respectively.[122,123] A reference material for comparison of photophysical characterizations was also necessary, therefore the previously synthesized dimeric complex Pt-2[88,108] was chosen.

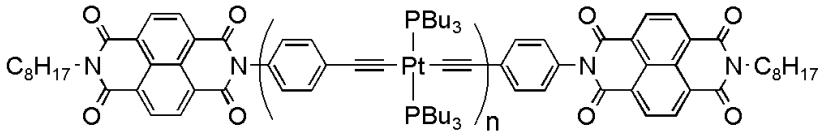

Pt_nNDI_2

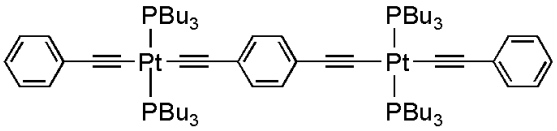

Pt-2

Figure 2-1. Chemical structures of the end-capped Pt-acetylide oligomers.

The synthesis of the longer oligomers of the series (i.e., n = 6 and 10) presented a general synthetic challenge. Three basic synthetic routes were considered when outlining the synthesis, as each had advantages and drawbacks. The simplest synthetic approach would perhaps have been use of the fractionation method.[90] Here, a short-lived AA/BB type polymerization reaction of $Pt(PBu_3)_2Cl_2$ and 1,4-diethynylbenzene could be carried out, followed by quenching the reaction early with the appropriate end-cap. The drawback in this approach would be the separation and isolation of the oligomers because the reaction would be uncontrolled, resulting in a complex mixture of oligomers with different chain lengths. A stepwise, totally directed approach[90] was perhaps most obvious, but this would involve a completely linear synthesis with group protection/deprotection needed at each step in the sequence. While product isolation via this route would be much less difficult, the synthesis would require many steps, compromising the overall yields of the target oligomers.[121]

Previously, our group as applied the iterative method toward preparation of monodisperse platinum acetylide oligomers,[88,103,104,108] however because of the need for longer chain lengths in the for dynamics experiments we chose the iterative-convergent approach for the task.[90,124,125] This method involves the synthesis of an unsymmetric platinum acetylide oligomer segment containing orthogonal protecting groups as a primary synthon (structure **7**, Figure 2-2). Synthetically building from the center of the oligomer and out also ultimately reduced the number of overall steps involved in assembly of the longer oligomers.

Synthesis

The route used to construct the primary synthon **7** is outlined in Figure 2-2 below. Monomeric complex **3** was first prepared via selective deprotection of the

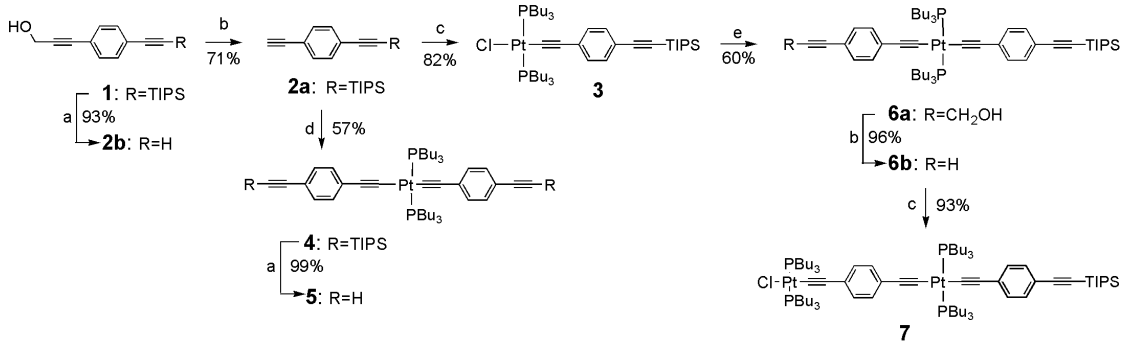

a) TBAF, THF, rt, 1h; b) MnO_2, KOH, ether, rt, 5h; c) *cis*-$Pt(PBu_3)_2Cl_2$, Et_2NH, reflux, 12h; d) *cis*-$Pt(PBu_3)_2Cl_2$, cat. CuI, THF/Et_2NH, rt, 2h; e) **2b**, cat. CuI, Et_2NH, rt, 12h.

Figure 2-2. Synthesis of orthogonally-protected synthon 7.

hydroxymethyl (HOM) group of known compound **1**[88,114] to afford an unsymmetrically protected 1,4-diethynybenzene (**2a**) in which one of the ethynyl groups is free and the other is protected with the triisopropylsilyl (TIPS) unit. The use of the Hagihara coupling[66] of *cis*-$Pt(PBu_3)_2Cl_2$ with **2a** in refluxing diethylamine afforded the mono-substituted product **3** in a 58% overall yield from **1**. A copper-catalyzed Hagihara coupling of complex **3** was then run with compound **2b**, which contains one free ethynyl group and one protected with the HOM group. This reaction produced the orthogonally-protected organometallic intermediate **6a**, a key building block toward the synthesis of the longer oligomers, in 60% yield. Either of the acetylene protecting groups (HOM or TIPS) of **6a** can be selectively removed. Moreover, the complex is soluble in non-polar solvents due to incorporation of alkyl groups, and it can be easily separated by silica chromatography from less polar impurities due to the polar HOM unit that interacts more strongly with the silica support, increasing its retention time on a column. Deprotection

of the HOM group from **6a** produces **6b** which was coupled with *cis*-$Pt(PBu_3)_2Cl_2$ to afford the TIPS-protected synthon **7** in an 89% yield.

Synthesis of the shorter oligomers **11** and **12** did not require synthon **7** as the synthesis was relatively straight forward (Figure 2-3). The end-capped dimer, **Pt_2NDI_2** (**11**), was prepared by the copper(I) catalyzed Hagihara coupling of known compounds **8**[126] and **10**.[108] The end-capped trimer, **Pt_3NDI_2** (**12**), was prepared by coupling known complex **5**[88] with the NDI synthon **9**. Synthon **9** was previously prepared via Hagihara coupling of *cis*-$Pt(PBu_3)_2Cl_2$ with **8**.

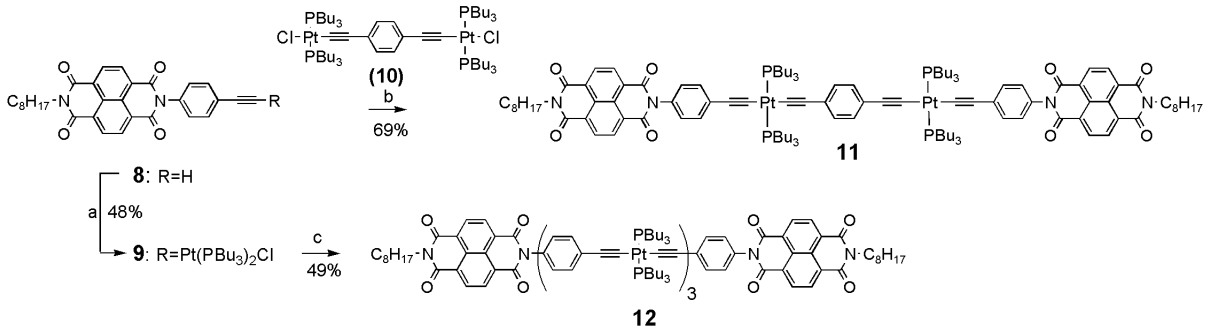

a) *cis*-$Pt(PBu_3)_2Cl_2$, iPr_2NH/MeCN, reflux, 12h; b) cat. CuI, THF/Et_2NH, rt, 3h; c) **5**, cat. CuI, THF/Et_2NH, rt, 3h.

Figure 2-3. Synthesis of **Pt_2NDI_2 (11)** and **Pt_3NDI_2 (12**).

The synthons **7** and **9** were both used to afford rapid construction of the longer end-capped oligomers Pt_6NDI_2 and Pt_6NDI_2 (**15** and **17**) as shown in Figure 2-4. Both end-capped oligomers were synthesized via tetramer **14a**, which was synthesized in high yield by coupling two equivalents of synthon **7** with diethynylbenzene. Deprotection of the TIPS groups in **14a** using tetrabutylammonium fluoride (TBAF) followed by coupling of the resulting free acetylenes in tetramer **14b** with the NDI end-cap **9** afforded

Pt_6NDI_2. Finally, the final decamer **$Pt_{10}NDI_2$** was synthesized via copper(I) catalyzed coupling of **14b** with synthon **7** to yield octamer **16a**. The TIPS protecting groups were then removed from **16a** with TBAF, and the resulting free acetylenes of the deprotected octamer (**16b**) were coupled with end-cap **9** to yield the decamer **$Pt_{10}NDI_2$**.

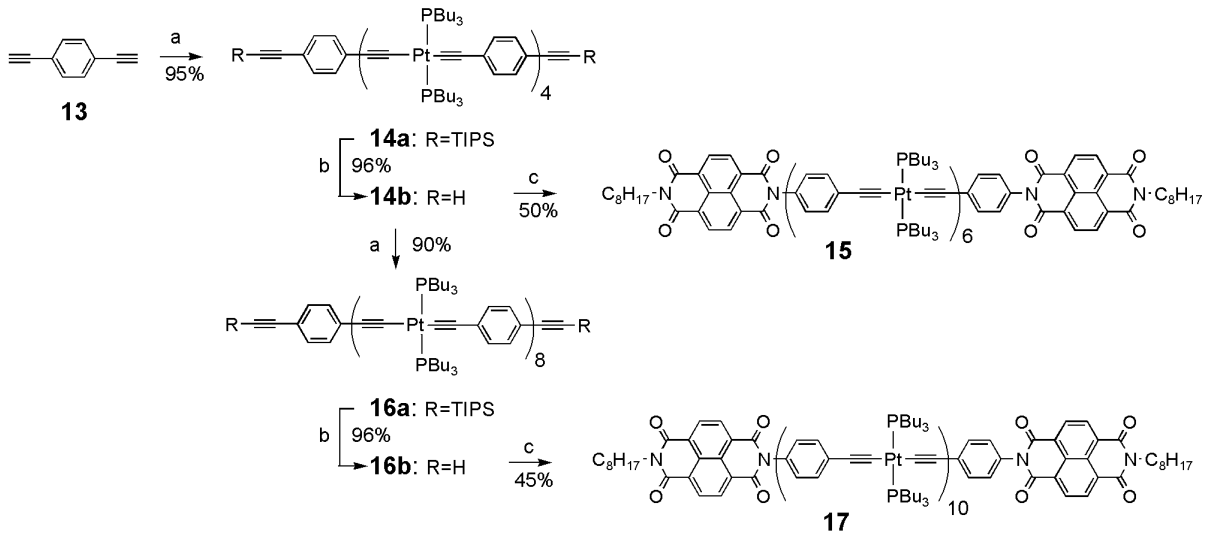

a) **7**, THF/Et_2NH, cat. CuI, rt, 4h; b) TBAF, THF, rt, 1h; c) **9**, THF/Et_2NH, cat. CuI, rt, 3h.

Figure 2-4. Synthesis of **Pt_6NDI_2 (15)** and **$Pt_{10}NDI_2$ (17)** oligomers

^{31}P NMR Characterization

The oligomer structures were confirmed by ^{1}H NMR, ^{31}P NMR and elemental analysis as further described in the experimental section. The ^{31}P NMR spectra of the oligomers are especially interesting in revealing characteristics of the oligomer structures (Figure 2-5). The ^{31}P spectra appear as a pattern of three resonances centered at δ ~ 4 ppm for each oligomer; the weak "doublet" with J ~ 2350 Hz is characteristic of the ^{195}Pt-^{31}P coupling, and the central resonance is due to the PtP_2 units with NMR inactive Pt isotopes. Splitting of the three individual resonance peaks is observed for the trimer, hexamer and decamer and is discussed below. The *trans*

stereochemistry of the PtP_2 units is confirmed by the magnitude of the ^{195}Pt-^{31}P coupling constant.[69]

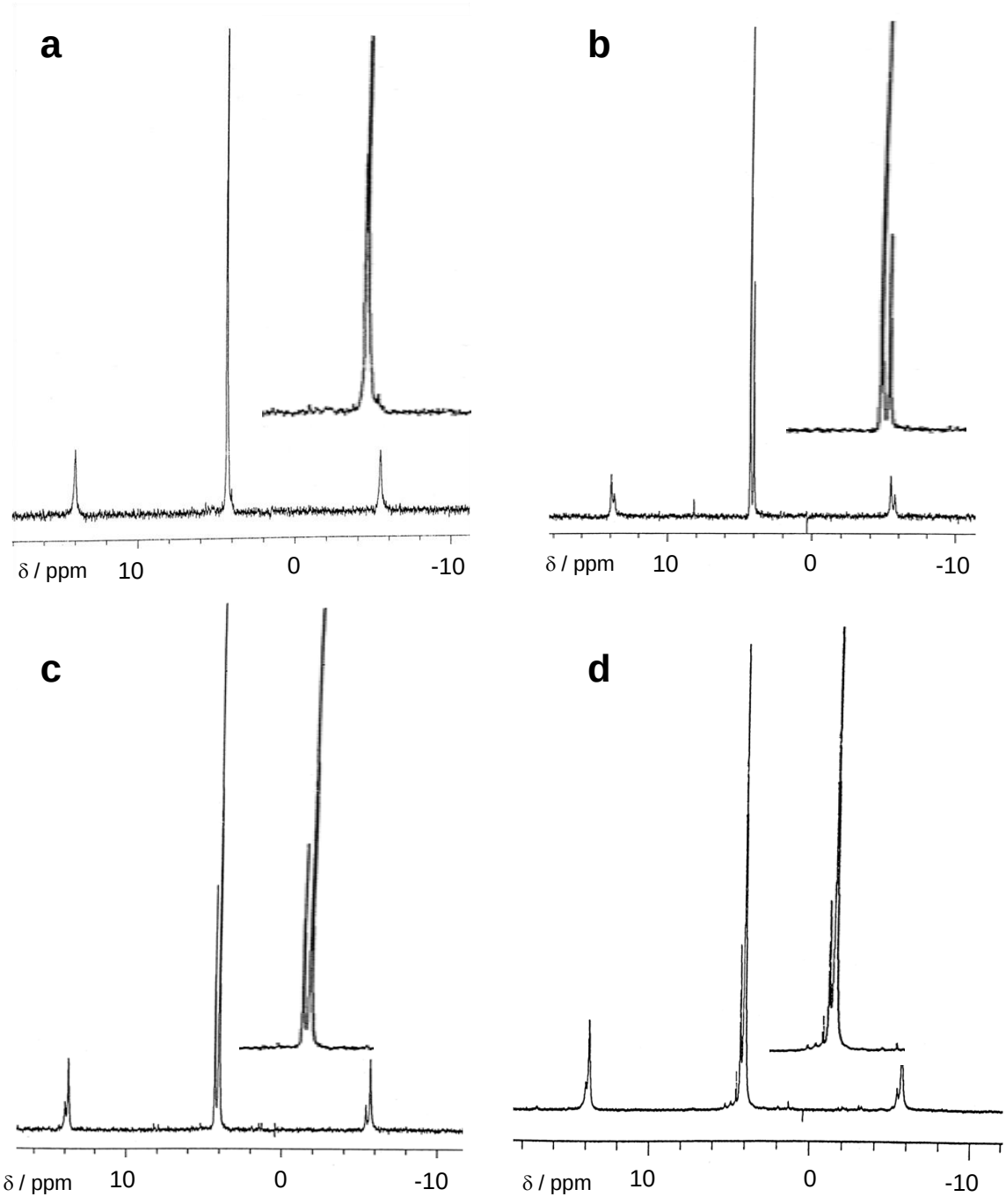

Figure 2-5. ^{31}P NMR spectra for the $\mathbf{Pt_nNDI_2}$ series. (a) n = 2; (b) n = 3; (c) n = 6; (d) n = 10

To better discuss the pattern of splitting which results from the oligomer structures, we focus attention on the central resonance (δ ~ 4 ppm). The expanded insets of Figure 2-5 highlight these signals. In Figure 2-5a, the central resonance signal for **Pt_2NDI_2** is a singlet. This observation is consistent with the fact that the two PtP_2 centers are equivalent in the dimer. For the trimer, **Pt_3NDI_2** (Figure 2-5b), the center resonance appears as two closely spaced singlets with the downfield:upfield ratio of approximately 2:1. This splitting is consistent with the fact that there are two chemically inequivalent sets of phosphines in the oligomer structure: those on the terminal PtP_2 units and those on the central PtP_2 unit. On the basis of the ratios for each signal, we conclude that the resonance for the terminal PtP_2 units is downfield by *ca.* 0.2 ppm relative to that for the central PtP_2. The downfield shift for the terminal PtP_2 units may arise due to the electron withdrawing effect of the NDI unit, which is a relatively strong π-acceptor. Examining the signals for the hexamer, **Pt_6NDI_2**, in Figure 2-5c is also interesting; the center resonance also appears as two closely spaced singlets, however the downfield:upfield ratio is 1:2, reversed from that of the trimer. This spectrum is also consistent with the structure of the hexamer, which features two terminal PtP_2 units and four central PtP_2 units: on the basis of the structure we would predict the ratio of the terminal and central resonance peaks to be 1:2. Finally, the decamer, **$Pt_{10}NDI_2$**, shows a similar trend in which the downfield peak apparently due to the terminal PtP_2 units is considerably weaker compared to the upfield signal due to the central $PtPt_2$ units. While we are unable to report the numerical integration values for the two signals, inspection of the expanded spectrum in Figure 2-5d indicates that the downfield:upfield

peak ratio is in qualitative agreement with the 1:4 ratio expected on the basis of the oligomer's structure.

Electrochemistry

The objective of the synthesis of the NDI end-capped Pt-acetylide oligomers is to use them to investigate charge and exciton transport in π-conjugated organometallic systems. In order to understand the properties of the excited and charged states of these systems, it is essential to characterize the accessible redox states within the materials. Hence, cyclic voltammetry was performed on the simplest oligomer of the series, **Pt_2NDI_2**, to obtain information regarding the redox states of both the core and the end-groups together.

The cyclic voltammagram of **Pt_2NDI_2** in Figure 2-6 features two reversible cathodic waves with $E_{1/2}$ = -0.65 and -1.05 V, as well as a single reversible anodic wave at $E_{1/2}$ = 0.89 V (potentials vs. SCE). The cathodic waves are assigned to sequential one-electron reduction of the two NDI end-groups. Most likely, each cathodic wave likely corresponds to simultaneous one-electron reduction of both of the NDI units, for example for the first wave at $E_{1/2}$ = -0.65 V: NDI-Pt_2-NDI + $2e^-$ → $(NDI^{-\bullet}\text{-}Pt_2\text{-}NDI^{-\bullet})^{2-}$, however quantitative measurements with ferrocene proved difficult to further lend to this assumption. This assignment is supported by a number of previous studies of the NDI unit (including a study of a platinum acetylide complex that contains NDI units) which demonstrate that the NDI electrophore is reduced in two sequential one-electron processes at potentials in the range -0.6 and -0.8 V vs. SCE.[122,123,126]

The anodic wave observed for **Pt_2NDI_2** is assigned to a one-electron oxidation of an electrophore consisting of the platinum acetylide unit, [-$Pt(PBu_3)_2$-C≡C-Ph-C≡C-

$Pt(PBu_3)_2$-]. This assignment is in agreement with our recent work on the electrochemical properties of the model complex Pt-2; a series of platinum acetylide oligomers with a repeat unit structure $[-Pt(PBu_3)_2-C\equiv C-Ph-C\equiv C-]_n$ were previously characterized.[108] The study showed that Pt-2 exhibits a one-electron oxidation at $E_{1/2}$ = 0.89 V, while the longer oligomers display similar waves at slightly less anodic potentials.

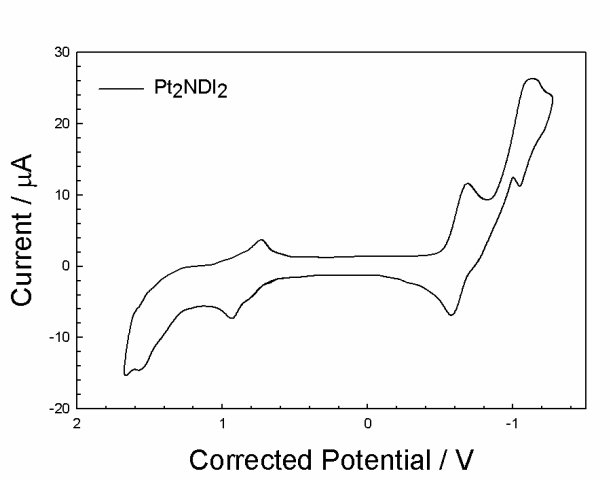

Figure 2-6. Cyclic voltammagram of **Pt_2NDI_2** (**11**) in methylene chloride with 0.1 M TBAH as electrolyte, vs. SCE.

Absorption and Photoluminescence Spectroscopy

The UV-visible absorption spectra of the Pt_nNDI_2 oligomer series were measured in THF (Figure 2-7, left). Each of the molecules exhibit strong absorption in the near UV region, with the molar absorptivity increasing with chain length to a maximum of nearly 800,000 $M^{-1}cm^{-1}$ for the decamer. The near-UV absorption arises from π,π^* transitions localized on the Pt-acetylide chain and on the NDI end-groups (both chromophores absorb in the 340 – 370 nm region). Interestingly, the shape of the near-UV absorption varies within the series. In particular, for the **Pt_2NDI_2** and **Pt_3NDI_2** oligomers, there are two well-defined absorption band maxima at *ca.* 360 and 375 nm; however, for the

hexamer and decamer the band sharpens and only a single band maximum is seen at 370 nm. This variation is believed to arise due to the relative contribution of the platinum acetylide chain and NDI chromophores across the series. More specifically, the absorption is dominated by π,π^* transitions localized on the NDI end-group chromophore for the shorter oligomers. The absorption of the NDI chromophore features a pronounced vibronic progression with maxima at 360 and 380 nm,[122] which

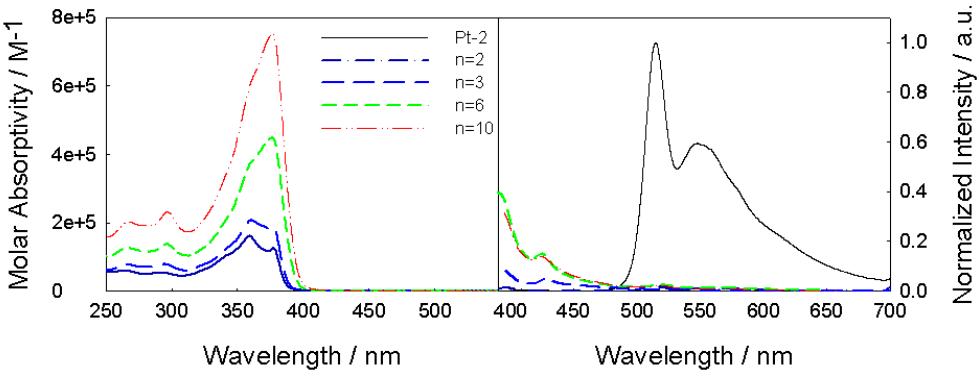

Figure 2-7. UV-Vis (left) and steady state emission spectra (right) of **Pt_nNDI_2** series in degassed THF at 298K.

are clearly resolved in the **Pt_2NDI_2** spectrum. The near-UV absorption is increasingly dominated by the long-axis polarized π,π^* transition localized on the organometallic conjugated core segment as the length of the Pt-acetylide chain increases. The near-UV absorption in **$Pt_{10}NDI_2$** measures *ca.* 85% absorption on the Pt-acetylide chain, with *ca.* 15% or less of the oscillator strength on the NDI end-caps. The series of weaker transitions at higher energy also become more prominent in the longer oligomers; these transitions have been previously assigned as arising from short-axis polarized π,π^* transitions on the platinum acetylide chain.[88,127]

Photoluminescence spectroscopy is also important in the characterization of these materials as it provides insight into the excited state dynamics of the NDI end-capped oligomers. A comparison in the emission of the **Pt_nNDI_2** series with the emission of the model complex, Pt-2 is plotted in Figure 2-8 (right). The spectra were measured for argon-degassed solutions and the intensities are normalized to demonstrate the relative emission quantum yields of the NDI end-capped oligomers vs. the model comparison compound Pt-2. The Pt-2 the emission is dominated by a structured band with λ_{max} = 519 nm with a vibronic shoulder at lower energy. This emission is observed for all platinum acetylide oligomers with the repeat unit structure [-Pt$(PBu_3)_2$-C≡C-Ph-C≡C-] and has phosphorescence characterized as arising from the triplet excited state (exciton). Previous studies have shown that the phosphorescence energy is invariant with oligomer chain length, an observation that suggests that the spatially confined nature of the triplet exciton to a relatively short chain segment.[88,104]

Notably, the phosphorescence emission is hardly observed for any of the **Pt_nNDI_2** oligomers, a result which clearly indicates the accessibility of a more competative non-radiative pathway that very efficiently quenches the triplet exciton prior to phosphorescence. Emission quantum yield studies were performed and conclude that the quenching of the Pt-acetylide phosphorescence is nearly quantitative, with the quantum yields for the NDI end-capped oligomers in the range Φ_P ~ 0.1-0.2 % compared to the yield of Pt-2 which has Φ_P ~ 5%.[88]

The electrochemical studies of **Pt_2NDI_2** provide insight concerning the mechanism for the triplet exciton quenching. In particular, on the basis of the cyclic voltammetry studies it is concluded that a charge separated state in which one NDI acceptor is

reduced and the Pt-acetylide chain is oxidized, e.g., NDI-[-(Pt(PBu_3)$_2$-C≡C-Ph-C≡C-)$^{+\bullet}$]-NDI$^{-\bullet}$, lies at *ca.* 1.55 eV relative to the ground state. (The charge transfer state energy is estimated by taking the difference in the oxidation and reduction potentials of Pt_2NDI_2.)[128] This state lies well below the energy of the triplet exciton state, which lies at *ca.* 2.4 eV, as estimated from the band maximum of the phosphorescence. Thus, we conclude that the triplet quenching arises from rapid intramolecular photoinduced electron transfer,

NDI-[-^{3}(Pt(PBu_3)$_2$-C≡C-Ph-C≡C-)*]-NDI → NDI-[-(Pt(PBu_3)$_2$-C≡C-Ph-C≡C-$^{+\bullet}$)]-NDI$^{-\bullet}$,

which is much faster compared to radiative decay of the triplet exciton. In the following chapter details of picosecond transient absorption spectroscopy experiments will be provided that confirm that this process occurs, and that also provide very significant insight concerning the dynamics of triplet exciton diffusion within the longer platinum acetylide oligomers.

Summary and Conclusions

An iterative-convergent synthetic method to prepare a series of mono-disperse platinum acetylide oligomers that contain as many as 10 repeat units has been successfully developed. The oligomers are end-functionalized with naphthalene diimide electron acceptors for use in studies of exciton and electron transport. The iterative-convergent synthetic approach uses organometallic synthons that feature either (or both) HOM or TIPS as protecting groups for the terminal acetylene moieties. These protecting groups are orthogonal: they are removed under different conditions in high synthetic yields affording monofunctional synthons that can be used in subsequent iterative react-deprotect sequences to construct the longer oligomers. In addition to

serving as a protecting group, the polar nature of the HOM unit also has the benefit of facilitating the chromatographic separations. In particular, oligomers that are end-functionalized with the HOM group elute more slowly on silica gel columns compared to the (less polar) reaction by-products and oligomers that contain only the TIPS protecting groups.

Precedence for the use of the HOM and TIPS as orthogonal protecting groups in synthesis of oligomers comes from the work of Godt *et al*;[114] this group demonstrated the strategy in the synthesis of phenylene ethynylene oligomers with nine repeat units. Takahashi et al[121] used a TIPS protected terminal acetylene organometallic intermediate in a platinum acetylide dendrimer synthesis that was carried out through four generations. However, prior to this work we are unaware of the prior use of orthogonal acetylene protecting groups in the synthesis of organometallic oligomers.

Experimental

Materials and Instruments

All solvents and chemicals used for synthesis of the platinum acetylide oligomers were reagent grade and used without purification unless noted. Silica gel (Silicycle Inc., 230-400 mesh, 40-63 microns, 60 Å) was used for all flash chromatography. All silyl-acetylene starting materials were purchased from GFS Chemical; potassium tetrachloroplatinate and palladium-bis(triphenylphosphyl) dichloride were purchased from Strem Chemicals; all other chemicals were purchased from Sigma-Aldrich. ^{1}H and ^{31}P NMR spectra were obtained on a Varian 300-MHz spectrometer using deuterated chloroform ($CDCl_3$) as the solvent and tetramethylsilane (TMS) as the internal reference. Elemental analysis was performed from Robertson Microlit Laboratories for all of the final oligomers. Decomposition temperatures were also estimated for all

oligomers synthesized using a standard Melt-temp apparatus. All newly-synthesized intermediates were characterized by TOF-MS and elemental analysis.

Cyclic voltammetry experiments were performed in dry methylene chloride (CH_2Cl_2) solution containing 0.1 M tetra-*n*-butylammonimum hexafluorophosphate (TBAHFP) as the supporting electrolyte. The three-electrode setup consisted of a platinum microdisk (2 mm^2) working electrode, a platinum wire auxiliary electrode and a silver wire reference electrode. Solutions were degassed with argon flow prior to measurements, maintaining positive argon pressure during the measurements. The concentrations of oligomers in the solutions were 1 mM. A scan rate of 100 mV/s was used. All potentials were internally calibrated against the ferrocene/ferricinium couple (E = 0.43 V vs. SCE in CH_2Cl_2) and potentials plotted vs. SCE.

Steady-state absorption spectra were recorded on a Varian Cary 100 dual-beam spectrophotometer. Corrected steady-state emission measurements were conducted on a SPEX F-112 fluorescence spectrometer. Samples were degassed by argon purging for 30 min and concentrations were adjusted to produce "optically dilute" solutions (i.e., A_{max}< 0.20) in THF. Quantum yields were calculated using $Ru(byp)_3Cl_2$ as a known reference.[129]

Synthesis

cis-bis(Tributylphosphine)dichloroplatinum(II) was prepared by literature methods. Yield = 1.45 g (89.5%). M.p. 138-139^oC.[130]

*3-{4-[(Triisopropylsilyl)-ethynyl]-phenyl}-prop-2-yn-1-ol (**1**).* This compound was synthesized by literature methods. [88,103,104,108] Yield 3.1 g (32.7%). M.p. 61-63^oC. ^1H NMR (300 MHz, $CDCl_3$) δ 1.20 (s, 21H), 3.82 (br s, 1H), 4.58 (s, 2H), 7.40 (dd, 4H).

*1-Ethynyl-4-(tri-iso-propylsilylethynyl)-benzene (**2a**)* was prepared by literature methodology.[108] Yield = 1.31 g (71.2%). M.p. 47-48°C. ^{1}H NMR (75 MHz, $CDCl_3$) δ 1.18 (s, 21H), 3.15 (s, 1H), 7.45 (s, 4H). Mass spec. (DIP-CI-HRMS) calc'd for $C_{19}H_{26}Si$ $[M+H]^+$ 283.1877, found $[M+H]^+$ 283.1867.

*3-(4-Ethynyl-phenyl)-prop-2-yn-1-ol (**2b**).* To a 25 mL round bottom flask with a stir bar was added **1** (1.5 g, 4.80 mmol) and THF (5 mL). The solution was degassed 5 min under argon, followed by the addition of TBAF, 1 M in THF (11.9 mL, 11.9 mmol). The reaction was let stir at room temperature for 1 h. After this time, the solution was diluted with Et_2O and washed with both D.I. water and brine. The organic layer was then dried over $NaSO_{4(s)}$. The solvent was evaporated to give a crude brown solid that was purified by flash chromatography (silica gel, 1:1 to 3:1 hexane/CH_2Cl_2, then addition of 1% MeOH to afford fraction 2 as product). The solvent of the second fraction was evaporated to afford a dark brown oil as the product. Yield 0.70 g (93%). ^{1}H NMR (300 MHz, $CDCl_3$) δ 1.25 (br, 1H), 3.15 (s, 1H), 4.45 (s, 2H), 7.38 (dd, 4H). M.p. 70-71°C.[114]

*trans-Bis(tributylphosphine)chloro{(4-Ethynyl-phenylethynyl)-triisopropyl-silane}platinum(II) (**3**).* **2a** (0.36 g, 1.28 mmol) and $HNEt_2$ (30 mL) were added to a round bottom flask with a stir bar. The mixture was stirred and degassed with argon for 10 min, follow by the addition of *cis*-$Pt(PBu_3)_2$ Cl_2 (0.95 g, 1.41 mmol). The reaction was stirred at reflux under argon overnight, then cooled and diluted with CH_2Cl_2. The organic solution was washed with both d.i. water and brine then dried over $NaSO_{4(s)}$. TLC in 5:1 hexane/CH_2Cl_2 gave 4 spots (spot 3 was product). Solvent was evaporated to give a crude solid that was purified by flash chromatography (silica gel, 9:1 to 3:1 hexane/CH_2Cl_2). Fraction 3 solvent was evaporated to afford a yellow crystalline solid

that did not phosphoresce under a long wave UV lamp. Yield 0.97 g (82.6%). M.p. 65-67^{o}C. ^{1}H NMR (300 MHz, $CDCl_3$) δ 0.89 (t, 18H), 1.18 (s, 21H), 1.3-1.6 (br m, 24H), 1.98 (br m, 12H), 7.14 (d, 2H), 7.31 (d, 2H). ^{31}P NMR ($CDCl_3$) δ 8.0 (J = 2356 Hz). Mass Spec. (+TOF-HRMS) Calc'd for $C_{43}H_{79}ClP_2PtSiNa$ $[M+Na]^+$ 939.4658; Found $[M+Na]^+$ 939.4685. Anal. Calcd. for $C_{43}H_{79}ClP_2PtSi$: C, 56.34; H, 8.69; N, 0.0. Found C, 56.62; H, 9.05; N, 0.01.

*trans-Bis(tributylphosphine)bis{(4-Ethynyl-phenylethynyl)-triisopropyl-silane}platinum(II) (**4**).* To a 50 mL round bottom flask with a stir bar was added **2a** (0.30 g, 1.06 mmol), *cis*-Pt $(PBu_3)_2Cl_2$ (0.33 g, 0.48 mmol) and $HNEt_2$ (10 mL). The solution was degassed with argon for 10 min, followed by the addition of CuI (~3 mg). Within minutes, the reaction was a bright yellow color with salt formation. After 1 h, the solvent was evaporated and the solid diluted with CH_2Cl_2. The organic solution was washed with D.I. water and brine, then dried over $NaSO_{4(s)}$. Evaporation of solvent afforded a crude yellow oil that was purified by flash chromatography (silica gel, 100% hexane to 4:1 hexane/CH_2Cl_2). Fractions 1 and 2 were impurities; fraction 3 was eluted as a large yellow band. Solvent was removed to yield a yellow crystalline solid as product. Yield 0.32 g (57%). M.p. 65-68^{o}C. ^{1}H NMR (300 MHz, $CDCl_3$) δ 0.88 (t, 17H), 1.08 (s, 39H), 1.19 (sextet, 12H), 1.55 (br m, 12H), 2.05 (br m, 12H), 7.13 (d, 4H), 7.29 (d, 4H); ^{31}P NMR ($CDCl_3$) δ 4.2 (J_{Pt-P} = 2346.94 Hz).[88]

*trans-Bis(tributylphosphine)bis(4-ethynyl-phenylethynyl)platinum(II) (**5**).* To a 25 mL round bottom flask with a stir bar was added **4** (300 mg, 0.26 mmol) and THF (5 mL). The solution was degassed 5 min with argon, followed by the addition of TBAF, 1 M in THF (0.77 mL, 0.77 mmol). The reaction was stirred at room temperature for 1 h.

TLC (silica, 10:1 hexane/acetone) revealed complete transformation of the starting material. The solution was diluted with Et_2O and washed with both D.I. water and brine. The organic solution was dried over $MgSO_{4(s)}$, and the solvent was removed to give a crude yellow solid that was purified by a short flash chromatography column (silica gel, 10:1 hexane/acetone). The eluted yellow fraction solvent was evaporated to afford a yellow crystalline solid (starburst-like crystals). Yield 218 mg (99%). M.p. 85-88^oC. ^1H NMR (300 MHz, $CDCl_3$) δ 0.91 (t, 18H), 1.45 (m, 12H), 1.55 (m, 12H), 2.10 (br m, 12H), 3.09 (s, 2H), 7.19 (d, 4H), 7.32 (d, 4H).[88]

*trans-Bis(tributylphosphine)-[2-{4-(prop-1-yn-3-ol)phenyl}ethyne]-[2-{4-(2-triisopropylsilyl-1-phenylethynyl}ethyne (**6a**).* To a round bottom flask with a stir bar was added **3** (0.55 g, 0.60 mmol) and **2b** (94 mg, 0.60 mmol). $HNEt_2$ (15 mL) was added and the solution was degassed for 10 min under argon. CuI (2 mg) was then added under argon flow, and the reaction was let stir at room temperature overnight. The solution was then diluted with CH_2Cl_2 and washed with D.I. water and brine. The bright yellow organic solution was dried over $MgSO_{4(s)}$, then solvent was evaporated to give a dark yellow oil. The crude product was purified by flash chromatography (silica gel, CH_2Cl_2). Fraction 2, a bright yellow band on the column, was evaporated to afford a yellow solid. Yield 0.37 g (60%). ^1H NMR (300 MHz, $CDCl_3$) δ 1.0 (t, 19 H), 1.2 (s, 21H), 1.4-1.8 (br m, 24H), 2.05 (br, 1H), 2.21 (br m, 12H), 4.60 (br s, 2H), 7.28 (dd, 4H), 7.41 (dd, 4H); ^{31}P NMR ($CDCl_3$) δ 4.1(J_{Pt-P} = 2346.33 Hz).

*Complex (**6b**).* To a 100 mL round bottom flask with a stir bar was added **6** (0.40 g, 0.39 mmol) and Et_2O (20 mL). The solution was degassed with argon, followed by the addition of powdered KOH (0.22 g, 8.86 mmol) and activated MnO_2 (0.67 g, 7.72

mmol). The reaction was let stir at room temperature for 12 h, and then it was quenched with D.I. water. The solution was diluted with Et_2O and washed with 5% $HCl_{(aq)}$, D.I. water, and brine. The organic layer was dried over $NaSO_{4(s)}$, and the solvent was removed to give a crude orange oil that was purified by flash chromatography (silica gel, 9:1 CH_2Cl_2/hexane). Fraction 1 eluted as a yellow band off of the column, and this was evaporated to give the product as a yellow oil. Yield = 0.38 g (96%). ^{1}H NMR (300 MHz, $CDCl_3$) δ 0.91 (t, 18H), 1.13 (s, 20H), 1.35-1.70 (br m, 24H), 2.10 (br m, 12H), 3.1 (s, 1H), 7.19 (dd, 4H), 7.35 (dd, 4H); ^{31}P NMR ($CDCl_3$) δ 4.1(J_{Pt-P} = 2346.34 Hz).

*Complex (**7**).* To a 100 mL round bottom flask with a stir bar was added **6b** (250 mg, 0.25 mmol) and $HNEt_2$ (30 mL). The mixture was stirred and degassed at room temperature under argon for 10 min, followed by the addition of *cis*-$PtCl_2(PBu_3)_2$ (200 mg, 0.30 mmol). The reaction was heated to reflux and let stir under argon overnight. After 15 h, the reaction was cooled and the solvent evaporated to give a crude yellow oil. The sample was diluted with CH_2Cl_2 and washed with D.I. water and brine. The organic layer was dried over $NaSO_{4(s)}$, and then the solvent was removed to afford a yellow oil. The crude oil was purified by flash chromatography (silica gel, 4:1 then 2:1 hexane/CH_2Cl_2). Fraction 2 moved as a large yellow band through the column. Solvent was evaporated then put under vacuum 2 h to give a yellow solid product, although residual hexane was difficult to completely remove. Yield = 380 mg (93%). M.p. 73-74^{o}C. ^{1}H NMR (300 MHz, $CDCl_3$) δ 0.8-1.0 (m, 45H *some hexane incorporated), 1.12 (s, 21H), 1.26 (m, *hexane), 1.37-1.70 (br m, 50H), 1.92-2.22 (br m, 24H), 7.07 (dd, 4H), 7.18 (d, 2H), 7.30 (d, 2H); ^{31}P NMR ($CDCl_3$) δ 4.2 (J_{Pt-P} = 2346.34 Hz). Mass Spec.

(+TOF-HRMS) Calc'd for $C_{154}H_{274}Cl_2P_8Pt_4Si_2Na_2$ $[2M+2Na]^{+2}$ 1663.3327; Found $[2M+2Na]^{+2}$ 1663.8327. Anal. Calcd. for $C_{77}H_{137}ClP_4Pt_2Si$: C, 56.37; H, 8.42; N, 0.0. Found C, 56.65; H, 8.75; N, 0.04.

*N-(4'-Ethynylphenyl)-N'-(octyl)naphthalene-1,8:4,5-tetracarboxydiimide (**8**).* This compound was prepared via routes previously decribed in the literature. All intermediate data given. *N-(n-octyl)naphthalene-1,8-dicarboxyanhydride-4,5-dicarboximide*[122]*:* Yield = 2.87 g (20.4%). 1H NMR (300 MHz, $CDCl_3$) δ 0.88 (t, 3H), 1.30 (br m, 12H), 4.20 (t, 2H), 8.80 (s, 4H). M.p. 173-175^{o}C. Mass spec. (DIP-CI-HRMS) calc'd for $C_{22}H_{21}NO_5$, $[M+H]^+$ 380.1492; found, $[M+H]^+$ 380.1510. *N-(4'-iodophenyl)-N'-(octyl)naphthalene-1,8:4,5-tetracarboxydiimide*[131]: Yield 1.31 g (85.6%). ^{1}H NMR (300 MHz, $CDCl_3$) δ 0.90 (t, 3H), 1.30 (br m, 10H), 1.70 (m, 2H), 4.20 (t, 2H), 7.2 (d, 2H), 7.6 (d, 2H), 8.80 (s, 4H). M.p. 252-253^{o}C. Mass spec. (DIP-CI-HRMS) calc'd for $C_{28}H_{25}N_2O_4I$ $[M+H]^+$ 581.0932, found $[M+H]^+$ 581.0884. Anal. Calcd. for $C_{28}H_{25}N_2O_4I$: C, 57.94; H, 4.34; N, 4.83. Found C, 58.23; H, 4.27; N, 4.77.

N-(4'-(2-Triisopropylsilyl-ethynylphenyl)-N'-(octyl)naphthalene-1,8:4,5-tetracarboxydiimide. To a 250 mL schlenk flask with stir bar was added *N*-(4'-iodophenyl)-*N*'-(octyl)naphthalene-1,8:4,5-tetracarboxydiimide (1.88 g, 3.24 mmol) and 1:1:1 THF/iPr_2NH/CH_3CN (120 mL). The solution was stirred and degassed at room temperature for 30 min, followed by addition of $Pd(PPh_3)_4$/CuI via schlenk technique. The solution was further degassed and heated to 40^{o}C, followed by addition of TIPS acetylene (1.18 g, 6.48 mmol) via syringe. The light yellow solution turned a darker yellow color immediately, and the reaction was let stir under argon for 12 h, in which time the reaction turned a dark brown color. After 12 h the solution was cooled and

diluted with $CHCl_3$, then washed with satd' $NH_4Cl_{(aq)}$, 10% $HCl_{(aq)}$, and brine. The organic layer was dried over $NaSO_4$(s), then the solvent was evaporated to give a crude brown solid. The product was purified by flash chromatography (silica, CHCl3). The second fraction was isolated as the yellow solid product. Yield = 1.97g (95.6%). M.p. 253-255^oC. ^1H NMR (300 MHz, $CDCl_3$) δ 0.88 (t, 3H), 1.15 (s, 21H), 1.30 (br m, 10H), 1.70 (m, 2H), 4.20 (t, 2H), 7.28 (d, 2H), 7.68 (d, 2H), 8.80 (s, 4H). Mass Spec. (+TOF-HRMS) Calc'd for $C_{39}H_{46}N_2O_4SiNa$ $[M+Na]^+$ 657.3119; Found $[M+Na]^+$ 657.3119. Anal. Calcd. for $C_{39}H_{46}N_2O_4Si$: C, 73.78; H, 7.30; N, 4.41. Found C, 73.51; H, 7.51; N, 4.28.

*N-(4'-Ethynylphenyl)-N'-(octyl)naphthalene-1,8:4,5-tetracarboxydiimide (**8**):* To a round bottom flask with a stir bar was added *N*-(4'-(2-TIPS-ethynylphenyl)-*N*'-(octyl)naphthalene-1,8:4,5-tetracarboxydiimide (1.97 g, 3.10 mmol) and THF (45 mL). The solution was stirred and degassed under argon for 15 min, followed by addition of TBAF, 1M in THF (6.83 mL, 6.83 mmol) to the reaction. This was stirred at room temperature for 4 h, followed by dilution with CH_2Cl_2. The organic layer was washed with D.I. water and brine, then it was dried over $NaSO_{4(s)}$. The solvent was evaporated to give a dark yellow solid. Flash chromatography (silica gel, 10:1 $CHCl_3$/Hexane, 4:1 $CHCl_3$/THF) was used to purify the solid. The product was recovered as a yellow solid in the second eluted fraction. Yield = 1.07 g (72.3%). M.p. 257-259^oC. ^1H NMR (300 MHz, $CDCl_3$) δ 0.88 (t, 3 H), 1.30 (br m, 10H), 1.75 (m, 2H), 3.10 (s, 1H), 4.20 (t, 2H), 7.28 (d, 2H), 7.68 (d, 2 H), 8.80 (s, 4H). Mass spec. (DIP-CI-HRMS) for $C_{30}H_{26}N_2O_4$ $[M+H]^+$ 479.1965, found $[M+H]^+$ 479.1972.[131]

*Complex (**9**).* To a 200 mL round bottom flask equipped with a stir bar was added **8** (0.82, 1.71 mmol), *i*Pr_2NH (30 mL) and MeCN (60 mL). The mixture was stirred and

degassed with argon for 10 min, followed by addition of *cis*-$Pt(PBu_3)_2$ Cl_2 (1.49 g, 2.23 mmol). The reactions was refluxed overnight, then cooled to room temperature and diluted with CH_2Cl_2. The organic solution was washed with D.I. water and brine, then it was dried over $NaSO_{4(s)}$. The solvent was removed to give a dark red solid. The crude product was purified by flash chromatography (silica gel, CH_2Cl_2). The first fraction eluted was a yellow band of Pt (II) starting material**;** the second fraction was the pure product **9** as a bright orange band. All other color remained at the top of the column. The solvent was evaporated from fraction 2 to yield an orange powder. This product was recrystalized in hexane to afford a very small, shiny needle-like powder. Yield 0.91g (48%). M.p. 145-146^{o}C. ^{1}H NMR (300 MHz, $CDCl_3$) δ 0.8-1.0 (br m, 19H), 1.2-1.8 (br m, 25H), 2.0 (br m, 11H), 4.20 (t, 2H), 7.15 (d, 2H), 7.40 (d, 2H), 8.80 (s, 4H); ^{31}P NMR ($CDCl_3$) δ 8.1 (J_{Pt-P} = 2365.26). Mass Spec. (+TOF-MS) Calc'd for $C_{54}H_{79}ClN_2O_4P_2PtNa$ $[M+Na]^+$ 1135.4751; Found $[M+Na]^+$ 1135.4768. Anal. Calcd. for $C_{54}H_{79}ClN_2O_4P_2Pt$: C, 58.29; H, 7.16; N, 2.52. Found C, 58.43; H, 7.36; N, 2.42.

*Complex (**10**).* This compound was prepared by literature procedure.[108] Yield = 0.58 g (90%). M.p. 103-104^{o}C. ^{1}H NMR (75 MHz, $CDCl_3$) δ 0.91 (t, 36H), 1.45 (m, 24H), 1.55 (m, 24H), 2.0 (br m, 24H), 7.05 (s, 4H); ^{13}C NMR (300 MHz, $CDCl_3$) δ 14.0, 22.1, 24.5, 26.3, 101.6, 215.3, 130.5; ^{31}P NMR (121 MHz, $CDCl_3$) δ +7.89 (J_{Pt-P} = 2390.8 Hz). Mass Spec. (+TOF-HRMS) Calc'd for $C_{58}H_{112}Cl_2P_4Pt_2Na$ $[M+Na]^+$ 1416.6276; Found $[M+Na]^+$ 1416.6275.

*Pt_2NDI_2 (**11**).* To a 50 mL flask with stir bar was added the **8** (60 mg, 0.13 mmol), **10** (80 mg, 0.06 mmol), THF (3.5 mL) and diethylamine (2 mL). The solution was stirred and degassed with argon for 30 min, followed by the addition of CuI (3 mg) under argon

flow. The reaction was stirred at room temperature for 1.5 h. The orange/brown reaction mixture was diluted with CH_2Cl_2, then washed with D.I. water and brine, and dried over $NaSO_{4(s)}$. Evaporation of the organic solvent gave a crude dark green solid. The product was purified by flash chromatography (silica gel, 1:1 hexane/CH_2Cl_2, then 5:2:1 CH_2Cl_2/$CHCl_3$/hexane) to elute the product as the second fraction. Solvent was evaporated to give the product as a dark green solid. Yield = 90 mg (69.4%). Decomposition temperature: 197-199^oC. ^1H NMR (300 MHz, $CDCl_3$) δ 0.90 (m, 42H), 1.20-1.80 (br m, 74H), 2.15 (br m, 27H), 4.20 (t, 4H), 7.15 (d, 8H), 7.42 (d, 4H), 8.80 (s, 8H); ^{31}P NMR ($CDCl_3$) δ 4.27 (J_{Pt-P} = 2354.33 Hz). Mass Spec. (MALDI-TOF) Calc'd for $C_{118}H_{126}N_4O_8P_4Pt_2$ [$M^{+\cdot}$] 2278.07; Found [$M^{+\cdot}$] 2278.06. Anal. Calcd. for $C_{118}H_{126}N_4O_8P_4Pt_2$: C, 62.20; H, 7.17; N, 2.46. Found C, 62.40; H, 7.22; N, 2.27.

*Pt_3NDI_2 (**12**).* To a 50 mL round bottom flask equipped with a stir bar was added **5** (76 mg, 89.9 μmol), **9** (220 mg, 0.20 mmol), $HNEt_2$ (5 mL) and THF (3 mL). The solution was degassed under argon for 10 min, followed by the addition of CuI (~1 mg) to the solution. The reaction was stirred under argon for 2 h. In this time, the mixture turned from a light orange color to a dark orange/brown color. TLC (silica, 1:1 hexane/CH_2Cl_2) revealed a complete consumption of the starting materials. The solution was diluted with CH_2Cl_2 and washed with both D.I. water and brine. The organic layer was dried over $NaSO_{4(s)}$, and the solvent was removed to give a dark green solid that was purified by flash chromatography (silica gel, 1:1:0 to 1:1:(1%) hexane/CH_2Cl_2/(acetone)). Fraction 2 moved as a dark orange band down the column; solvent was removed to afford a green solid product. Yield 290 mg (49%). Decomposition temp. 216-217^oC. ^1H NMR (300 MHz, $CDCl_3$) δ 0.8-1.1 (br m, 59H),

1.1-1.8 (br m, 99H), 2.08 (br m, 34H), 4.20 (t, 4H), 7.1 (br m, 12H), 7.41 (d, 4H), 8.80 (s, 8H); ^{31}P NMR ($CDCl_3$) δ 4.2 (J_{Pt-P} = 2355.49 Hz), 4.0 (J_{Pt-P} = 2363.43 Hz). Anal. Calcd. for $C_{152}H_{220}N_4O_8P_6Pt_3$: C, 60.81; H, 7.39; N, 1.87. Found C, 60.62; H, 7.40; N, 1.78.

*1,4-Diethynylbenzene (**13**)* was prepared by previous literature methods.[88,103] Yield = 0.92 g (88.5%). M.p. 91-93^{o}C (90-94^{o}C). ^{1}H NMR (300 MHz, $CDCl_3$) δ 3.18 (s, 2H), 7.42 (s, 4H).

*Complex (**14a**).* To a 50 mL round bottom flask with stir bar was added 1,4-diethynylbenzene **13** (15 mg, 0.12 mmol), **7** (425 mg, 0.26 mmol), THF (5 mL) and $HNEt_2$ (15 mL). The solution was degassed for 10 min under argon, followed by the addition of CuI (3 mg). The reaction was stirred under argon for 3 h at room temperature, followed by quenching it with D.I. water. The solution was diluted with CH_2Cl_2, washed with D.I. water and brine, and dried over $NaSO_{4(s)}$. The solvent was evaporated to afford a crude yellow solid that was purified by flash chromatography (silica gel, 100:1 hexane/ acetone). Fraction 1 traveled as a yellow band down the column, and solvent was evaporated to give a yellow solid as product. Yield = 0.38 g (95%). M.p. 161-162^{o}C. ^{1}H NMR (300 MHz, $CDCl_3$) δ 0.91 (t, 72H), 1.13 (s, 42H), 1.38-1.48 (br m, 99H), 2.15 (br m, 49H), 7.10 (s, 12H), 7.18 (d, 4H), 7.32 (d, 4H); ^{31}P NMR ($CDCl_3$) δ 4.0 (J_{Pt-P} = 2365.87 Hz), 4.2 (J_{Pt-P} = 2355.49 Hz). Mass Spec. (MALDI-TOF-HRMS with HABA as matrix) Calc'd for $C_{1654}H_{278}P_8Pt_4Si_2$ $[M]^+$ 3333.7813; Found $[M]^+$ 3333.7568.

*Complex (**14b**).* To a 25 mL round bottom flask with a stir bar was added **14a** (230 mg, 0.07 mmol) and THF (5 mL). The mixture was degassed for 10 min, followed by the addition of TBAF, 1 M in THF (0.69 mL, 0.69 mmol) via syringe. The reaction was

let stir at room temperature with the flask covered in aluminum foil for 1 h, and then it was quenched with D.I. water and diluted with CH_2Cl_2. The organic layer was washed with D.I. H_2O and brine, and it was dried over $NaSO_{4(s)}$. Once the organic solvent was evaporated, the crude yellow solid was purified by flash chromatography (silica gel, 20:1 hexane/acetone). Fraction 1 was collected as a yellow solution. The solvent was evaporated to afford a light yellow solid as product. Yield = 210 mg (96%). ^{1}H NMR ($CDCl_3$) δ 0.91 (t, 71H), 1.05 (s, 5H *TIPS-F salt contaminate in NMR sample), 1.38-1.48 (br m, 99H), 2.15 (br, 48H), 3.09 (s, 2H), 7.10 (s, 12H), 7.18 (d, 4H), 7.32 (d, 4H) ; ^{31}P NMR ($CDCl_3$) δ 3.95 (J_{Pt-P} = 2352.43 Hz), 4.2 (J_{Pt-P} = 2356 Hz).

*Pt_6NDI_2 (**15**).* To a 50 mL round bottom flask with a stir bar was added **9** (163 mg, 146 µmol), **14b** (200 mg, 66 µmol), THF (5 mL) and $HNEt_2$ (5 mL). The solution was degassed with argon for 5 min, followed by the addition of CuI (2 mg). Within 2 min the reaction turned a dark orange color and became somewhat opaque with salt formation. After 3 h, the reaction was quenched with D.I. H_2O, diluted with CH_2Cl_2 and washed twice with brine. The organic layer was dried over $NaSO_{4(s)}$ and then the solvent removed to give a crude green/brown solid. The product was purified by flash chromatography (silica gel, 2:1 $CHCl_3$/hexane), eluting the product as a red band down the column. Solvent was removed from this fraction to afford a dark green solid product, although some residual hexane proved difficult to remove. Yield 170 mg (50.1%). Decomposition Temp. > 400^{o}C. ^{1}H NMR (300 MHz, $CDCl_3$) δ 0.90 (m, 108H) 1.2-1.7 (br m, 171H), 2.15 (br m, 74H), 4.20 (t, 4H), 7.0-7.2 (br d, 25H), 7.42 (d, 4H), 8.8 (s, 7H); ^{31}P NMR ($CDCl_3$) δ 4.04 (J_{Pt-P} = 2365.3 Hz), 4.28 (J_{Pt-P} = 2356.1 Hz); Anal.

Calcd. for $C_{254}H_{394}N_4O_8P_{12}Pt_6$: C, 58.96; H, 7.68; N, 1.08. Found C, 58.78; H, 8.00; N, 0.98.

*Complex (**16a**).* To a 50 mL round bottom flask with a stir bar was added **14b** (218 mg, 0.07 mmol), **7** (249 mg, 0.15 mmol), *i*Pr_2NH (8 mL) and THF (3 mL). The solution was degassed with argon for 10 min, followed by addition of CuI (~1 mg). The reaction was stirred under argon at room temperature overnight. After 15 h, the solvent was evaporated and the crude solid diluted in CH_2Cl_2. The organic solution was washed with D.I. water and brine, and then dried with $NaSO_{4(s)}$. The solvent was evaporated to give a crude yellow solid that was purified by flash chromatography (silica gel, 1:1 to 2:1 CH_2Cl/hexane) as fraction 2 (fraction 1 was a very small band on the column; fraction 2 was a very large yellow band). Solvent was evaporated from this fraction to afford a light yellow solid as product. Yield 395 mg (90%). ^{1}H NMR (300 MHz, $CDCl_3$) δ 0.90 (t, 145H), 1.12 (s, 40H), 1.3-1.7 (br m, 201H), 2.15 (br m, 97H), 7.05-7.20 (m, 30H), 7.32 (d, 4H); ^{31}P NMR ($CDCl_3$) δ 4.0 (J_{Pt-P} = 2349.38 Hz), 4.2 (J_{Pt-P} = 2369.53 Hz).

*Complex (**16b**).* To a 25 mL round bottom flask with a stir bar was added **16a** (120 mg, 19 μmol) and THF (5 mL). The solution was degassed with argon for 5 min, followed by the addition of TBAF, 1 M in THF (56.4 μL, 56.5 μmol) via syringe. The reaction was stirred at room temperature under argon with the flask covered in aluminum foil (to prevent light exposure) for 1 h. After this time, the reaction was diluted with CH_2Cl_2 and washed with D.I. water and brine. The organic layer was dried over $NaSO_{4(s)}$ and solvent then evaporated to afford a crude yellow solid. The product was purified by flash chromatography (silica gel, 3:1 CH_2Cl_2/hexane). Fraction 1, a yellow band on the column, was collected and the solvent evaporated to give a yellow solid

product, however some residual hexane proved difficult to remove. Yield 100 mg (96%). ^{1}H NMR (300 MHz, $CDCl_3$) δ 0.90 (br t, 180H *with hydrocarbon solvents), 1.26 (s, 42H *TIPS-F salt contaminate), 1.3-1.7 (br m, 203H *with hc solvents), 2.15 (br m, 96H), 3.10 (s, 2H), 7.05-7.20 (m, 31H), 7.32 (d, 4H); ^{31}P NMR (300 MHz, $CDCl_3$) δ 4.0 ($J_{Pt\text{-}P}$ = 2366.87 Hz), 4.2 ($J_{Pt\text{-}P}$ = 2348.24 Hz).

*$Pt_{10}NDI_2$ (**17**).* To a 25 mL round bottom flask with a stir bar was added **16b** (400 mg, 65.9 µmol), **9** (161 mg, 145.2 µmol), $HNEt_2$ (8 mL) and THF (8 mL). The solution was degassed under argon for 10 min, followed by the addition of CuI (~1 mg). The reaction was stirred at room temperature under argon for 4 h. After this time, the solution was diluted with CH_2Cl_2 and washed with both D.I. water and brine. The organic layer was dried over $NaSO_{4(s)}$, and then the solvent was evaporated to give a dark green crude solid. The product mixture was purified by flash chromatography (silica gel, 2:1:(1%) to 3:1:(1%) to 5:1:(1%) CH_2Cl_2/hexane/(MeOH)). Fractions 1 and 2 (both yellow color) were degraded starting materials, and fraction 3 (dark orange band) was eluted, samples collected and solvent evaporated to afford a dark green solid as product. Yield 240 mg (45.0%). Decomposition temp. > 400^{o}C. ^{1}H NMR (300 MHz, $CDCl_3$) δ 0.95 (m, 188H), 1.1-1.9 (br m, 263H), 2.15 (br s, 120H), 4.20 (br t, 4H), 7.13 (br s, 38H), 7.45 (br d, 4H), 8.80 (s, 8H) ; ^{31}P NMR ($CDCl_3$) δ 4.0 ($J_{Pt\text{-}P}$ = 2365.26 Hz), 4.2 ($J_{Pt\text{-}P}$ = 2365 Hz); Anal. Calcd. $C_{390}H_{626}N_4O_8P_{20}Pt_{10}$: C, 58.05; H, 7.82; N, 0.69. Found C, 57.98; H 7.68; N, 0.72.

CHAPTER 3
NEGATIVE POLARON AND TRIPLET EXCITON DIFFUSION DYNAMICS IN PLATINUM-ACETYLIDE OLIGOMERS

Introduction

Electron and energy transfer are two of the most significant and fundamental processes in chemistry and in biology, and especially so for optical and electronic applications. However, while many issues remain to be clarified for these materials, even more challenges occur in trying to manipulate, by synthesis, positioning and excitation, the rate processes within these materials. Conjugated organic materials have been the focus of a vast amount of research directed toward addressing fundamental scientific questions, as well as developing new advanced materials, for these applications.[30] While a great deal of effort has been directed toward organic materials, the more recent incorporation of various transition metals (i.e. Ir^{III}, Pd^{II}, Pt^{II}, Ru^{II}, Os^{III}, Hg^{I}, etc.) within the framework of selected conjugated organic chromophores has created a wide range of new materials that exhibit interesting photophysical properties.[94,132-141] One such example has been in the area of organic light emitting diode (OLED) research, where the use of metal-organic materials has increased the device efficiencies substantially to afford more efficient electrophosphorescence.[64,142-147] Among these metal-organic materials, platinum-acetylides have generated attention in both optical and optoelectronic applications due to both their interesting excited state properties which are dominated by highly populated, long-lived triplet states, as well as their known charge carrier properties.[88,103,104,108]

In our group's ongoing efforts to explore the fundamental properties of these materials, we have previously defined the triplet exciton as a spatially confined state localized on a chromophore consisting of one to two Pt-acetylide repeat units.[104,108]

Experimental results and DFT calculations also imply that delocalization in these materials is heavily influenced by the relative conformation of the phenylene rings and the square planar PtL_2C_2 units along the backbone.[148] More recent work suggests that charge is also relatively localized within the cation and anion radicals, with the confinement of the anion radical (negative polaron) being somewhat more pronounced.[108] Evidence of exciton and polaron diffusion were also described, addressing the question of transport mechanisms in these materials.

By focusing energy or charge transfer processes within a given molecule, i.e. the platinum acetylide moiety, it may be possible to characterize both the response (kinetics) and the mechanism for such transfers.[149] Therefore, in continuation of our ongoing work, development toward further understanding of the dynamics of both the charge and triplet exciton migration is crucial in gaining insight into the nature of these states—a need recently highlighted by several senior researchers in the field.[36]

The methods used in this study as well as other techniques have been successfully applied in investigations of charge and energy transport in all-organic conjugated compounds, as well as in a few metal-organic systems more recently reported.[20,150] This current project expands on work from the previous chapter, providing the spectroscopic analysis of a series of monodisperse Pt-acetylide oligomers end-capped with naphthalene diimide units designed to act as electron traps (Pt_nNDI_2, where n = 2, 3, 6, and 10 shown in Figure 3-1). Variable temperature steady state emission studies, pulse radiolysis measurements and ultrafast transient absorption measurements were applied to study the transport dynamics of both Pt-acetylide negative polaron and triplet exciton diffusion, respectively.

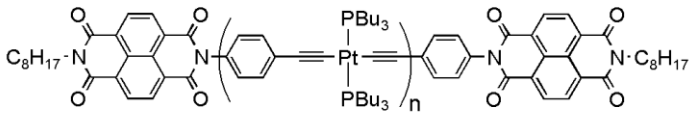

Pt_nNDI_2

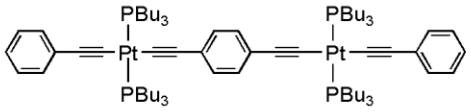

Pt_2

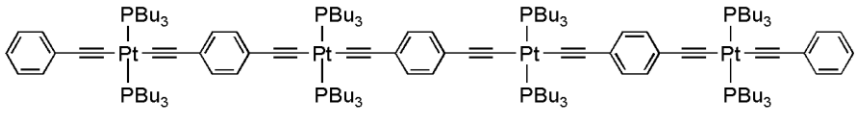

Pt_4

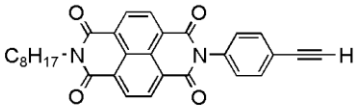

NDI-H

Figure 3-1. Structures of the current study: Pt_nNDI_2, Pt_2, Pt_4, and NDI-H.

Experimental

Synthesis

In an effort directed towards developing an understanding of charge and energy transfer in conjugated metal-organic materials, an extended series of naphthalene diimide (NDI) end-capped Pt-acetylide oligomers, Pt_nNDI_2, have been prepared, where n = 2, 3, 6, and 10 (Figure 3-1). Preparation of these compounds was described in Chapter 2.

Steady State Photophysics

Steady-state absorption spectra were recorded on a Varian Cary 100 dual-beam spectrophotometer. Corrected steady-state emission measurements were conducted on a SPEX F-112 fluorescence spectrometer. Samples were degassed by argon purging for 30 min and concentrations were adjusted to produce “optically dilute”

solutions (i.e., $A_{max} < 0.20$). Photoluminescence quantum yields were determined according to the "optically dilute" method described by Demas and Crosby.[151] Low-temperature fluorescence measurements were made by cooling the samples in a LN2 cooled Oxford Instruments OptistatDN-1704 optical cryostat connected to an Omega CYC3200 temperature controller, and emission measurements were conducted on a PTI fluorescence spectrometer. Samples were degassed by four repeated cycles of freeze-pump-thaw on a high vacuum line.

Electrochemistry

Cyclic voltammetry (CV) experiments were performed in a dry methylene chloride (CH_2Cl_2) solution containing 0.1 M tetra-*n*-butylammonium hexafluorophosphate (TBAHFP) as the supporting electrolyte. The three-electrode setup consisted of a platinum microdisk (2 mm^2) working electrode, a platinum wire auxiliary electrode and a silver wire reference electrode. Solutions were degassed with argon flow prior to measurements, maintaining positive argon pressure during the measurements. The concentrations of oligomers in the solutions were 1 mM. A 100 mV/s scan rate was used. All potentials were internally calibrated against the ferrocene/ferricinium couple (E = 0.43 V vs. SCE in CH_2Cl_2) and potentials plotted vs. SCE.[134]

Pulse Radiolysis

This work was carried out at the Brookhaven National Laboratory Laser-Electron Accelerator Facility (LEAF). The LEAF facility and the methods used are described elsewhere,[107,152,153] as are application to conjugated polymers.[110,111,150] Briefly, the electron pulse (≤ 50 ps duration) was focused into a quartz cell with an optical path length of 20 or 5 mm containing tetrahydrofuran (THF) solutions under argon. The monitoring light source was a pulsed xenon arc lamp. Wavelengths were selected

using either 40 nm or 10 nm bandpass interference filters. Transient absorption signals were detected with either silicon (EG&G FND-100Q, ≤ 1000 nm), or InGaAs (GPD Optoelectronics GAP-500L, ≥ 1100 nm) photodiodes or a biplanar phototube (Hamamatsu R1328U-03, ≤ 650 nm) and digitized with a LeCroy 8620A-oscilloscope. While most measurements have 2-4 ns time resolution, 125 ps system rise time was attained in the visible using the biplanar phototube, and short path cells. Molar extinction coefficients of the radical anions were calculated using $G(e^-_{THF})=0.60$ in THF,[154,155] where G is the radiation chemical yield. To account for capture of geminate electrons, many of which decay in times near 1 ns, electron decay in neat THF was analyzed within Figure 3-2 below. The extinction coefficients obtained were smaller than those reported earlier for Pt_n ions.[108]

The Optical Fiber Single-Shot (OFSS) system obtains still faster time resolution. It operates on a beamline at LEAF where the electron pulse is compressed to ~5 ps duration. The OFSS system is a new instrument that obtains 15 ps overall time resolution using single electron pulses.[156] Signal to noise is enhanced by averaging data from ~25 pulses. Briefly it measures transient absorption utilizing laser probe pulses with wavelengths selected by an optical parametric amplifier. Each probe pulse passes through an optical fiber bundle composed of ~100 fibers having different lengths, separating the probe pulse into 100 mini-pulses having different time delays. The bundle is then imaged into the region of the sample irradiated by the 5 ps electron pulse, and then imaged on a CCD array camera.

Charge transport to the NDI end caps was analyzed in the scheme below (Figure 3-2). Fast electrons pass through the sample cell creating ionization that primarily

results in reactive solvated electrons (e^-_s) in THF, abbreviated as RH in the scheme. The electrons are thermalized within a few ps and attach to the oligomers in bimolecular charge transfer reactions 1-2. The solvent cations $RH^{+\bullet}$ fragment to solvated protons in RH_2^+ and radicals $R^\bullet$.[157] Neither RH_2^+ or radicals $R^\bullet$ react with the oligomers on the time scales investigated, but both react with radical anions of the oligomers in geminate and homogeneous recombination.

$RH \rightarrow RH^{+\bullet} + e^{-\bullet}$	(ionization)	(i)
$e^{-\bullet} \rightarrow e_s^{-\bullet}$	(thermalization, solvation)	(ii)
$RH^{+\bullet} + RH \rightarrow R^\bullet + RH_2^+$	(proton transfer)	(iii)
$e_s^{-\bullet} + Pt_nNDI_2 \rightarrow Pt_n^{-\bullet}NDI_2$	(e^- attachment)	(1)
$e_s^{-\bullet} + Pt_nNDI_2 \rightarrow Pt_nNDI_2^{-\bullet}$	(e^- attachment)	(2)
$Pt_n^{-\bullet}NDI_2 + RH_2^+, R^\bullet \rightarrow$ products		(3)
$e_s^{-\bullet} + RH_2^+, R^\bullet \rightarrow$ products		(4)
$Pt_n^{-\bullet}NDI_2 \rightarrow Pt_nNDI_2^{-\bullet}$	(intramolecular ET)	(5)

Figure 3-2. Scheme depicting the transport of charge to the NDI end caps via pulse radiolysis.

The reaction rate constants were determined within this scheme to account for both geminate and homogeneous recombination with the counter ions by dividing the system into a homogeneous fraction and two geminate fractions. In the geminate fractions k_3 and k_4 are faster. A kinetic model was fit to the data using non-linear least squares fitting in Igor Pro software (Wavemetrics). Where not stated, uncertainties are 15%.

Ultrafast Transient Absorption Spectrometry

Femtosecond time-resolved experiments were performed using the spectrometer available at the Ohio Laboratory for Kinetic Spectroscopy at Bowling Green State University. The laser system output consisted of pulses of 352 nm, 0.5 mW, 1 μJ/pulse,

100 fs (FWHM) operating at a repetition rate of 1 kHz. Additional details of the experimental parameters have been cited elsewhere.[158]

Results

Oligomer Structure

The Pt_nNDI_2 oligomers synthesized were designed for two different aspects of study: the investigation of dynamics of triplet exciton migration and dynamics of a charge (e-) transport. The Pt-acetylide core was chosen because the well-characterized excited state properties of these materials are dominated by highly populated, long-lived triplet states which are highly phosphorescent and are thus easily monitored by photoluminescence spectroscopy.[31,64,82]Furthermore, polymers of these materials are easily synthesized by use of copper iodide catalyzed Hagihara condensation polymerization; these materials possess a rigid rod “molecular wire” structure which has many benefits in optioelectric applications, and they have also demonstrated excellent charge carrier properties.[108,159-161] The endcaps were intended to act as electron traps. The NDI moiety suited this design, as it is known to be easily reducible.[122]

The dynamics of negative polaron diffusion in the oligomers would be investigated by pulse radiolysis techniques (Figure 3-3a) by monitoring spectral differences in the transient absorption of charges on the chain vs. the trap. Diffusion-controlled electron attachment would produce radical anions statistically within the oligomers. Electrons captured within the Pt-core of the oligomers would undergo subsequent electron transport before being trapped at the NDI endcap, while electrons captured directly near the endcap would be trapped instantly.

Dynamics of triplet exciton migration would be monitored in the endcapped oligomers via spectral differences in the transient absorption of the Pt-acetylide triplet exciton vs. the charge-separated (CS) species (Figure 3-3b). Photoexcitation of the Pt-acetylide core, followed by fast ISC would produce high yields of the localized triplet. Photoinduced electron transfer (PET) from the triplet state of the PAO core to a neighboring diimide (DI) trap would yield the CS species. Excitons residing within the Pt-core would have to diffuse toward the chain-end before being quenched, while excitons directly neighboring an endcap would be instantaneously quenched. It is envisioned that both triplet exciton and negative polaron diffusion occur via a random walk mechanism along the chain, meaning "steps" in either direction within the core are isoenergetic and equally favorable; only when directly at the chain end would the states be trapped by electron transfer to the DI endcap.

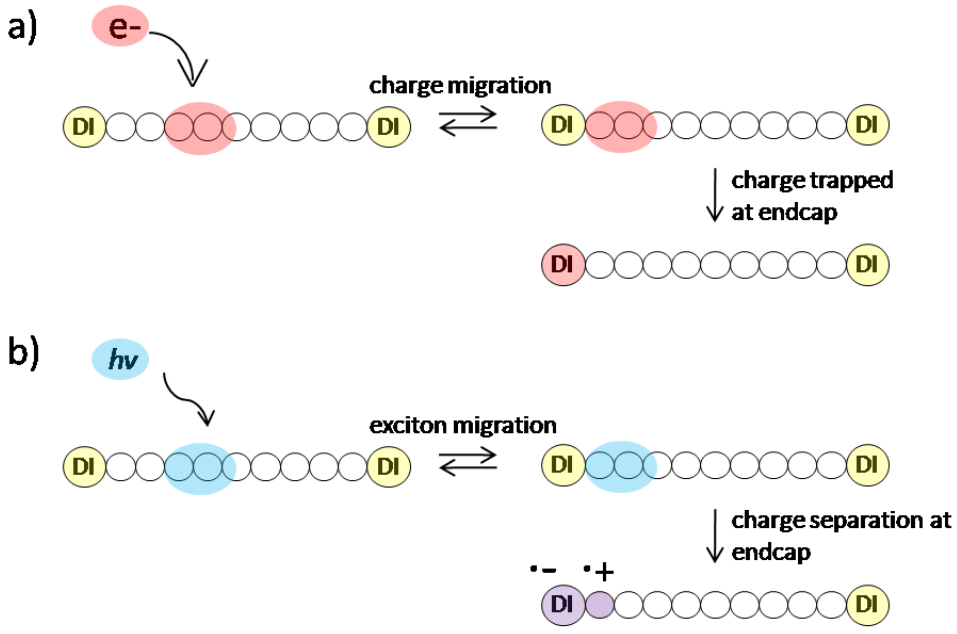

Figure 3-3. Schematic of charge (a) and exciton (b) migration in Pt_nNDI_2 oligomers.

The dynamics of either process were expected to be very fast within the PAO core. Therefore, to increase the chance of success in measuring the e- hopping or exciton migration dynamics, oligomers with relatively long chains were prepared to increase the overall lifetimes of the exciton or polaron. Known compounds NDIH[38], Pt_2 and Pt_4[88,108] were used in understanding the properties of the Pt_nNDI_2 series.

Characterization

The steady state photophysical and electrochemical characterization of these compounds were a meaningful prerequisite to pulse radiolytic and transient absorption studies. Results are summarized in Table 3-1 below. The UV-Vis absorption spectra (Figure 2-7) of the oligomers were recorded in THF; Pt_2NDI_2 displays a strong absorption band at λ_{max} = 359 nm (~3.4 eV). As the core Pt-acetylide chain was extended, the maximum absorbance shifted to λ_{max} = 361, 376 and 376 nm, respectively. The cyclic voltammagram of Pt_2NDI_2 displayed two different standard half potentials (Figure 2-6) of +0.89 V and -0.66 V, correlating well to oxidation within the core ($Pt_n^{0/\bullet+}$) and reduction of the endcap ($NDI^{0/\bullet-}$), respectively.[122] This result confirmed that the NDI trap is reduced at a potential that is ca. 0.7 V less negative than the PAO core and gave rise to the energy of the charge separated species E_{CS} ~ +1.54 V (Figure 3-4).

Table 3-1. Table of Energetics

Oligomer	$E_{Singlet}$ /eV	$E_{Triplet}$ /eV	E_{red} /V[a]	E_{ox} /V[a]	E_{CS} /V[b]
Pt-2[108,162]	3.32	2.40	-1.27	0.89	---
Pt-4[108,162]	3.19	2.39	-1.30	0.89/0.88	---
Pt_2NDI_2	3.12	2.41	-0.65	0.89	1.54
NDI-H	3.21	2.04	-0.53[122]	---	---

[a] potential reported versus SCE
[b] $E_{CS} = E_{ox} - E_{red}$

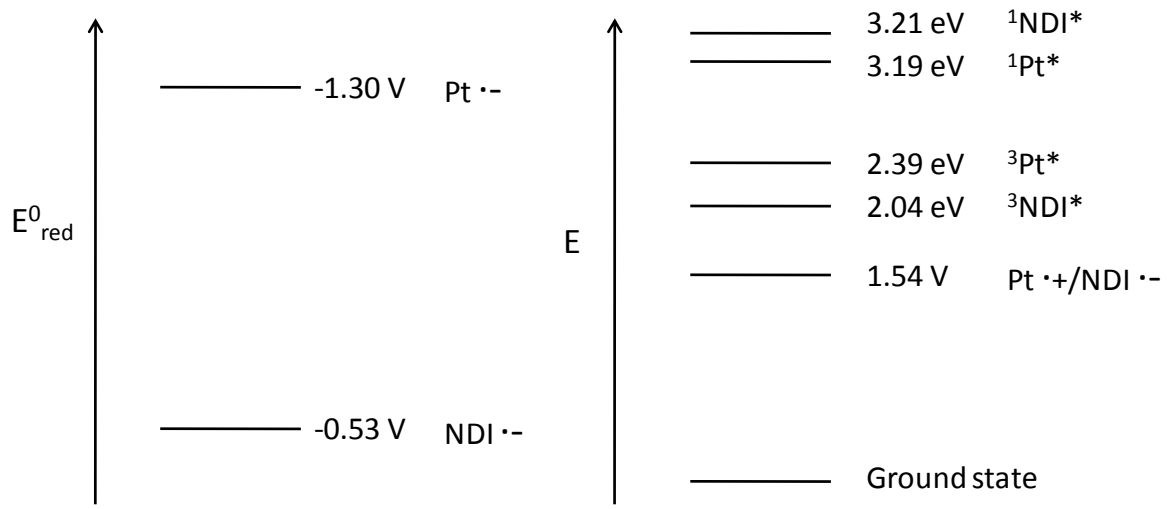

Figure 3-4. Energy level diagram of different charged and excited states of the Pt_nNDI_2 oligomers.

Pulse Radiolysis and Negative Polaron Migration

Pulse radiolysis was carried out on THF solutions of the NDI end-capped oligomers Pt_2NDI_2, Pt_6NDI_2, $Pt_{10}NDI_2$ and model compounds Pt_4 and NDI-H. As described in the experimental section (Figure 3-2), electron beam irradiation in THF rapidly produces solvated electrons (e^-_s) which serve as a promiscuous reducing agent, rapidly generating anion radical states of the oligomers. The electron attachment (reduction) reaction is pseudo-first order in the (oligomer) substrate, and therefore in order to decrease the timescale of the reduction reaction pulse radiolysis was carried out at relatively high oligomer concentration, 7.3 mM.

Figure 3-5 compares the visible region absorption spectra for the radical anions of Pt_4, NDI-H and $Pt_{10}NDI_2$ observed ~20 ns following pulse radiolysis in THF solution. The spectra also feature near infrared bands shown in an extended version of the plot (Figure 3-6). The absorption spectra of the anion radicals of Pt_2NDI_2 and Pt_6NDI_2,

shown in Figure 3-7, are similar to that for $Pt_{10}NDI_2$ and the isolated end-cap anion NDI-H.

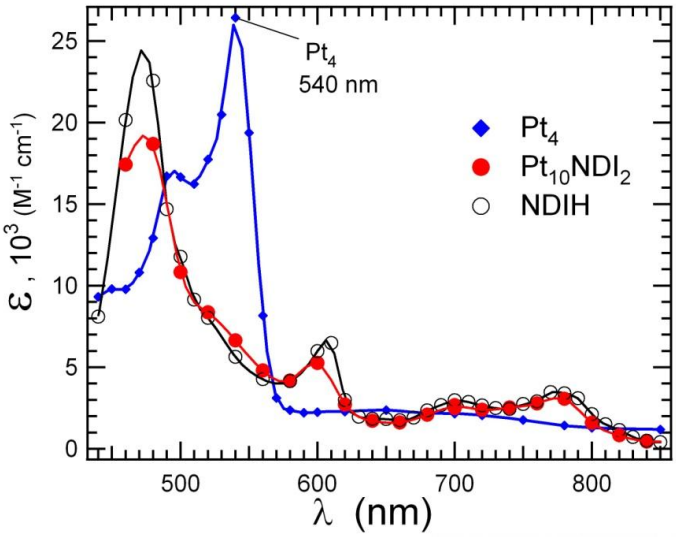

Figure 3-5. Spectra of $Pt_{10}NDI_2^{-\bullet}$ and $NDIH^{-\bullet}$ obtained from transient absorptions at 60 and 30 ns after pulse radiolysis in THF. The spectra are compared with that for $Pt_4^{-\bullet}$.

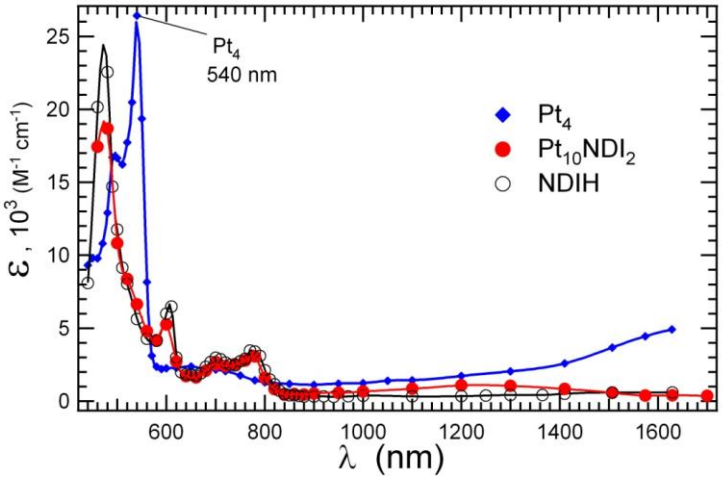

Figure 3-6. Visible and near infrared spectra of $Pt_{10}NDI_2^{-\bullet}$ and $NDIH^{-\bullet}$ obtained from transient absorptions at 60 and 30 ns after pulse radiolysis in THF. The spectra are compared with that for $Pt_4^{-\bullet}$.

With the exception of Pt_4, the spectra of all of the anion radicals are the same with λ_{max} ~ 475 nm and weaker bands at 610, 700 and 780 nm; this is consistent with the spectrum of the naphthalene diimide anion radical, $NDI^{-\bullet}$.[163] The spectrum observed for

Pt_4 features a prominent absorption with λ_{max} ~ 540 nm, and the spectrum is the same as reported in our earlier study,[108] where the band was assigned to the platinum acetylide chain localized negative polaron state, $-(PtL_2\text{-}C{\equiv}C\text{-}Ph\text{-}C{\equiv}C\text{-})_n^{-\bullet}$. The important conclusion that can be made on the basis of the transient absorption spectra is that electrons attached to Pt_2NDI_2, Pt_6NDI_2 and $Pt_{10}NDI_2$ appear rapidly (t < 20 ns) on the NDI groups. From this we can infer that even in the long oligomers Pt_6NDI_2 and $Pt_{10}NDI_2$, transport of the negative polaron to the NDI end-groups is rapid, occurring on a timescale faster than is accessible on the conventional pulse radiolysis system used for the transient absorption spectral studies (risetime ~ 2 ns, k > 5 x 10^8 s^{-1}). As outlined below, kinetic studies on $Pt_{10}NDI_2$ using the optical fiber single-shot (OFSS) system which has significantly better time resolution (risetime ~ 15 ps) provides direct insight into the polaron transport dynamics.

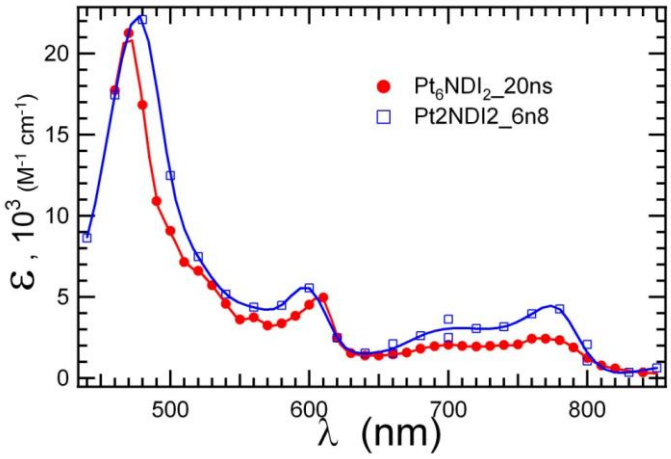

Figure 3-7. Spectra of $Pt_2NDI_2^{-\bullet}$ and $Pt_6NDI_2^{-\bullet}$ obtained from transient absorptions at 60 and 30 ns after pulse radiolysis in THF.

Prior to discussing the OFSS data, we report rate constants for electron attachment, which are needed to evaluate of rates of polaron transport, reaction 5 in Figure 3-2. Rate constants for attachment of solvated electrons in THF to oligomers

having NDI endcaps are given in Table 3-2, along with those recently reported[108] for attachment to a series of Pt_nPh_2 oligomers, n=1-5.

Table 3-2. Rate Constants for electron attachment to Platinum oligomer molecules (M) in THF at 296 K.

M	k ($M^{-1}s^{-1}$)	M	k ($M^{-1}s^{-1}$)[108]
Pt_2NDI_2	1.24 x10^{11}	Pt_1	9.8 x 10^{10}
Pt_6NDI_2	1.70 x10^{11}	Pt_2	1.7 x 10^{11}
$Pt_{10}NDI_2$	3.60 x10^{11}	Pt_3	2.1 x 10^{11}
NDIH	4.78 x10^{10}	Pt_4	2.5 x 10^{11}
		Pt_5	3.2 x 10^{11}

Using the OFSS pulse radiolysis system, we reexamined the fast-timescale dynamics of the $Pt_{10}NDI_2$ oligomer anion states to seek insight regarding the dynamics of polaron transport from the platinum acetylide chain to the NDI end-groups. As can be seen in Figure 3-5, the absorption spectrum of the chain localized polaron exhibits a maximum at 540 nm, whereas the NDI localized anion radical absorbs at shorter wavelength (475 nm). Thus, by monitoring the transient absorption at 540 nm it is possible to monitor the dynamics of the chain localized polaron state, with little interference from the NDI anion radical state (the ratio of the chain polaron:NDI end-group absorptivity at 540 nm is ~ 4:1). Figure 3-8 compares the transient absorption dynamics at 540 nm for Pt_4 (c = 19 mM) and $Pt_{10}NDI_2$ (c = 7.3 mM) in THF solution obtained using the OFSS system. The Pt_4 anions are seen to form in a prompt component (τ < 20 ps) followed by an additional 160 ps growth component which is due to attachment of solvated electrons. The prompt component is due to capture of electrons before they are solvated,[164] that is prior to step (ii) in Figure 3-2. The efficiency of this prompt capture of unsolvated or “dry electrons” was recently found to be proportional to the length of polymer or oligomers, making Pt_4 a good reference for

$Pt_{10}NDI_2$ when used at a concentration almost three times larger, although the slower component due to capture of solvated electrons is faster (160 ps) in the 19 mM Pt_4 solution than in the 7.3 mM $Pt_{10}NDI_2$ solution (300 ps).

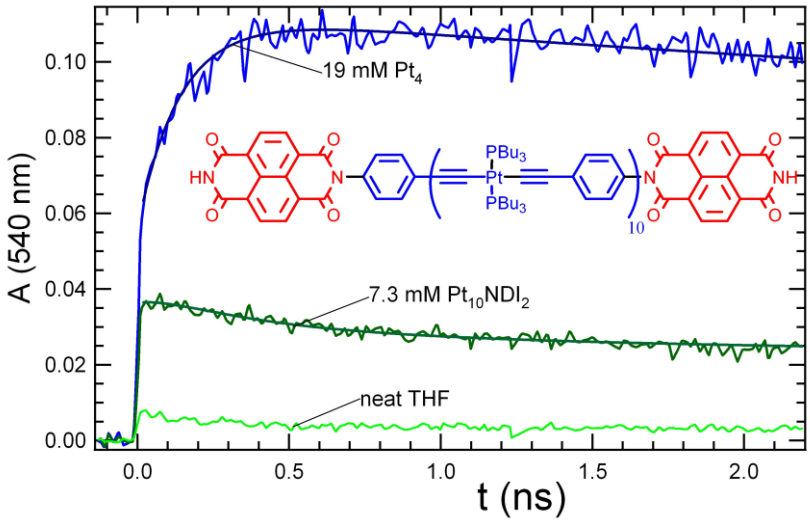

Figure 3-8. Transient absorption at 540 nm of 7.3 mM $Pt_{10}NDI_2$ in THF compared with that for Pt_4 and with neat THF solvent. The single-shot instrument enabled 15 ps time resolution. Fits with the kinetic model in Figure 3-2 are shown passing through the data. For $Pt_{10}NDI_2$ the fits indicate that electrons in the Pt chains transport to and are captured by the NDI end caps with two rates with $1/k_f$= 540 ps (0.53) and 140 ps (0.09). Also shown is the fit curve with both components of k_f set to infinity.

Interestingly, the transient absorption profile at 540 nm for $Pt_{10}NDI_2$ is distinctly different compared to that of the Pt_4 reference. In particular, the absorption exhibits only a prompt rise component and then a small amplitude decay occurs over a 500 ps timescale. The final transient absorption amplitude is ~ 4 times less than that of Pt4, consistent with the weaker absorption of the $NDI^{\bullet-}$ state at 540 nm. It is important to note that the transient absorption dynamics of the $Pt_{10}NDI_2$ anion at 540 nm do not feature a slow rise as observed for Pt_4. Qualitatively this difference in the observed dynamics arises because of a superposition of a decay (due to disappearance of the chain localized anion state) on the rise due to the attachment of solvated electrons.

In order to extract more quantitative information from the $Pt_{10}NDI_2$ anion dynamics, the data in Figure 3-8 was fitted using the reactions in Figure 3-2. (Before fitting, a small contribution from Pt_n triplet excited states was subtracted. This correction utilized a measured triplet contribution triplet absorption at 650 nm and the ratio extinction coefficients for the triplet determined in the photoexcitation experiments.) The fitting strategy, discussed previously,[165] begins with a description of electron production and decay in neat THF solvent. The solvent parameters are then held fixed during fitting the attachment dynamics to Pt_4, and decay of $Pt_4^{-\bullet}$, before fitting $Pt_{10}NDI_2$. In Figure 3-8, absorbance due to $Pt_4^{-\bullet}$ is seen to grow with a time constant of 0.13 ns. This is faster by a factor of 1.6 than expected from the rate constant in Table 3-2 due to transient terms found for diffusion-controlled reactions of long molecules.[164,166] Measurement of fast transport is facilitated by fast production of a fraction of the anions in a "step" process that is complete our 15 ps time resolution. The step process is due to capture of electrons prior to solvation, which occurs with probability 1-exp(-qc), where c is the concentration of the Pt_4 or $Pt_{10}NDI_2$ molecules. As expected, capture of pre-solvation electrons is found to be more effective for $Pt_{10}NDI_2$, ($q=72\ M^{-1}$) than for the shorter Pt_4, ($q= 29.9\ M^{-1}$). Fitting the OFSS data for $Pt_{10}NDI_2$ with the kinetic model in Figure 3-2 find that electron transport from the platinum acetylide chain to the NDI end groups occurs with biexponential kinetics: 540 ps (0.53) and 140 ps (0.09), where the fractions (parenthesized) refer to the total number electrons attached to $Pt_{10}NDI_2$. The fit curve giving these rates is seen passing through the data in Figure 3-8. The results indicate that a substantial fraction, 0.38, of electrons attached to $Pt_{10}NDI_2$ are captured immediately (<< 10 ps) by the NDI trap groups. The NDI trap groups are similar in size

to one repeat unit of the Pt chain, so $Pt_{10}NDI_2$ can be considered to comprise twelve units. If each of these twelve units captures electrons with equal probability, then the observed 38% immediate capture corresponds to electrons attached centering on the NDI groups and the first 1.3 Pt units adjacent to NDI: if a $Pt^{-\bullet}$ polaron is centered on or within 1.3 repeat units of and NDI, it transfers immediately to the NDI. Those polarons formed in the central 7.4 units of the chain are observed as $Pt^{-\bullet}$ that must diffuse along the chain to react with the NDI trap.

It would be desirable to monitor the 475 nm absorption due to $NDI^{-\bullet}$ in order to observe fast appearance of electrons at the NDI end groups. However, measurement at 475 nm is difficult because the intense absorption of ground state neutral $Pt_{10}NDI_2$ molecules at the high concentration needed to capture electrons reduces the analyzing light intensity by a factor of ~100. In addition the OFSS instrument is not yet able to operate effectively at 475 nm. A measurement at 480 nm with a biplanar phototube detector (150 ps nominal resolution) is shown in Figure 3-9. While the data are very noisy because of the low transmittance of the solution and consequently weak probe light intensity, it does indicate that the $NDI^{-\bullet}$ absorption rises within 500 ps to the level expected based on the $Pt_{10}NDI_2^{-\bullet}$ absorption spectrum in Figure 3-5. While the S/N of this data does not allow quantitative determination of the growth rate of the $NDI^{-\bullet}$ absorption, the data is fully consistent with the observations at 540 nm, supporting the conclusion that almost all electrons attached to $Pt_{10}NDI_2$ appear within 700 ps on the NDI end groups.

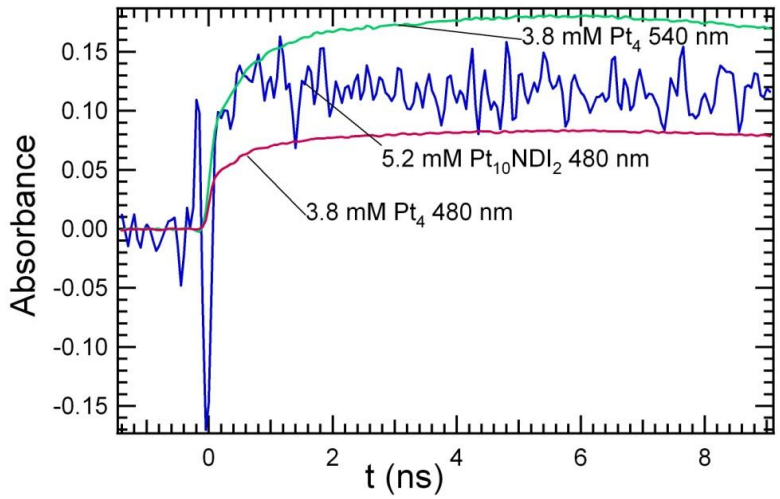

Figure 3-9. Transient absorption at 480 nm showing the formation of $NDI_2^{-\bullet}$ in a 5.2 mM solution of $Pt_{10}NDI_2$ in THF. The data are very noisy due to intense absorption by the $Pt_{10}NDI_2$ molecules, which reduces the probe light intensity by a factor of ~100 at this high concentration. In addition to noise the data are affected during the first ~300 ps by emission. The noisy measurements on $Pt_{10}NDI_2$ are compared with observations on Pt_4 at 480 nm, and at the 540 nm spectral maximum of $Pt_4^{-\bullet}$. The absorption at 480 nm in the $Pt_{10}NDI_2$ solution, relative to those in the Pt_4 solution, is consistent with nearly complete transfer of electrons to the NDI end groups by ~500 ps.

Photophysics and Exciton Transport

The second investigation for these oligomers was to examine the dynamics of triplet exciton transport along the Pt-acetylide chain (Figure 3-3b). Because absorption spectra of the PAOs are dominated by π,π^* transitions from the Pt-acetylide backbone, photoexcitation mainly affords excitons which are localized on the conjugated chain. Due to incorporation of the heavy metal in the backbone, intersystem crossing is rapid (~10^{12} s^{-1}) and relatively high yields of the triplet exciton are generated; fluorescence yields are relatively low due to the slower rate of radiative decay (~10^9 s^{-1}). Therefore, within very short times of excitation the triplet state is almost quantitatively poplulated. It has been shown that the triplet exciton in these systems is spatially confined, with a chromophore structure consisting of the single -[-$Pt(PR_3)_2$-C≡C-Ar-C≡C-$Pt(PR_3)_2$-]- unit,

and the exciton was demonstrated to be transient species that diffuses along the PAO backbone.[103]

It is envisioned that exciton diffusion is a random walk along the chain until it encounters the NDI trap, triggering a PET reaction. Charge recombination of the $Pt_nNDI_2^{\bullet+/\bullet-}$ ion pair is a non-radiative decay process; therefore, for every PET process that occurs, some amount of phosphorescence decay from the triplet exciton is quenched. Should exciton migration and subsequent charge transfer processes occur more quickly than radiative decay processes, it was expected that the triplet emission quantum yields should be quenched by some amount, depending on the rate differences of either kinetic process.

Steady state emission.

The steady state emission spectra of the Pt_nNDI_2 oligomers were previously measured in deoxygenated THF solutions at room temperature with an excitation wavelength corresponding to the maximum absorbance energy for all oligomers (Figure 2-7). A summary of this data, discussed in Chapter 2, is given in Table 3-1. The phosphorescence of a Pt-acetylide moiety has a characteristic triplet emission at ca. 520 nm (ca. 3.4 eV). The photoluminescence quantum yields at room temperature for the Pt_nNDI_2 series indicated strong emission quenching compared to the Pt_2 model oligomer.

Based on these findings, steady state emission spectra were also recorded in deoxygenated 2-MeTHF (T_g = 137 K) at lower temperatures. The Pt_nNDI_2 spectra, along with NDI-H, are shown in Figure 3-10. As the temperature was decreased, the triplet-based emission intensity was slowly recovered (ca. 520 nm) for the n = 6 and n = 10 oligomers once the solvent had reached glass transition temperatures (T<140 K).

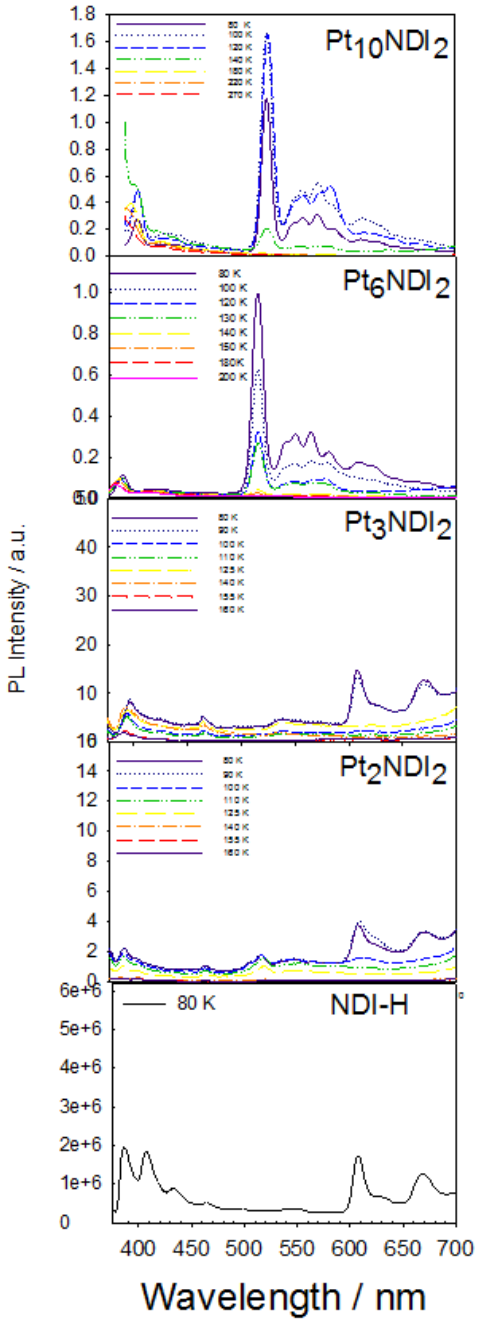

Figure 3-10. Variable temperature steady state emission spectra of the Pt_nNDI_2 oligomers vs. the low temperature emission of the NDI-H endcap (bottom) in degassed THF.

However, for the n = 2 and n = 3 oligomers relatively no gain in phosphorescence yield is seen, even at 80 K. The weak emission seen in **Pt_2NDI_2** and **Pt_3NDI_2** at cryogenic

temperatures correlates with the fluorescence (ca. 400 nm) and phosphorescence (ca. 610 and 670 nm) of the NDI endcaps. Although this emission also exists in the longer oligomers, it is elusive due to its relatively low intensity vs. the phosphorescence seen in these spectra.

Recall that the triplet exciton was defined as being localized across two Pt-atoms in Pt-acetylides oligomers, and the singlet exciton was defined as being somewhat more delocalized through several repeat units.[88] This suggests that for all of the Pt_nNDI_2 oligomers, the singlet exciton generated is always in direct contact, spatially, with the trap, while the more confined triplet exciton is only always directly neighboring a trap in the shorter oligomers **Pt_2NDI_2** and **Pt_3NDI_2** (Figure 3-11). Therefore, no diffusion of the confined triplet exciton or delocalized singlet exciton would be necessary for PET to occur in the shorter molecules.

The absence of phosphorescence in the shorter oligomers, even at 80 K, suggests two things: the activation barrier for the PET reaction is extremely low, due to the large $-\Delta G^o$, and the process perhaps requires little change in structural geometry of the molecule (as the oligomers are frozen and relatively immobile in a glass at low temperature). Insight into whether PET is occurring directly after excitation from the singlet excited state, or if it is occurring after ISC to the triplet state, is evasive in these systems, however, because the excitons of both spin states would directly neighbor the trap in these shorter chains. The recovery of phosphorescence emission below the glass transition temperature for the n=6 and n=10 oligomers does prove that indeed the triplet exciton is formed, but diffusion to the trap is slowed by a thermal barrier. The results of this data imply that electron transfer is *not* the rate determining step for

exciton quenching in the longer oligomers, but rather the triplet migration is the slow, rate determining step.

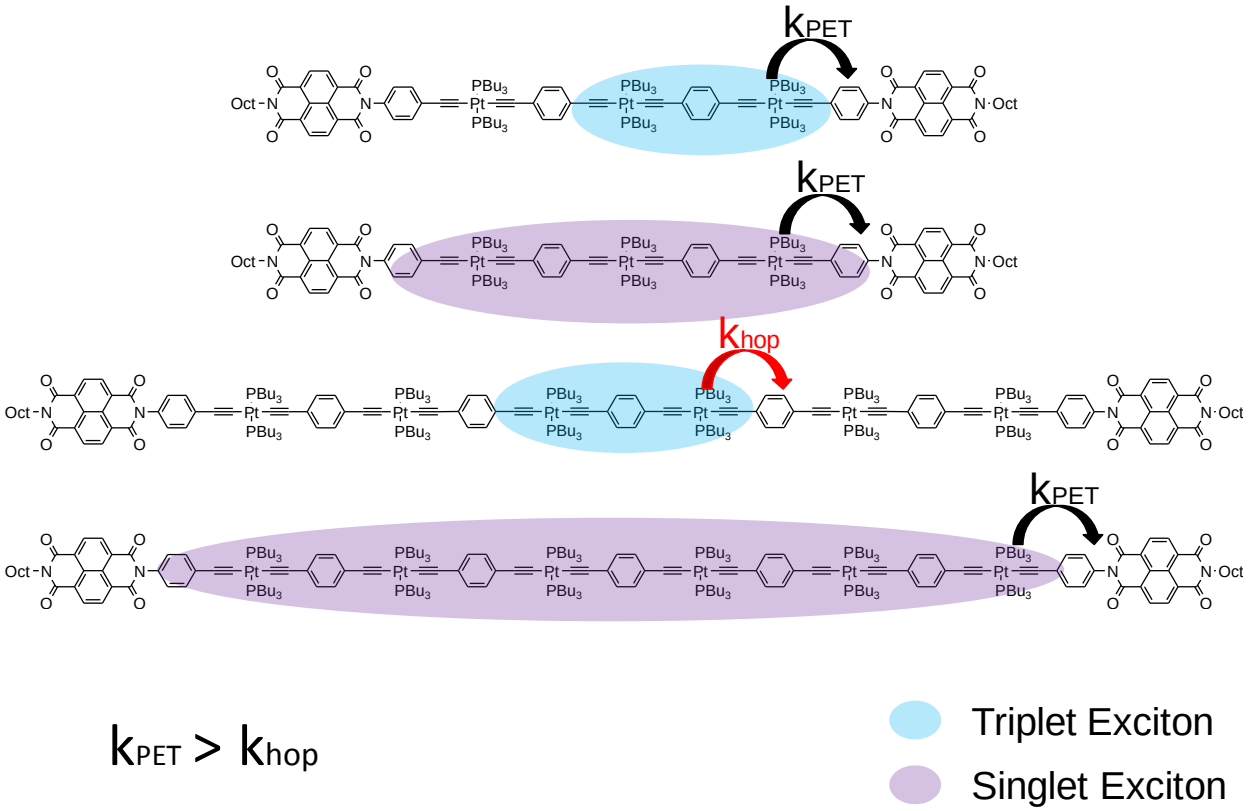

Figure 3-11. Confinement of the triplet and singlet exciton in relation to distance to the NDI trap for **Pt_3NDI_2** and **Pt_6NDI_2**.

Previous low temperature studies of Pt-acetylide oligomers found that in glass solvents, Pt_n oligomers exhibited luminescence similar to the longer Pt_nNDI_2 oligomers arising from several states due to differences in conformers that do not interconvert during the lifetime of the triplet state in frozen glass.[104] The different conformation states were said to arise as a result of rotation of the phenylene rings relative to the planes defined by the square planar PtP_2C_2 units (Figure 3-12). DFT calculations agreed with experimental observations, citing that the energy minimal ground state conformation for a Pt_n chain—in which all phenylene units are twisted out of the plane

(ttt)—lies ca. 3.1 kcal·mol^{-1} higher in energy than the minimum energy conformer of the localized triplet state—in which one phenylene unit is parallel to the PtP_2C_2 plane (tpt). Triplet exciton diffusion, or hopping, was found to be accompanied by a small activation energy arising from a reorganizational energy caused by the geometric difference between the two states/conformers—a phenomenon known as conformational gating.

The loss of phosphorescence emission in the n = 6 and 10 oligomers above 140 K (T_g = 137 K) is consistent with these previous findings in that at ambient temperatures, triplet exciton hopping via configurational reorganization is thermally accessible. However, at cryogenic temperatures (T<140 K in glass solvent) it is slowed such that hopping is competitive with the lifetime of the exciton (μs)[167] affording emission prior to diffusion/quenching of the triplet. The slowing of the triplet hopping via conformational gating is consistent with the notion that the migration does indeed have a small/medium activation barrier (~3-5 kcal·mol^{-1}), thus triplet migration is the rate-determining step of the quenching process.

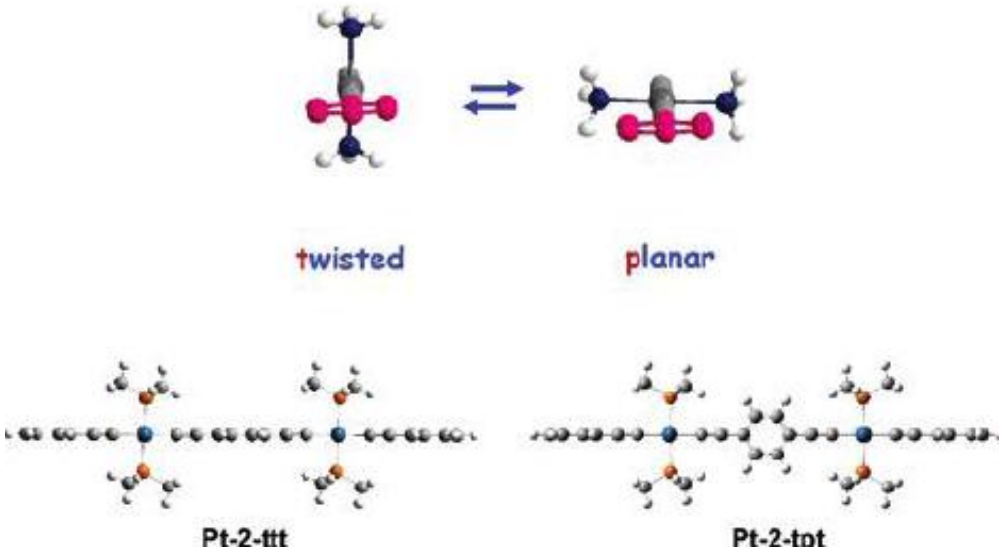

Figure 3-12. Conformational differences between energy minima of the ground state (left) and triplet state (right) of Pt_2. Figure adapted from Glusac *et al.*[104]

Femtosecond transient absorption.

By use of ultrafast transient absorption spectroscopy (λ_{ex} = 352 nm), both the rise times of the $NDI^{-\bullet}$ and the decay times of the ($^3\pi,\pi$)-PAO core were determined. The spectra for the Pt_nNDI_2 series are presented in Figure 3-13.

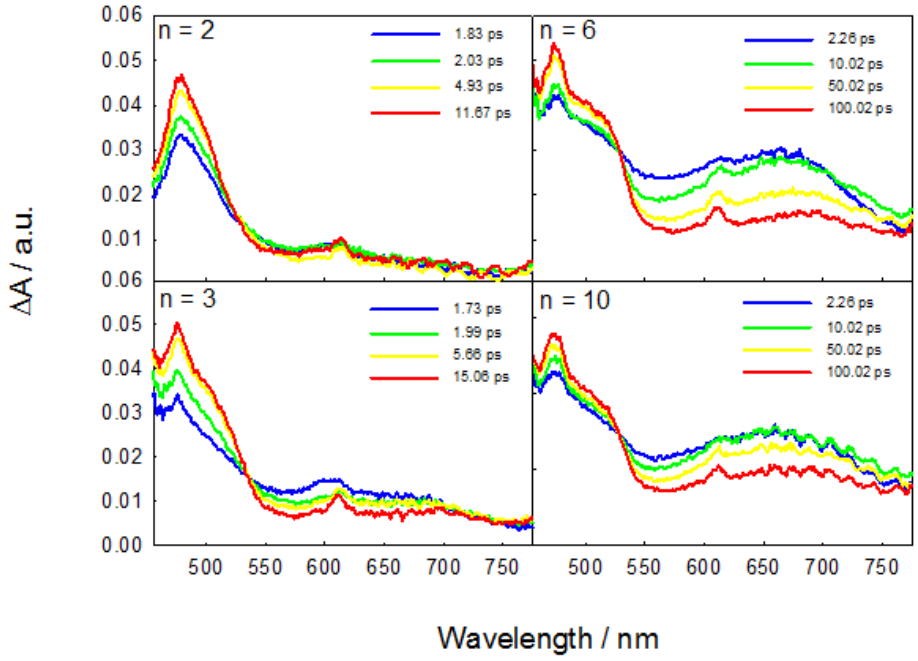

Figure 3-13. Spectra of radical anion at various time intervals for n = 2 (top left), 3 (bottom left), 6 (top right) and 10 (bottom right).

Comparison of the spectra in the 550-750 nm region within the series show both a broadening with a systematic red-shifting as 'n' becomes larger (Figure 3-13). This can be attributed to further delocalization, or increased length, of the triplet exciton as the PAO core is expanded, which shifts the absorbance to lower energies and also enhances band broadening. Again, the spectral absorbance at λ_{max}~ 480 nm is consistent with the absorbance spectra of the $NDI^{-\bullet}$ previously reported by Wasielewski et al.[163]

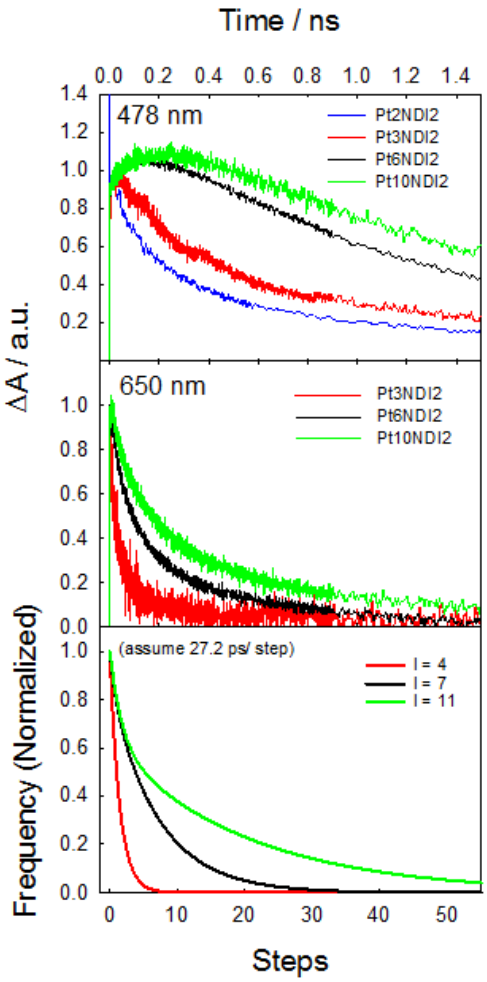

Figure 3-14. Plot of the normalized TA kinetic traces of the Pt_nNDI_2 series at 650 nm (top), 478 nm (middle) and simulated decay of the triplet exciton (bottom) assuming 27.2 ps/step.

The kinetic traces for the Pt_nNDI_2 series at 478 nm and 650 nm are plotted in Figure 3-14. As seen the middle plot, the decay kinetics of the ($^3\pi,\pi$) PAO core at ca. 650 nm contain both a fast and slow component, which could be explained by both initial location of the created triplet exciton with respect to proximity to the end cap, and also by the proposed random-walk hopping mechanism described in which some excitons are quenched statistically more quickly than others. The overall decay rates for the series do differ, however. The lifetime of the triplet exciton for Pt_2NDI_2,

measured at 650 nm, is extremely short, τ_T ~ 0.43 ps (Table 3-3). For $Pt_{10}NDI_2$, however, the overall decay of the triplet at 650 nm is somewhat slower, τ_T ~ 373 ps. The kinetics intrinsically include both PET and statistical exciton diffusion processes, lending to the longer lifetime of the triplet.

Figure 3-14(top) presents the normalized kinetic traces of each end-capped oligomer at ca. 480 nm. The initial rise of the signal is fast for all oligomers (~2 ps < ΔA_{max} < 200 ps), but does show a trend of slowing down in overall growth as chain length increases.

Table 3-3. Kinetics of triplet exciton decay at 650 nm for the Pt_nNDI_2 series.

n	$\tau_{av,\ 650\ nm}$ (ps)	$k_{av,\ 650\ nm}$ (s^{-1})
2	0.43	2.32×10^{12}
3	8.3	1.20×10^{11}
6	203	4.93×10^{9}
10	373	2.68×10^{9}

Random walk numerical simulation.

To simulate the random walk process numerically, a program was written with Visual Basic in SigmaPlot. Briefly, the oligomer chain length (defined as 'm', not including the trap sites on both ends) and the desired number of program repetitions (n) are input as simulation parameters. A random integer is generated representing where the exciton is initially created, IniPos, within the oligomer chain ($1 \leq IniPos \leq m$). If the IniPos is in the middle of the chain ($1 < IniPos < m$), another random number between 0-1 is generated. If this number is in the range between 0.5 and 1, the IniPos is moved to the right (IniPos + 1). Otherwise, it is moved to the left (IniPos - 1). In either case, the counter for random walk steps is increased by 1 (Steps + 1). When the IniPos

reaches the chain end (IniPos = 1 or IniPos = m), the random walk stops and the counter for steps (Steps) is recorded. The same procedure is repeated for the desired number of repetition times (n), and the obtained numbers of random walk steps (Steps) are subjected to histogram analysis (Bin Width = 5). A visual representation of how the program is written and run is presented in Figure 3-15 below.

As an example, shown in Figure 3-14 is the comparison of the experimental (middle) and the simulated (bottom) results. In this particular case, the chain length for the oligomer Pt_nNDI_2 is considered to be n + 1. Thus, for the corresponding oligomers n = 3, 6 or 10, 'm' = 4, 7 or 11, respectively. For m = 4, the histogram can be sufficiently fit with a single exponential function. However, for m = 11, a double exponential function has to be used. For m = 7, either single or double exponential function gives a reasonably good fit. The only variable used to fit experimentally obtained data with simulated data is the time per step. As shown in the figure, the simulation reproduces the experimental data relatively well when each step for the random walk simulation was fitted to be about 27.2 ps.

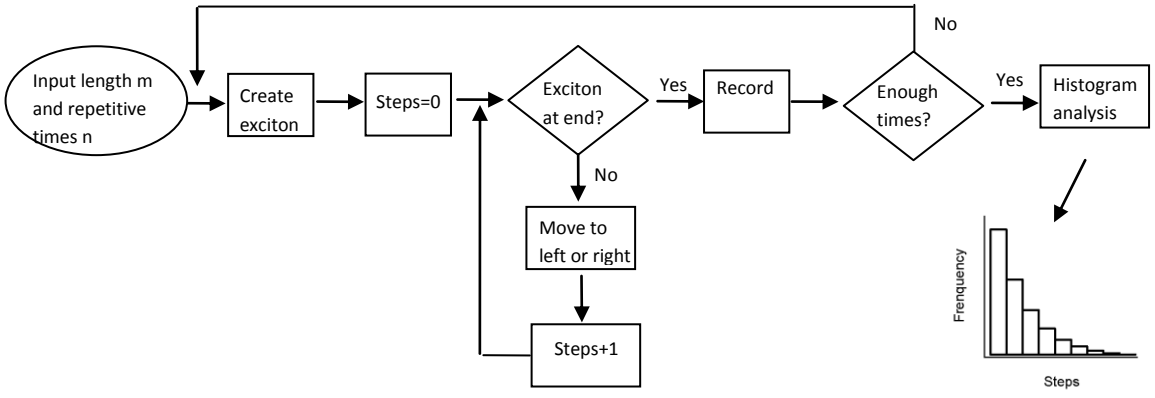

Figure 3-15. Schematic of the random walk simulation program.

Discussion

States are Concentrated

As discussed previously, optical data obtained from previous studies of the Pt_n series reveal that the polarons in PAOs are spatially confined.[108] More specifically, absorption spectra of the negative polarons generated via pulse radiolysis ionization techniques for the Pt_n series conclude virtually no change in spectra from the Pt_2 to Pt_7 oligomers; spectra of the $Pt_n^{-\bullet}$ generated display a characteristic maximum absorption at 540 nm. Similarly, the triplet exciton of the Pt_n series was found to be spatially concentrated between two platinum atoms; this conclusion was based on similar $^3\pi,\pi^*$ phosphorescence emission energies (ca. 520 nm) throughout the series, as well as very similar triplet-triplet absorption energies (ca. 650 nm) regardless of oligomer length.[88]

The spatial confinement of these states exists due to lattice polarization, or structural deformities, within the backbone that disrupt conjugation along the chains. Density functional calculations of both the triplet exciton and negative polaron of Pt_2 revealed differences in minimal energy geometries between the ground state species and the exciton or polaron states that contribute to the localization of these states.[104,108] Specifically, the lowest energy geometry of the ground state exists with all phenyl groups of Pt_2 in the plane perpendicular to the square planar platinum atoms (as discussed previously); the minimum energy geometry of the negative polaron was calculated with all phenyl moieties parallel to this plane. The calculated barrier to rotation of the phenyl ring in the radical anion species was estimated to be ~ 15 kcal/mol. The calculated geometry energy minimum for the triplet exciton exists with only the center phenylene unit in plane; barrier to rotation was estimated to be ~ 3.1

kcal/mol. Compare this to the ground state barrier to phenylene rotation, calculated as ~0.5-0.8 kcal/mol.[104] Results of these studies allude to the dependence on structural conformations to the energetics of exciton or polaron confinement.

Mechanism of Transport

Charges and triplet excitons created in the Pt_n chains have been found to be localized to approximately two repeat units. These polarons are trapped in a part of the chain only by structural relaxation (reorganization). A polaron may move, in random directions, to adjacent locations on the chain, generating a diffusion ending at the trap. Figure 3-16 depicts this mechanism. Alternatively, it may leap directly to the trap.

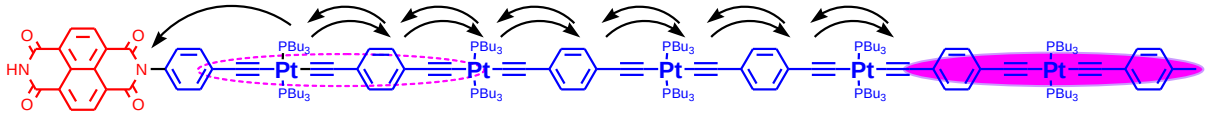

Figure 3-16. Polaron or exciton diffusion via a random hopping mechanism. Half (5 units) of a $Pt_{10}NDI_2$ molecule is shown. A polaron, either an exciton or electron, spread over ~2 repeat units near the middle of the chain is depicted as a solid magenta elipse at the right. Diffusion of the polaron to a location near the NDI trap group (dashed elipse) is followed by rapid transfer to the NDI trap.

The transitions that constitute diffusive steps along the chain or transfer from the chain to the trap require electronic couplings and nuclear overlap. Electronic couplings can arise from dipole (Förster resonance energy transfer, FRET) and exchange interactions. FRET does not apply to transfer of electrons, and dipole couplings are negligibly small for triplet excitons. FRET can occur only during the brief, ~1 ps, lifetime of the excitons as singlet excited states. For experiments on electrons and triplets in the chains, only one and two-electron exchange interactions are important. These fall exponentially with distance, giving rates that decrease by a factor of ten for each 1-3 Å change in distance.[168-177] For this reason, we will argue below that the dominant

mechanism is diffusive polaron transport to the ends of the chains. As depicted in Figure 3-16, the final step is transfer to the trap when the electron or exciton has reached a point sufficiently close, probably just a few Å from the trap. This "chain-end-polaron" might actually contact the end of the conjugated chain, or might be slightly farther from the trap as depicted.

Designating the rate of diffusional transport to the chain end as k_1, diffusion away from the end as k_{-1} and transfer from the chain end to the trap as k_2, we have the equation in Figure 3-17 below. The symbols designate a charge or exciton as a polaron in the chain (P_c), at the chain end (P_e) or on the trap (T). Kinetics for this scheme are well-known; the scheme is similar to the Michaelis-Menten mechanism for enzyme kinetics. We will analyze our observations assuming the limit, in which k_2 is fast. In that case, $k_2 >> k_1$, the observed rate approaches k_1. This assumption will be examined and other possibilities will be considered below. The diffusional transport, k_1, is not a single rate. We will describe it using numerical solutions for a random walk process described above. In that treatment, k_{-1} is not separate but is inherent in the random walk.

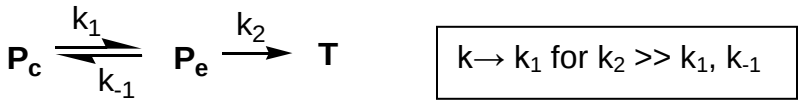

Figure 3-17. Calculating the rate of diffusional transport to the chain end.

For electron injection and transport in $Pt_{10}NDI_2$ (Figure 3-8), fits to the experimental data found that the capture of electrons in the Pt_{10} chains by the NDI end caps was described by biexponential decay. The random walk model with τ_{step}=27 ps is in excellent agreement with the biexponential decay, as seen in Figure 3-18 below.

Decay of triplet excitons could be observed in four lengths of Pt_nNDI_2. Random walk simulations describe those decays also with τ_{step}=27.2 ps. The simulations are in

fair agreement with the observations, with some differences. Notable is the slower decay in simulated traces compared to experimental ones in Figure 3-14. This difference could signal that relaxation of the polarons in the Pt_n chains is still occurring over the first ~100 ps, stabilizing the polaron and deepening the "self-trapping" which move with it. Transport would be slower after such a relaxation than before it. Structural reorganizations tend to be larger for triplets than for singlets or ions.

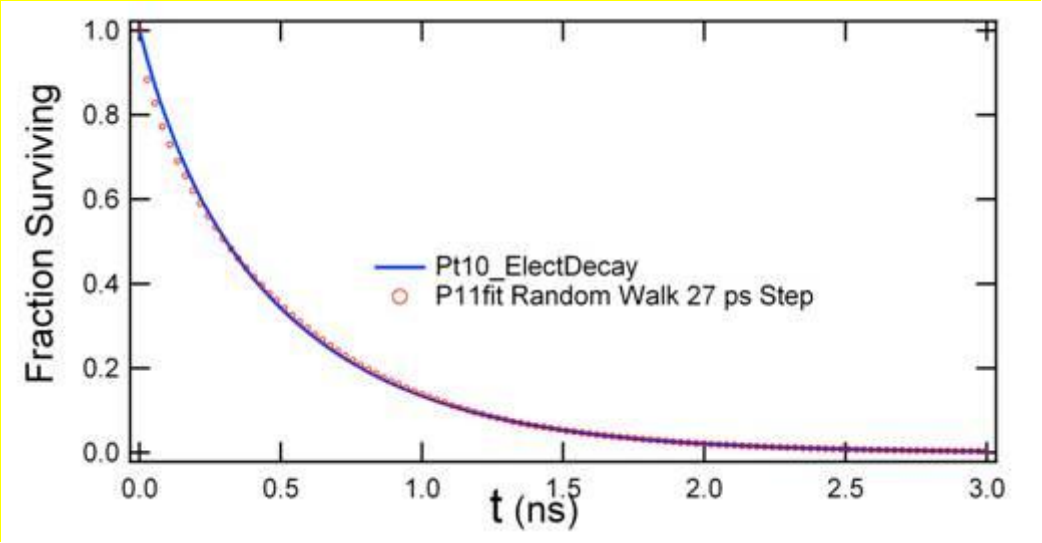

Figure 3-18. The bi-exponential function found to describe decay of electrons injected into the Pt chains of $Pt_{10}NDI_2$ molecules compared with random walk simulations having steps of 27 ps in which each step moves one repeat unit left or right along the Pt_{10} chain.

The discussion above assumed that observed rates of disappearance of Pt chain anions or triplets, and the appearance of NDI anions, measures the rate of transport because transport is rate limiting; k_2 is fast ($>>k_1$). If k_2 were slower than k_1, the overall rate would approximately equal k_2, independent of length of the Pt_n chain. For the triplets where rates were obtained for n = 3, 6 and 10, this is contrary to observation. In the absence of a direct measurement of k_2 it is useful to make a rough estimate by analogy to known rates. When electrons are injected into the chain k_2 is the rate of

electron transfer from an anion at the end of the chain, through two saturated bonds to the NDI group. From redox potentials in Table 3-1, the free energy change of this reaction is ΔG° = -0.65 eV. Closs[168] reported rates of intermolecular electron transfer from biphenyl anions to naphthalene, ΔG° = -0.05 eV, separated by 4-10 saturated bonds. Extrapolated of their fastest rate, 4 x 10^9 s^{-1}, from 4 to 2 saturated bonds, yields a value of 3 x 10^{10} s^{-1}. For ΔG° = -0.65 eV for ET from the Pt chain to NDI, the rate would be expected to further by a factor of 100 to 3 x 10^{12} s^{-1} (0.3 ps). This is 2000 times faster than the observed k_1, and 100 times faster than the time to diffuse the length of one repeat unit, τ_{step}=27 ps. While the extrapolated comparison is likely to contain substantial uncertainty, it seems very likely that $k_2 >> k_1$.

For triplets, k_2 comprises two possible reactions, shown in Figure 3-19. The electron transfer process would be expected to occur with a rate having an order of magnitude similar to that estimated for anions (~0.3 ps), so again that $k_2 >> k_1$. The triplet transfer rate estimated from intramolecular triplet transfer, is slower.[168] Thus, the triplet transfer route is expected to be a minor one. To the extent it occurs, it would be followed by rapid relaxation to the lower $Pt_n^{+\bullet}NDI^{-\bullet}$ charge transfer state, so this ion-pair is expected to be the product. For triplets it is also very likely that $k_2 >> k_1$, so the overall rate closely reflects the rate of transport along the chains.

Triplet transfer	^3Pt_n*NDI $\rightarrow$ $Pt_n{}^3$NDI*	ΔG° = -0.35 eV
Electron transfer	^3Pt_n*NDI $\rightarrow$ $^3(Pt_n^{+\bullet}NDI^{-\bullet})$	ΔG° = -0.85 eV

Figure 3-19. Two possible reactions of the triplet excitons for Pt_nNDI_2 oligomers.

Conclusion

Variable temperature steady-state emission studies, pulse radiolysis experiments and ultrafast transient absorption measurements were applied to examine the transport mechanism and dynamics of negative polaron and triplet exciton states in the Pt_nNDI_2 series. Pulse radiolysis experiments were applied to measure the rate of negative polaron diffusion within the series. While OFSS data obtained for growth kinetics in the 480 nm region was not quantitative (due to concentration issues as well as experimental limitations with OFSS), the biexponential decay data at 540 nm fit well with random-walk simulation data suggesting the time per 'step' of the negative polaron in the Pt-acetylide chain is about 27 ps. This data infers a fast ET from a chain-end polaron to the endcap and a slower, rate-determining diffusion of the negative polaron within the chain.

Emission spectra for the series at low temperatures (below the glass transition for Me-THF) revealed recovery of the phosphorescence in the n = 6 and 10 oligomers and not the n=2 or 3 oligomers. This data demonstrated the effective population of the triplet via ISC, and results implied the necessity of structural reorganization within the backbone of the oligomer for triplet exciton diffusion to occur. This was not necessary for PET processes to occur, as quenching of the triplet was evident for the short-chained oligomers even in the glass state of the solvent. This data provided evidence that PET is fast compared to the triplet exciton diffusion, which is rate-determining in the quenching process.

Ultrafast transient absorption measurements also confirmed population of the triplet exciton via absorption at *ca*. 650 nm. The decay of this state was found to be biexponential: the fast component is suggested to be PET from a triplet exciton at the chain end directly connected to the NDI trap, whereas the slow component consists of

random exciton diffusion toward the chain end. When compared to simulated random-walk decay data, a lifetime of ~27.2 ps/step for the triplet exciton was extrapolated. This is the first known report of intramolecular negative polaron or exciton hopping rates in platinum acetylide materials.

CHAPTER 4
SYNTHESIS AND PHOTOPHYSICS OF PLATINUM CAPPED PHENYLENE ETHYNYLENE OLIGOMERS

Introduction

There has been a wide range of platinum acetylide structures reported in the literature, including oligomers, polymers, and dendrimers, used for many different optical and electronic applications owing to the unique photophysical properties of these materials. In general, the key aspect toward the advancement of materials applications is to define distinct relationships between chemical structure and spectroscopic properties. The nature of the structure-property relationship is also fundamentally important in understanding the interaction of light with matter and the information that can be elicited from experiments. One such issue is the relationship between structure and the delocalization of the singlet and triplet excitons.

As discussed previously, our group has recently focused on studying delocalization of the singlet and triplet states of platinum acetylide oligomers.[88] It was found that ground state absorbance and fluorescence properties are dependent on the length of the material, as these states are defined as being delocalized through the metal-organic framework. The triplet state, however, was concluded to be confined, and the properties of this state change very little in relation to changes in the length of the Pt-acetylide.

Most of the studies investigating extended pi conjugation in the organic ligands of platinum acetylide oligomers focus on a single platinum atom and various ligands, or oligomers and polymers with identical repeat units; the understanding of delocalization in excited states is therefore limited. One example of such is a set of studies reported by Cooper and Rogers, *et al*.[77,87,178-182] Symmetrically substituted, mono-substituted

and asymmetrically substituted platinum acetylides were investigated and compared to the analogous organic butadienes, as shown in Figure 4-1 below.

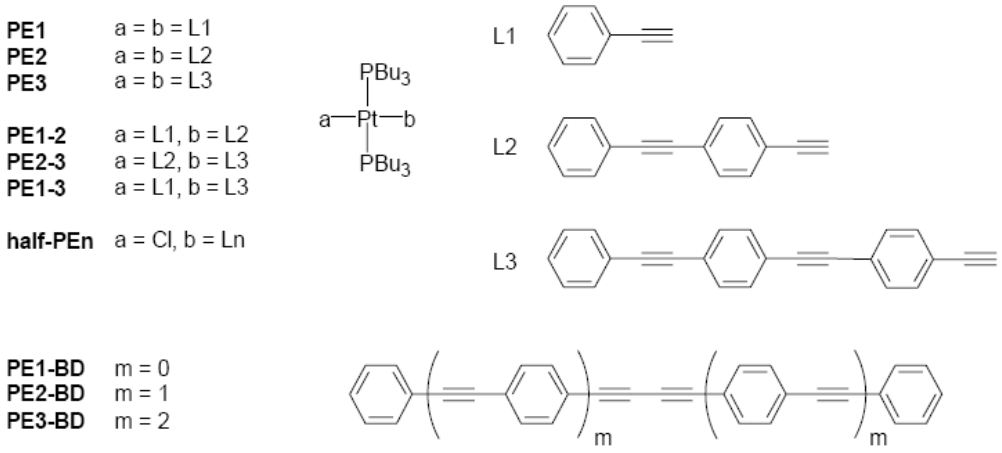

Figure 4-1. Various platinum acetylide compounds studied by Cooper, Rogers, *et al.*[77,87,178-182]

For the symmetrically substituted materials[87], increased conjugation gave rise to a red shifting of the S_0-S_1 and T_1-T_n processes. It was also concluded that the spin-orbit coupling effect of platinum on the ground and excited-state properties is reduced with increased conjugation length because the S_0-S_1 transition is more localized on the ligand. As the ligand size increased, the transition takes on more π-π^* character, therefore decreasing the mixing with orbitals localized on the platinum center. For the asymmetrically substituted complexes[182], absorption and emission data showed evidence of singlet exciton delocalization across the central platinum atom. The phosphorescence from the asymmetric complexes always arises from the largest ligand, verifying Kasha's Rule in that the triplet exciton migrates towards the lowest energy ligand. Comparison of these complexes with the mono-substituted compounds[180] concluded that while the singlet exciton was delocalized through the

platinum atom, the excited triplet states of each analogous compound were nearly identical, implying that the triplet exciton is confined to the larger organic ligand.

A series of dinuclear platinum acetylides complexes with various short spacers and end-caps were recently investigated in our group (Figure 4-2).[183] The ground-state and triplet-state absorbances were altered by the addition of the end-cap, whereas the triplet emission energies were less dependent on end-cap substitution. Phosphorescence was observed from both the spacer group and the higher energy end-cap, however. The results indicated that the singlet S_0 ground state, singlet S_1 excited state and triplet T_n excited state are delocalized throughout the molecule, but the T_1 states were localized on the ligand and spacer groups with no significant delocalization through the platinum atom in the triplet state.

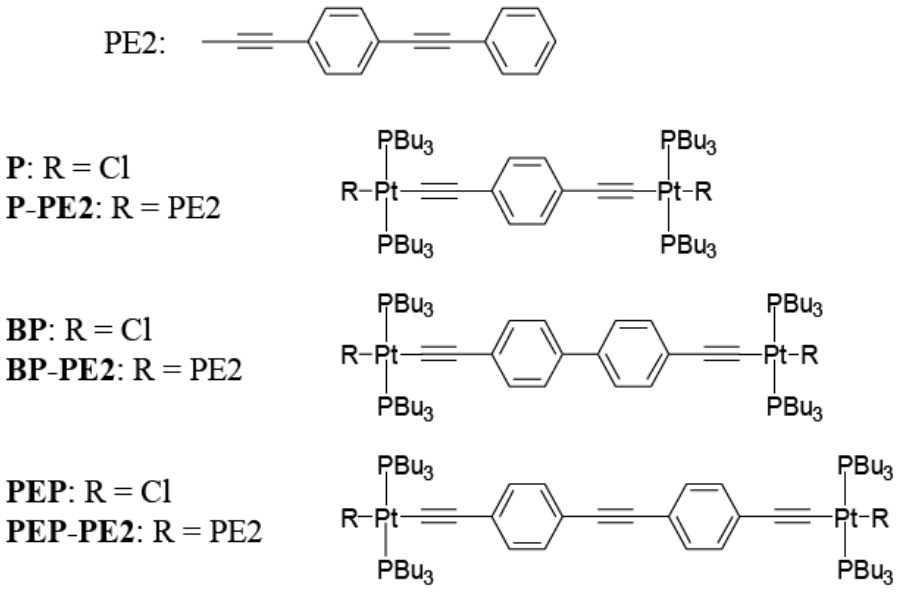

Figure 4-2. Series of dinuclear platinum acetylide complexes studied by Farley.[183]

This current study aims to examine effects of ground state and excited state delocalization between two platinum atoms as the length of a π-conjugated spacer is

extended. The spacer to be studied is a phenylene ethynylene repeat unit (Ph_n) in a series of platinum end-capped oligomers **Ph_nPt_2** (Figure 4-3).

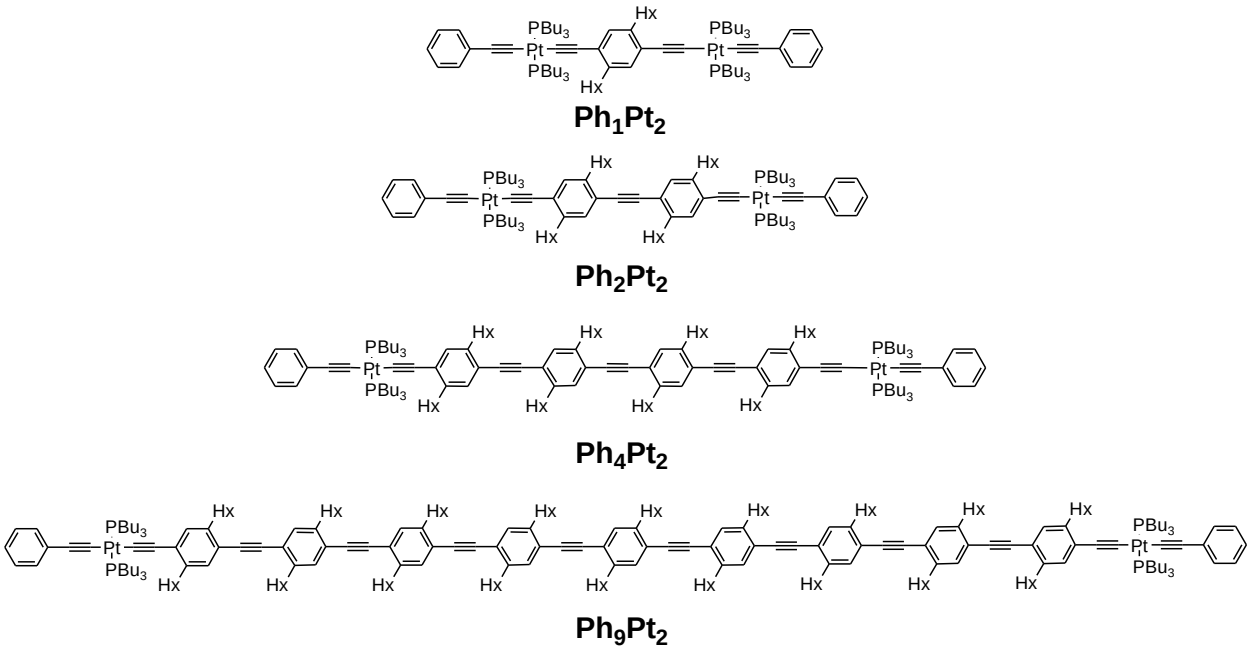

Figure 4-3. General structure of the **Ph_nPt_2** series, where n = 1, 2, 4, 9.

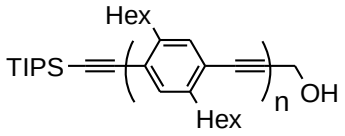

n = 1 (1a), 2 (1b), 4 (1d), 9 (1f)

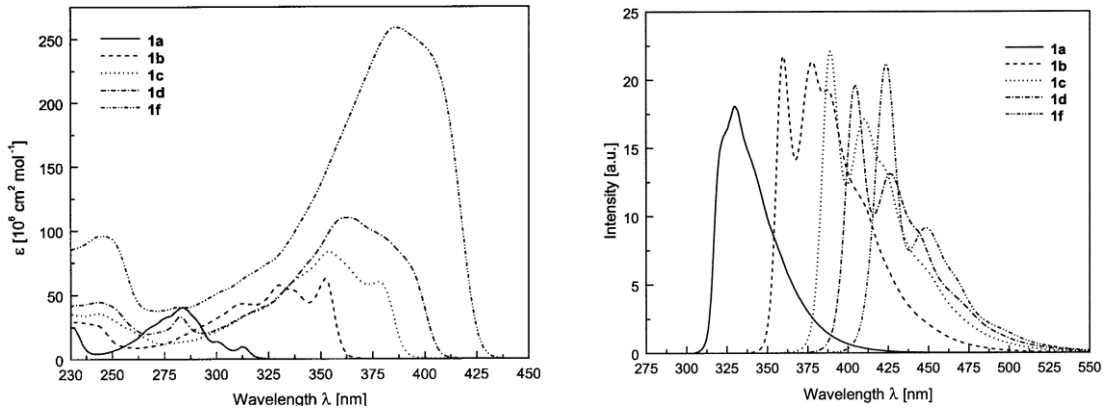

Figure 4-4. Oligo(PPE) structures (top), absorption (left) and emission (right) spectra reported by Godt.[114]

The analogous protected oligo(para-phenyleneethynylene)s of the spacers studied herein were previously synthesized and characterized by absorption and emission spectroscopy (Figure 4-4).[114] Increase of the length resulted in a bathochromic shift of the absorption and emission maxima. A unique feature of the dimers was the dinstinctive structure of the absorption and emission band, believed to be due to vibronically different electronic transitions.

Synthesis

The general synthesis of the Ph_nPt_2 series was modeled after the synthesis of monodisperse oligo(para-phenyleneethynylene)s,or oligo(PPE)s, reported by Godt and coworkers.[114] The strategy involved a divergent-convergent synthesis starting from 1,4-dihexyl-2-(3-hydroxyprop-1-ynyl)-5-[2-(triisopropylsilyl)ethynyl]benzene (**25**) via Pd/Cu-catalyzed alkyne-aryl couplings. The orthogonal acetylene protecting groups hydroxymethyl (HOM) and triisopropylsilyl (TIPS) were used to construct various smaller synthons that could be selectively deprotected and reacted, as well as to facilitate purification processes. The incorporation of the alkylated phenyl moieties is advantageous as well, as the hexyl (Hx) groups provide solubility in typical organic solvents. Deprotection of either the HOM or TIPS protecting group (one at a time) of the final oligo(PPE) synthons (top of Figure 4-4) would afford a somewhat stable terminal acetylene that could be reacted with a mono-substituted Pt(II) endcap, via Hagihara conditions, to afford the analogous platinum acetylides of the series, Ph_nPt_2 (as shown in Figure 4-3).

An inward-out, symmetrical synthesis of the oligomer was not implemented. Use of di-protected trialkylsilyl groups would make purification of the materials very difficult, as the compounds are already relatively nonpolar due to the presence of the alkylated

phenyl rings. Di-protection with two HOM groups could make the protected intermediates easier to separate; however, bis(terminal alkyne)s are oxidatively unstable and are therefore sensitive to the oxidative conditions required to deprotect both groups at once, ensuing *in situ* decomposition of the oligomers.[184]

The synthesis of **Ph_1Pt_2** is outlined in Figure 4-5 below. A copious amount of the main starting material, **19**, was initially prepared (~ 50 g). Iodination of **18** proved to be a challenge, as repetition of standard literature procedures gave mixed results from reaction to reaction. A reproducible yield of **19** was finally achieved when acetic anhydride was used in the reaction with both acetic acid and sulfuric acid, rather than the use of water as a co-solvent.[185]

Subsequent coupling of **19** with two equivalents of TMS-acetylene afforded the symmetrically-protected intermediate **20** in a high yield. Deprotection of this intermediate, followed by copper-catalyzed Hagihara coupling with endcap **22** yielded oligomer **Ph_1Pt_2** as a yellow solid, in 51% overall yield. The structure of this compound is analogous to the **Pt_2** oligomer studied in previous chapters 2 and 3.

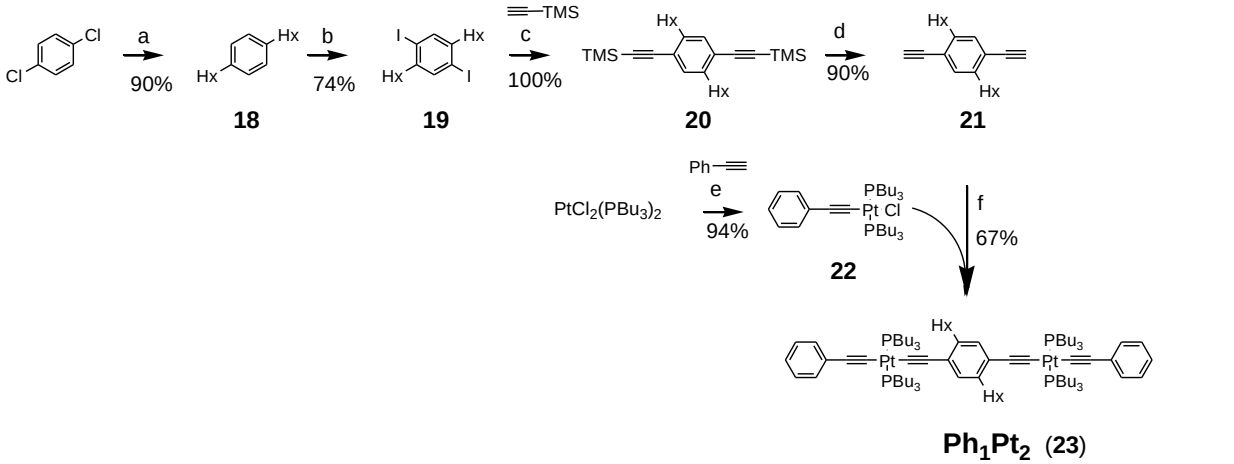

a) n-HxMgBr, $NiCl_2$dppp, dry ether, 0->35^oC, 20h; b) $I_2/NaIO_4$, H_2SO_4, $AcOH/Ac_2O$; c) $Pd(PPh_3)_2Cl_2$/CuI, THF/iPr_2NH, 70^oC,12h; d) TBAF, THF, rt, dark, 2h;e) Et_2NH, THF, 50^oC, 12h; f) CuI, THF/Et_2NH, rt, 1.5h.

Figure 4-5. Synthesis of the **Ph_1Pt_2** oligomer.

Construction of the longer oligomers required the use of orthogonal protecting groups, as discussed previously. Stepwise coupling of propargyl alcohol to **19** (Figure 4-6), followed by coupling of the mono-substituted adduct **24** with TIPS acetylene, afforded orthogonally-protected **25** in 63% yield overall (versus a statistical 33% overall yield of a one-pot synthesis). Selective deprotection of the HOM group followed by coupling with **24** gave the orthogonally-protected dimer **27**. Stepwise deprotection/Hagihara couplings with endcap **22** to each end of the oligomer yielded **Ph_2Pt_2** as a yellow solid.

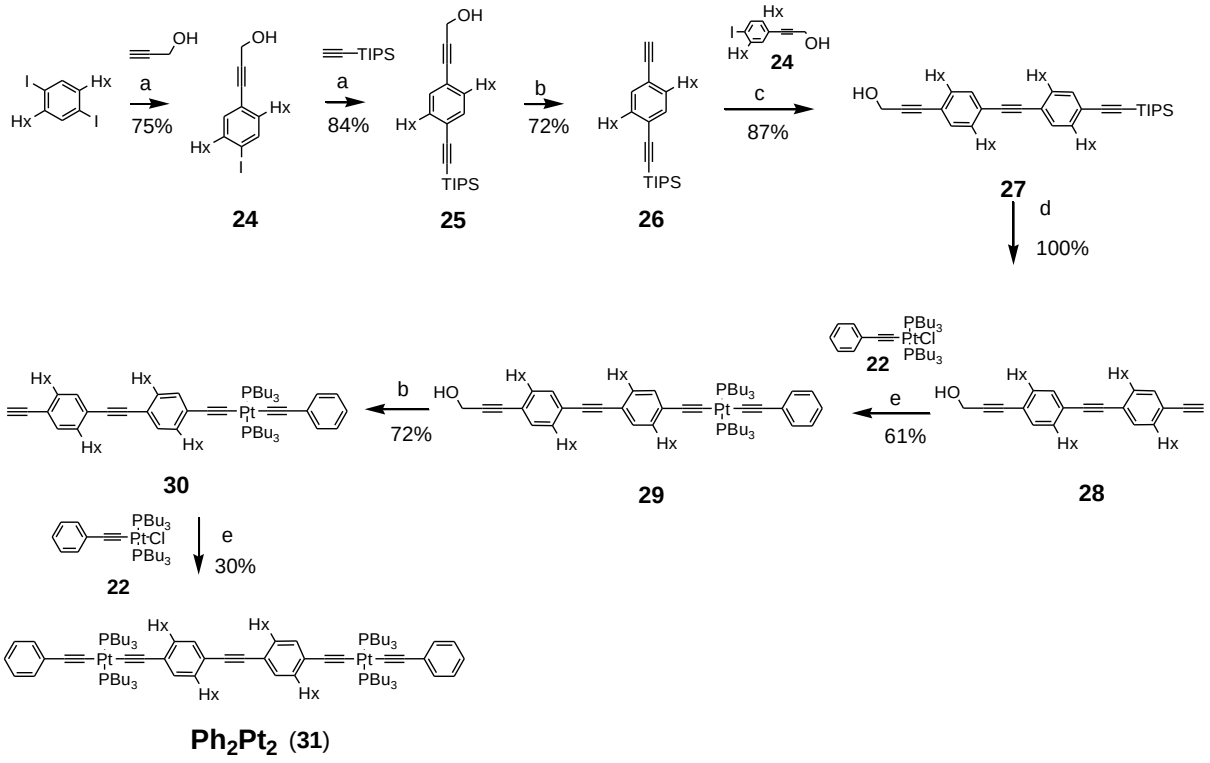

a) $Pd(PPh_3)_2Cl_2$/CuI, THF/piperidine, 50°C, 12h; b) MnO_2/KOH, ether, rt, dark, 12h; c)$Pd(PPh_3)_2Cl_2$/CuI, THF/piperidine, rt, 12h; d) TBAF, THF, rt, 2h; e) CuI, $NHEt_2$/THF, rt, 4h.

Figure 4-6. Synthesis of the **Ph_2Pt_2** oligomer.

The synthesis of **Ph_4Pt_2** was carried out in a similar manner. Synthesis of the orthogonally-protected tetramer **36** (Figure 4-7) was achieved via coupling of the mono-

HOM-protected iodo dimer **34** with the mono-TIPS protected acetylene dimer **35**. Again, stepwise deprotection/Hagihara couplings of each acetylene with endcap **22** afforded **Ph_4Pt_2** in moderate yields (Figure 4-8).

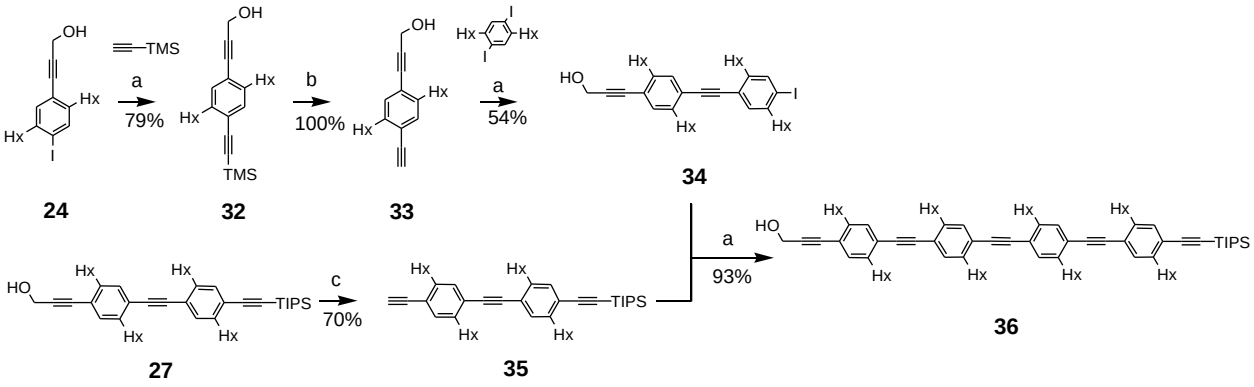

a) $Pd(PPh_3)_2Cl_2$/CuI, THF/piperidine, rt, 12h; b) KOH, MeOH/THF, rt, dark, 2h; c) MnO_2/KOH, ether, rt, dark, 12h.

Figure 4-7. Synthesis of orthogonally-protected intermediate **36**.

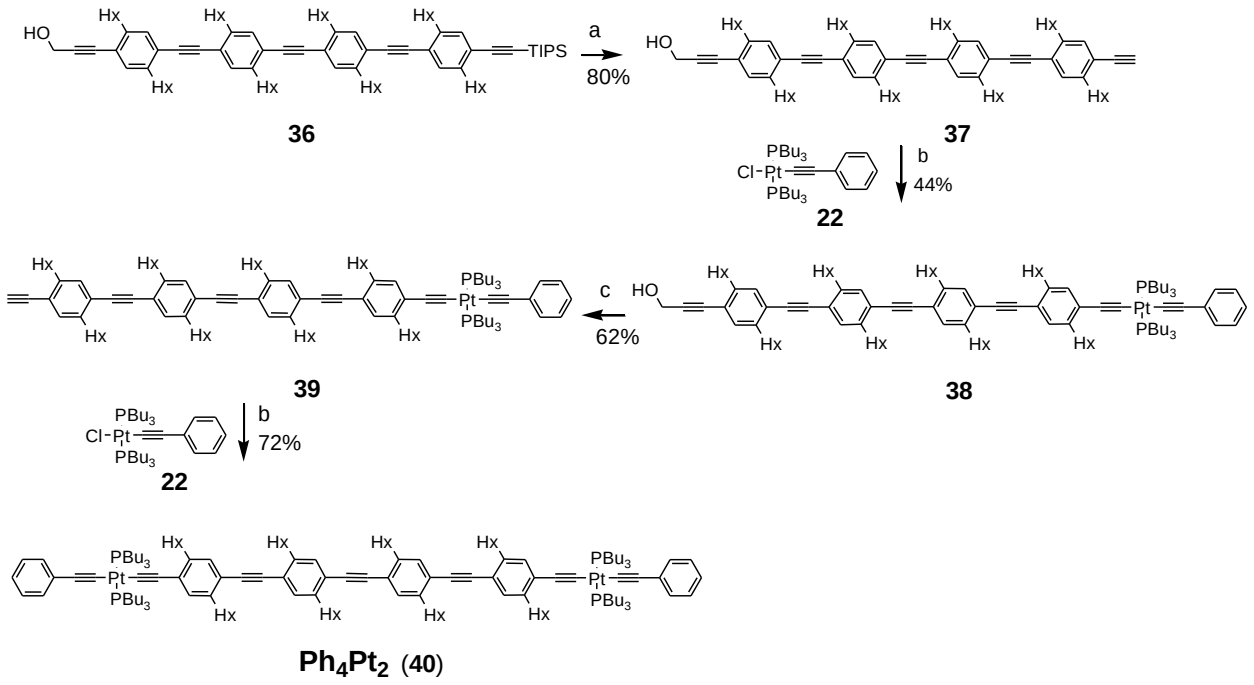

Ph_4Pt_2 (**40**)

a) TBAF, THF, rt, 2h; b) CuI, THF/$NHEt_2$, rt, 4h; c)MnO_2/KOH, ether, rt, dark, 4h.

Figure 4-8. Synthesis of the **Ph_4Pt_2** oligomer.

To this point, Sonogashira coupling of an aryl iodide with a free acetylene has been relatively clean with the use of $Pd(PPh_3)_2Cl_2$/CuI, as homocoupling of the free acetylene toward dimer formation has been minimal (with sufficient degassing). As the organic oligomers become longer, their sensitivity towards oxidative conditions increases, however. For the preparation of **Ph_9Pt_2**, a more active catalyst system was employed to prevent oxidative coupling of the acetylenes, $Pd_2(dba)_3$/CuI/PPh_3. Pentamer **42** and nonamer **43** were both prepared under these conditions (Figure 4-9). Once again, stepwise deprotection/Hagihara couplings of each end of the nonamer with **22** afforded **Ph_9Pt_2** as a yellow, paint-like solid in moderate yields (Figure 4-10).

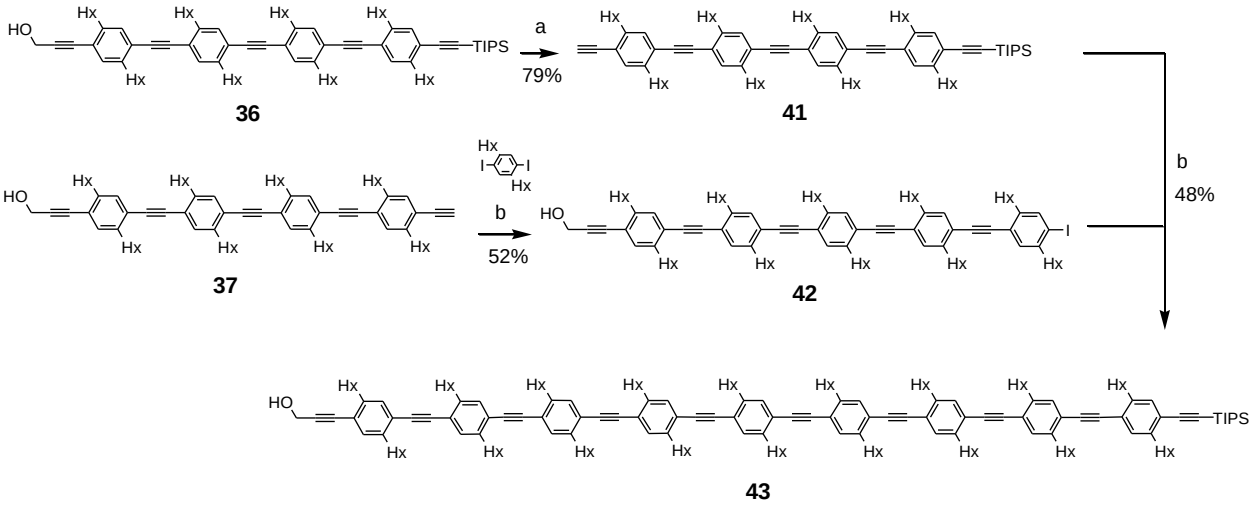

a) MnO_2/KOH, ether, rt, dark, 12h; b) $Pd_2(dba)_3$/CuI/PPh3, THF/piperidine, rt, 12h.

Figure 4-9. Synthesis of synthon **43**.

The final Ph_nPt_2 oligomers were all characterized by ^1H and ^{31}P NMR spectroscopy, as well as APCI high resolution mass spectrometry. The molecular weight of the **Ph_9Pt_2** oligomer, however, exceeded the limits for this type of ionization method. Other methods, including MALDI-TOF MS, were attempted but failed; therefore, this compound was further characterized by elemental analysis.

The ^{31}P NMR spectra revealed a pattern of three resonances for each final oligomer centered at δ ~ 4.5 ppm; each exhibited a weak "doublet" with J ~ 2360 Hz characteristic of the ^{195}Pt-^{31}P coupling, and a central resonance due to the PtP_2 units with NMR inactive Pt isotopes. The *trans* stereochemistry of the PtP_2 units was confirmed by the magnitude of the ^{195}Pt-^{31}P coupling constant.[69]

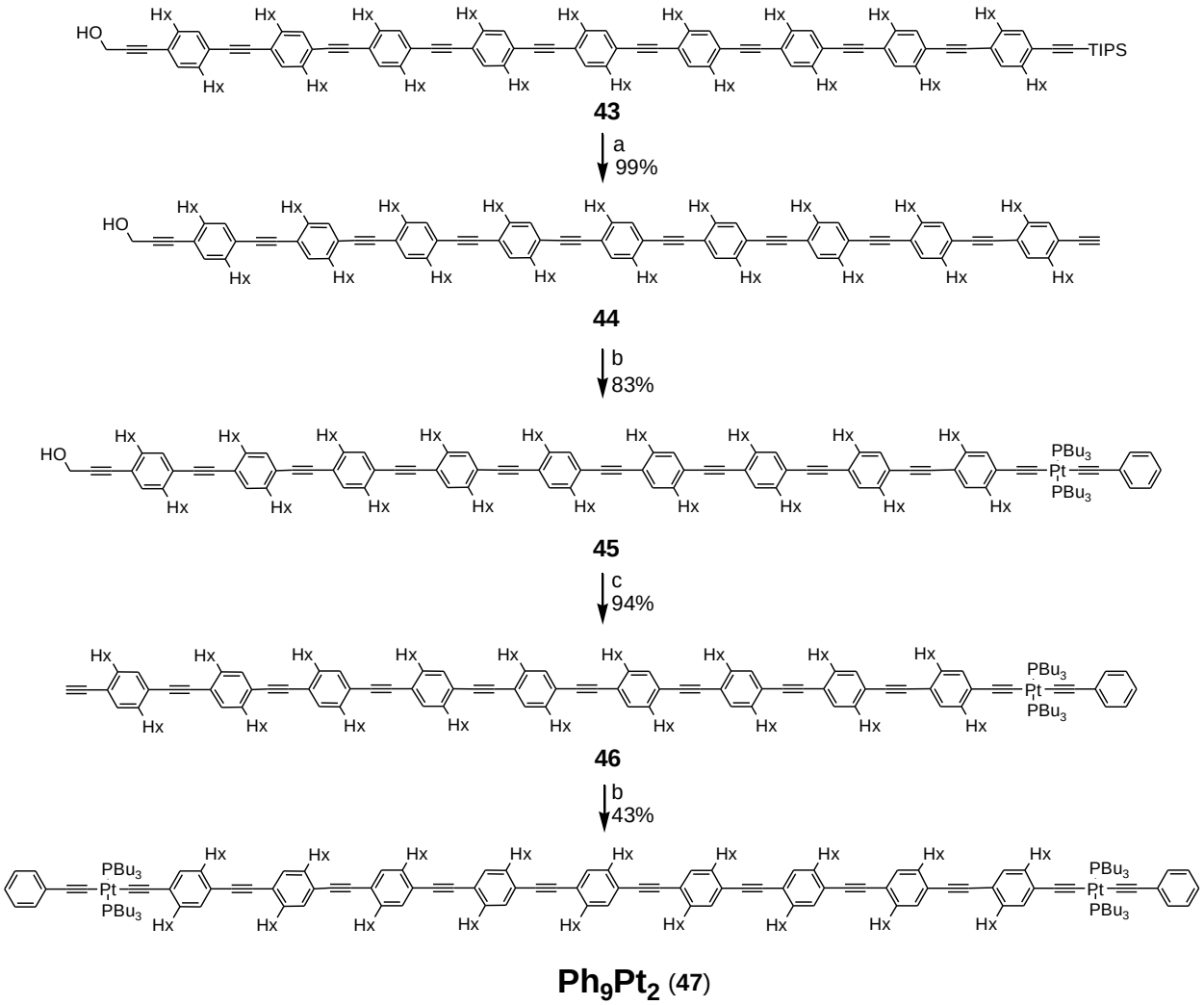

a) TBAF, THF, 2h, dark, rt; b) CuI, $NHEt_2$/THF, rt, 3h; c) MnO_2/KOH, ether, dark, rt.

Figure 4-10. Synthesis of the **Ph_9Pt_2** oligomer.

Results and Discussion

UV-Vis Absorbance

Table 4-1 lists a summary of the photophysical data collected for the Ph_nPt_2 oligomers. The absorption spectra for the series in THF solutions are shown below in Figure 4-11. The $S_0 \rightarrow S_1$ absorption maxima span over *ca* 0.3 eV range from 355 to 390 nm; these transitions arise from long axis polarized π,π^* transitions with some metal-to-ligand charge transfer (MLCT) character.[179] (Higher energy, short axis transitions remain fairly consistent throughout the series). The molar absorptivities for each of the compounds were measured (Table 4-1); the trend displays an increase with spacer length throughout the series.

Table 4-1. Summary of spectroscopic data for **Ph_nPt_2** series.

n	$E_{abs, max}$ (eV)	ε (M^{-1} cm^{-1})	$E_{F, max}$ (eV)	Φ_F (%)	$\tau_{F, av}$ (ns)	$E_{P, max}$ (eV)	Φ_P (%)	$E_{TA, max}$ (eV)	τ_T, (μs)
1	3.49	67500	3.12	0.2	0.001[a]	2.41	2.6	1.90	4.18
2	3.44	92000	3.07	0.1	0.036[b]	2.21	0.8	1.93	14.0
4	3.23	115000	2.92	0.2	0.111[c]	2.11	0.3	1.62	8.03
9	3.18	161000	2.92	2.2	0.179[d]	2.12[e]	--[f]	1.67	33.0

[a] τ_1 (α_1) = 0.404 ns (0.008%); τ_2 (α_2) = 0.001 ns (99.992%)
[b] τ_1 (α_1) = 0.036 ns (99.96%); τ_2 (α_2) = 0.497 ns (0.04%)
[c] τ_1 (α_1) = 0.101 ns (86.4%); τ_2 (α_2) = 0.550 ns (13.6%)
[d] τ_1 (α_1) = 0.322 ns (30.5%); τ_2 (α_2) = 0.115 ns (69.5%)
[e] Energy of emission recorded via gated-fluorescence TRE experiment.
[f] No phosphorescence emission was observed at room temperature.

The shortest oligomer **Ph_1Pt_2** exhibits the most blue-shifted maximum at 355 nm; the maximum absorbance is red-shifted to 360 nm for **Ph_2Pt_2**. The spectrum for this oligomer exhibits more fine structure than the others in the series, featuring another strong absorption at a slightly lower energy (*ca* 390 nm). Both the **Ph_4Pt_2** and **Ph_9Pt_2** oligomers display further red-shifting to 384 nm and 390 nm, respectively. The spectra of these larger compounds are slightly broader and less defined, and the change in absorbance is only slight considering the change in the length of the spacer.

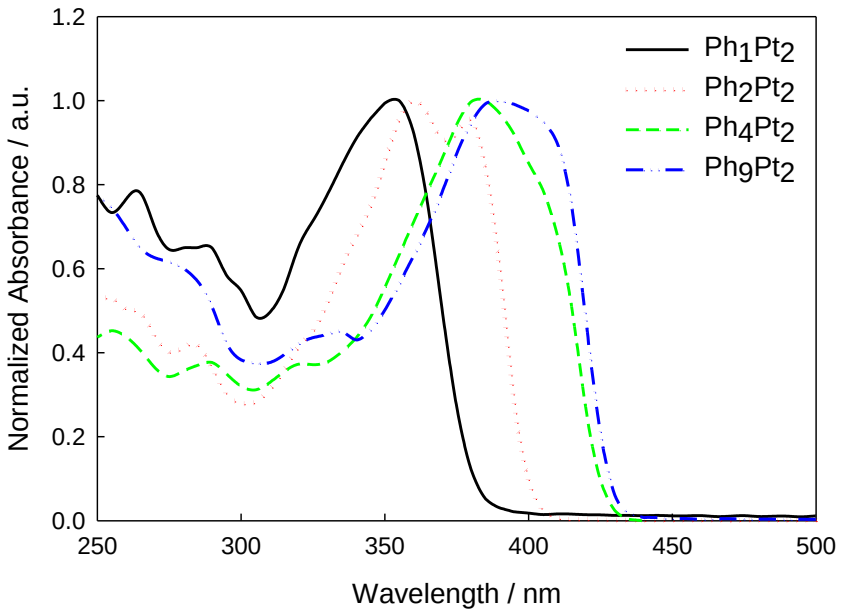

Figure 4-11. UV-Vis absorption spectra for Ph_nPt_2 series.

The red-shifting of the absorbance implies an increase in the delocalization of electrons in the ground state. In general, the absorption energies for the Ph_nPt_2 series are all red-shifted compared to the analogous organic oligomers reported by Godt *et al,*[114] suggesting that the incorporation of platinum has a direct effect on the electronic structure and conjugation length of the ground state, involving d,π orbital mixing of the organic spacers with the platinum atoms (Figure 4-12). The shapes of the spectra remain somewhat similar to their organic analogues, however. The effective conjugation length of the ground state chromophore seems to have nearly reached its limit in **Ph_9Pt_2**, as the change in energy from the n = 4 oligomer is relatively small.

Theoretical calculations of the highest occupied molecular orbital (HOMO) and lowest unoccupied molecular orbital (LUMO) for similar compounds have provided insight into these electronic transitions,[181,186] finding that the combination of the platinum d orbital and the aryl π orbitals contributes to the HOMO, while the LUMO consists of

only π^* orbitals with no contribution from the platinum d orbital. The lack of quantum chemical methods needed to further study the geometry and orbital configurations of this series only allows for limited conclusions to be made via comparison with the organic analogues.[114]

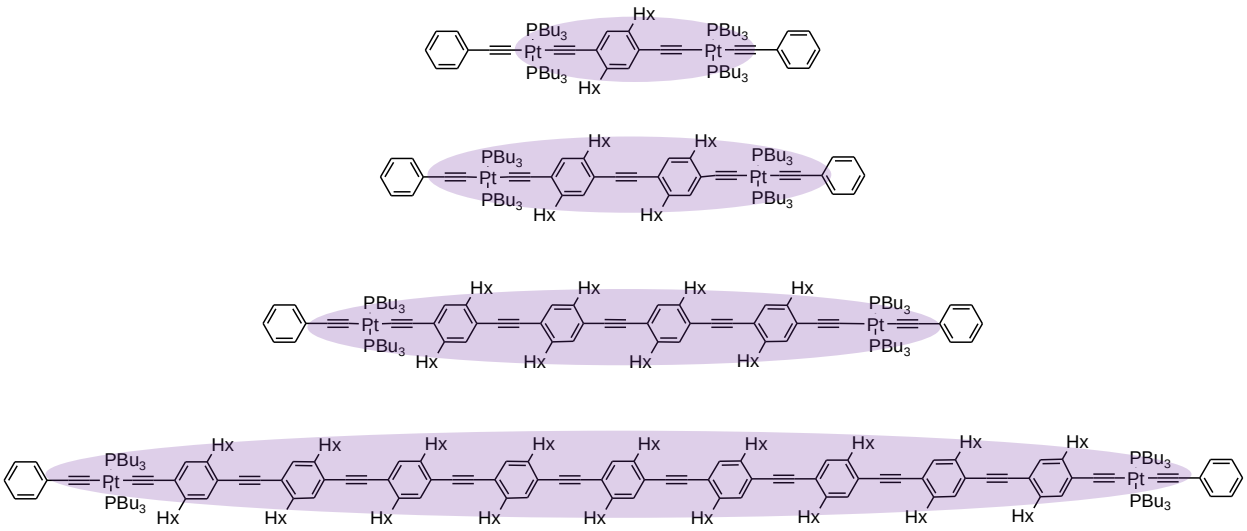

Figure 4-12. Delocalization of ground state within the Ph_nPt_2 series.

Steady State Photoluminescence

Fluorescence.

Steady state photoluminescence (PL) spectra of the series were recorded in THF at room temperature (Figure 4-13). Fluorescence emission for the oligomers exhibits red-shifting of the maximum with the extension of the spacer length over a similar range as ground state absorption (*ca* 0.3 eV). The fluorescence emissions of this series demonstrate a larger amount of stokes shifting (~0.3 eV) than for the Pt_n series reported by Liu *et al,*[88] but it is fairly consistent with the analogous organic series measured by Godt,[114] as is the general shape of emission. The fluorescence is relatively weak for the n=1, 2 and 4 oligomers (ϕ_F ~0.2%), but the quantum yield of the $S_1 \rightarrow S_0$ radiative

transition increases by an order of magnitude for **Ph_9Pt_2** (Table 4-1). The energy of emission, however, changes very little from **Ph_4Pt_2** (424 nm) to **Ph_9Pt_2**, (425 nm).

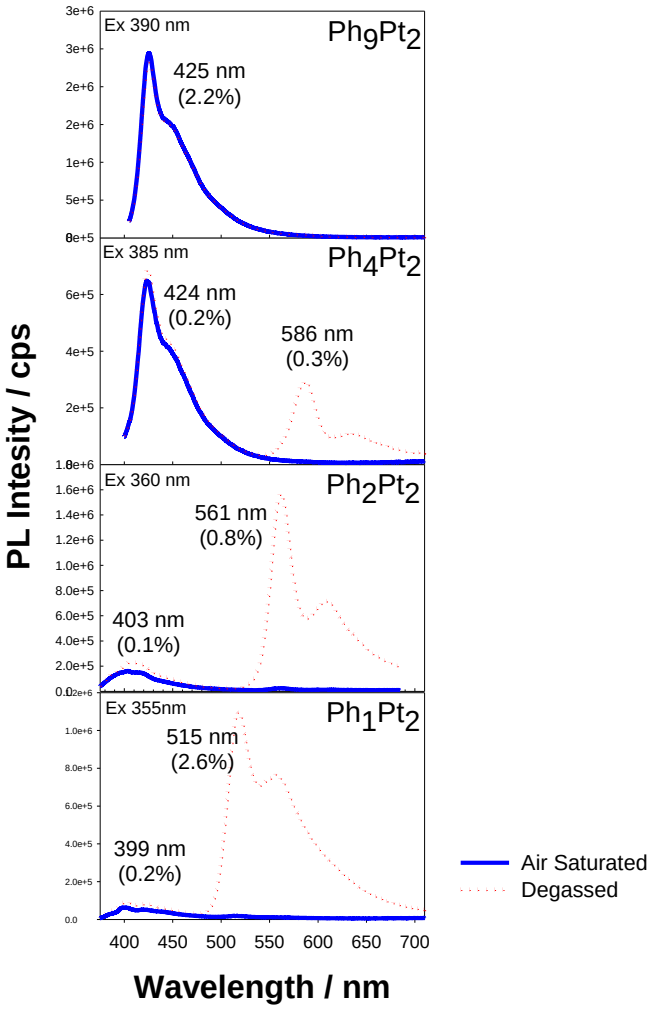

Figure 4-13. Steady state photoluminescence spectra of the Ph_nPt_2 series.

The fluorescence emission energies suggest that the singlet exciton is delocalized within the π^* framework of the organic spacer and with the d-orbitals of the platinum atoms for the n=1, 2 and 4 oligomers (Figure 4-14), as the fluorescence energies continually decrease with the increase in spacer length, and these energies are significantly red-shifted in comparison with the organic analogues previously

reported.[114] However, the emission from **Ph_9Pt_2** is almost identical to the analogous organic oligomer **1f** reported by Godt. This suggests that the singlet exciton is confined to the organic spacer and does not extend into the Pt atoms, and implies that the extent of conjugation involving d,π* mixing of the singlet exciton in the Ph_nPt_2 series has been reached. Definitive trends on conjugation length, however, cannot be determined by this experiment alone. The low yields of fluorescence in the emission spectra for the series indicates that intersystem crossing via spin-orbit coupling dominates decay of the singlet excited state. For other platinum-acetylide oligomers, the reported ISC quantum yields approach unity.[106,187] It is apparent from the data herein, however, that as the percent heavy metal character decreases in relation to the overall pi framework, the lower the rate of ISC.

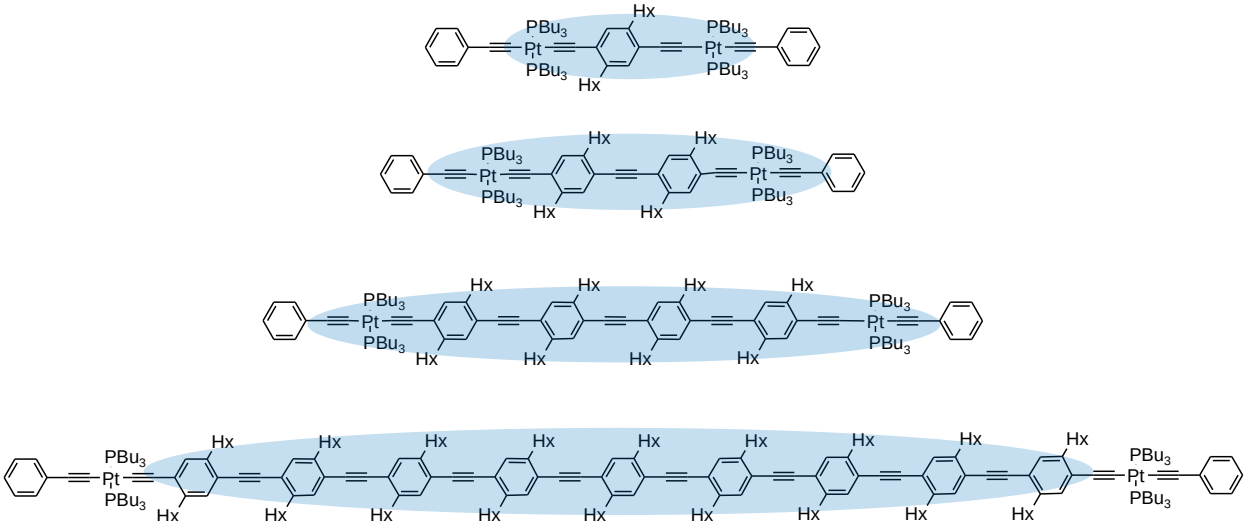

Figure 4-14. Delocalization of the singlet excitons for the Ph_nPt_2 series.

Fluorescence lifetime data is summarized in Table 4-1. Within the series, the lifetime of the singlet excited state increases along with the size of the oligomer. This trend is consistent with the premise that as the excited state is comprised of more π* character and less d-orbital character from the heavy Pt-atoms, the rate of ISC is

lowered; thus, the decay rate of the singlet excited state is lowered (it becomes longer-lived).

Phosphorescence.

The argon-degassed PL samples revealed lower energy phosphorescence emission at 515 nm, 561 nm and 586 nm in oligomers **Ph_1Pt_2**, **Ph_2Pt_2** and **Ph_4Pt_2**, respectively (Figure 4-12). At room temperature, these emission signals were generally broad, lacking vibronic structure. As the spacer length increases for the series, the maximum emission of phosphorescence red-shifted and the quantum yield decreased (2.6-0.3%), and no emission from the triplet was detected for **Ph_9Pt_2** at room temperature in the steady-state experiments. The quantum yield of phosphorescence in **Ph_9Pt_2** was expected to be significantly less; the lower Pt-metal contribution compared to organic contribution in this oligomer would lead to lower ISC yields; as well as lower rates of radiative decay.

To detect the energy of phosphorescence for **Ph_9Pt_2**, a time-resolved emission experiment was run in which the fluorescence signal was gated out via a 10 μs delay (Figure 4-15). A very weak phosphorescence signal (noted by the noise of the spectrum) was detected at 583 nm (some back-fluorescence is detected as well at ca. 425 nm). The phosphorescence energy measured for **Ph_9Pt_2** is roughly the same as the triplet energy measured for the **Ph_4Pt_2** oligomer, indicating the extent of delocalization for the triplet chromophore has been reached by **Ph_4Pt_2** in the series; it is suggested that the triplet exciton is most likely ligand-based in the nonamer, while the tetramer may include some d-character via delocalization across the Pt-atoms (similar to Figure 4-14). The reason for this conclusion is discussed below.

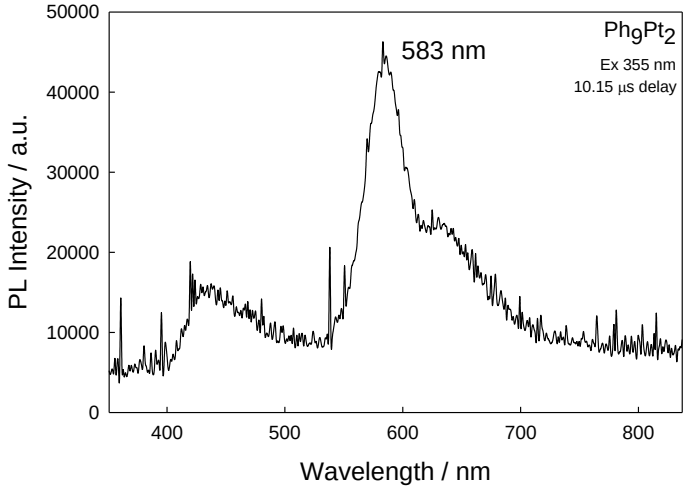

Figure 4-15. Time-resolved emission spectrum of **Ph_9Pt_2** in degassed THF. Excitation at 355 nm, spectrum recorded at a 10.15 μs delay.

The phosphorescence emission in dinuclear platinum compounds is generally characterized as originating from the π* ligand-based triplet state, even though population of T_1 occurs via efficient spin-orbit coupling between the excited organic ligands and the heavy metal platinum atom. Emission from this state is not typically seen at room temperature for strictly organic phenylene-ethynylene materials, however low temperature studies of similar monomers and polymers,[73] as well theoretical calculations of similar oligomer structures,[188] give insight into the energies of the triplet states in similar organic structures for comparison with the dinuclear platinum series herein. PL experiments of PPE films at 80K reveal triplet energies around 1.9 eV;[73] these values most likely correlate to the highest degree of delocalization within the $^3\pi^*$ exciton in PPEs. Similarly, quantum mechanical calculations of OPEs suggest similar lowest energies in oligomers greater than n = 10 repeat units.[188]

Predicted T_1 energies for OPEs with 'n' repeat units were also reported[188], and calculated values can loosely be compared to the E_{T1} of the platinum-capped Ph_nPt_2

series measured herein. Beljonne *et al* predicted that the $E_{S_o-T_1}$ for the n=2 OPE (analogous with **Ph_2Pt_2**) would be ~2.5 eV; this is comparatively higher than the phosphorescence energy measured for **Ph_2Pt_2** (2.21 eV). Similarly, the n=4 OPE triplet energy is calculated to be ~2.3 eV above ground state—also higher than the measured value for **Ph_4Pt_2** (2.11 eV). The differences in values decrease with the decrease in overall Pt-character in the Ph_nPt_2 molecules. The comparisons suggest that perhaps some d character does exist in the triplet exciton to further lower the energy of this state for the n = 1, 2 and 4 oligomers, however no real conclusions can be made without further investigation.

Transient Absorption

Transient absorption for the Ph_nPt_2 series were measured in deoxygenated THF solutions and spectra collected 30 ns after excitation by 355 nm pulse (10 ns, 8 mJ $pulse^{-1}$). The spectra are presented in Figure 4-16; maximum ΔA_{max} values and triplet lifetimes are summarized in Table 4-1.

Intense broad signals are exhibited in the visible region for all of the compounds in the series. Of all of the oligomers, **Ph_2Pt_2** surprisingly displays the most blue-shifted absorbance at *ca* 640 nm, a 12 nm shift from **Ph_1Pt_2** (652nm). **Ph_4Pt_2** displays a maximum absorbance at ca 760 nm. Of all the TA spectra, **Ph_9Pt_2** exhibits the broadest absorption; the maximum is centered at ca 745 nm, however there is a distinct broad shoulder centered around 670 nm as well.

The triplet state lifetimes (Table 4-1) were calculated from transient absorption decays. **Ph_1Pt_2** exhibits the shortest-lived triplet excited state (4.18 μs), followed by **Ph_4Pt_2** (8.03 μs). **Ph_9Pt_2** displayed the longest-lived triplet state lifetime at 33.0 μs.

Again, the **Ph_2Pt_2** oligomer fell slightly out of the trend (increasing lifetime with increasing organic spacer length) with a lifetime of 14.0 μs. The reason for this is unknown, but data eludes to perhaps a different structure of the excited state. While the relative error in measurement of lifetimes approaches almost 20%, the general trend is that the lifetime of the triplet exciton increases as the size of the organic spacer is lengthened (and the contribution of the metal decreases).

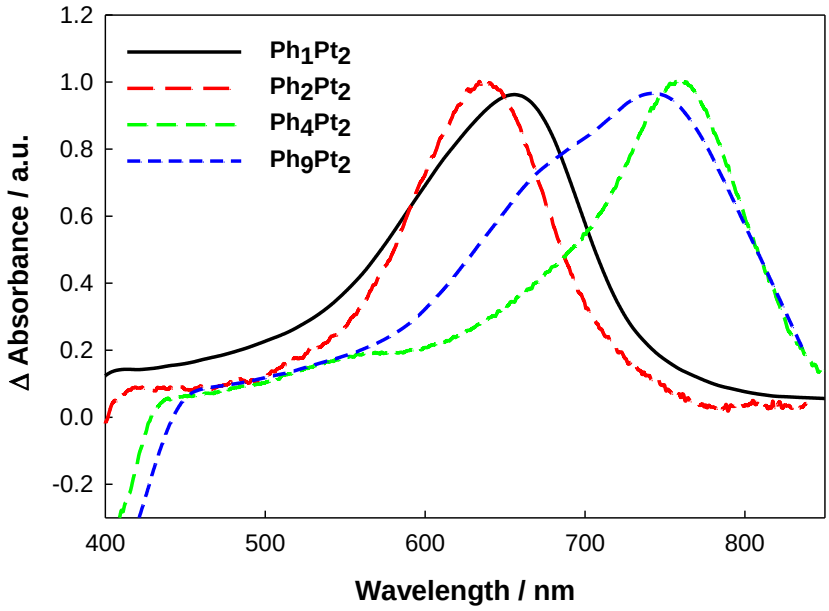

Figure 4-16. Transient absorption spectra of Ph_nPt_2 series.

The blue-shifting between dinuclear platinum oligomers **Ph_1Pt_2** and **Ph_2Pt_2** is rather intriguing. A similar phenomenon has been reported for a related dinuclear Pt series,[183] but this instance involved TA differences between a phenylene-ethynylene (P) and a biphenylene-ethynylene (BP) moiety in which the BP spacer was suggested to have an orthogonal-type structure with a ground state dihedral angle of 40°.[178] Due to the bulky hexyl side chains in the Ph_nPt_2 series, a similar phenomenon may exist (that is perhaps most evident in the dimer) even though the phenylene units in this case are

further spatially separated by an ethynyl linker. However, without quantum chemical methods to study the geometry and orbital configurations of this series, limited conclusions can be made. The idea that the central phenyl rings in the dimer-are twisted, which disrupts the conjugation, could be plausible; this could also explain oddities in the triplet lifetime of this oligomer, but because the exact conjugation length is not known for the Ph_nPt_2 series, it is not possible to determine trends based purely on conjugation length. The apparent blue-shifting between the n=4 and n=9 oligomers is not as surprising, as the nonamer does display a very broad absorption spectra in relation to the tetramer, suggesting multiple geometries of the excited T_n state exist in the longer oligomer. It is believed that the conjugation length of this excited triplet state had been reached based on the spectral data.

Conclusion

A series of platinum end-capped phenylene-ethynylene oligomers, Ph_nPt_2 were synthesized via an iterative-convergent route described by Godt *et al*[114] incorporating the use of orthogonal protecting groups to produce a variety of intermediate synthons. The molecules consisted of various sized organic spacer repeat units (n = 1, 2, 4 and 9) spanning two *trans*-$Pt(PBu_3)_2$(-C≡C-Ph) groups; the compounds were designed to characterize the influence of the heavy metal Pt atoms on the organic systems.

In comparison with the organic analogues previously reported[114], it was shown that the introduction of Pt in these systems affected the ground state absorption energies throughout the series, in which d,π-mixing was suggested to cause bathochromic shifting within the oligomers. The singlet excited state was also shown to be affected by the introduction of the Pt end groups; red-shifting of fluorescence emission was noted

for oligomers n = 1-4, while the singlet exciton was proposed to be mainly ligand-based in the nonamer. The fluorescence lifetimes of the oligomers were characterized, concluding that as the contribution of Pt vs. organic spacer decreased, the lifetimes of the singlet state increased, owing to less decay via ISC. The conclusion from the data was that the singlet ground and excited state were delocalized throughout the series, however the extent of delocalization in these states seemed to be reaching its limits.

Phosphorescence energies exhibited red-shifting (and a decrease in quantum efficiency) with an increase in spacer length for n=1-4 oligomers, but no emission was measured for the nonamer at via steady state experiments, as the quantum yield of this state was too low to detect vs. the fluorescence emission. Gated fluorescence experiments of the nonamer revealed very weak phosphorescence at the same energy as the tetramer, suggesting the extent of triplet exciton delocalization had been reached by n = 4. Population of the triplet state was also apparent in all oligomers, as all compounds exhibited broad transient absorptions. The general trend for T_n delocalization was similar to other states: an increase in organic spacer implied an increased conjugation length of the exciton. The data suggested that extent of delocalization of this state had been reached as well. **Ph_2Pt_2** was a bit of an anomaly in the group, displaying the highest energy TA transition. Reasons for this phenomenon are inconclusive in this study as more work is needed to investigate the structure/property relationships of the series.

Experimental

Materials and Instruments

All solvents and chemicals used for synthesis of the platinum acetylide oligomers were reagent grade and used without purification unless noted. Silica gel (Silicycle Inc.,

230-400 mesh, 40-63 microns, 60 Å) was used for all flash chromatography. All silyl-acetylene starting materials were purchased from GFS Chemical; potassium tetrachloroplatinate and palladium-bis(triphenylphosphyl) dichloride were purchased from Strem Chemicals; all other chemicals were purchased from Sigma-Aldrich. ^{1}H and ^{31}P NMR spectra were obtained on a Varian 300-MHz spectrometer using deuterated chloroform ($CDCl_3$) as the solvent and tetramethylsilane (TMS) as the internal reference. The synthesis of compounds **18**,[189] **19**,[185] **22**, [88] **24-29**, [114] **32-36**[114] and **41-43**[114] has been previously described in the literature.

Steady-state absorption spectra were recorded on a Varian Cary 100 dual-beam spectrophotometer. Corrected steady-state emission measurements were conducted on a PTI fluorescence spectrometer. Samples were degassed by argon purging for 30 min and concentrations were adjusted to produce "optically dilute" solutions (i.e., A_{max}< 0.20) in THF. Quantum yields were calculated using $Ru(byp)_3Cl_2$ as a known reference.[129]

Time-resolved emission measurements were carried out on a home-built apparatus consisting of a Continuum Surelite series Nd:YAG laser as the excitation source (λ = 355 nm, 10 ns fwhm, < 1mJ/pulse) and detection measured with a Princeton Instruments PI-MAX intensified CCD camera detector coupled to an Acton SpectraPro 150 spectrograph. The camera delay was set to 150 ns, and the gate set to 10 μs. The spectrum was recorded as an average of 500 images. The signal was relatively low, therefore the slit to the CCD was opened up (> 50 microns) until emission was detected. Samples were degassed in THF for 45 minutes with argon in a longneck fluorescence cell.

Transient absorption measurements were conducted on a home-built apparatus,[183] which used a Nd: YAG laser for excitation and PI-Max intensified CCD camera coupled with spectrograph as a detector. Sample concentration were adjusted so that $A_{355\ nm} \approx 0.8$. Triplet lifetimes were calculated using TA decay data via single exponential global fitting parameters in the SpecFit analysis software.

Fluorescence lifetimes were obtained using the time correlated single photon counting technique (TCSPC) with a PicoQuant FluoTime 100 Compact Fluorescence Lifetime Spectrophotometer. Excitation was achieved using a UV pulsed diode laser (λ_{max} 375 nm, P <10 mW). The laser was pulsed using an external BK Precision 4011A 5 MHz function generator. Decays were obtained using biexponential fitting parameters within the PicoQuant PicoHarp software.

Synthesis

cis-Bis(tributylphosphine)dichloroplatinum(II) was prepared by literature methods. Yield 70%. M.p. 138-139^{o}C.[130]

*1,4-di-n-hexylbenzene (**18**)* is a known compound and was prepared by the literature method.[189] Yield 90%. B.p.(100 mtorr) 90^{o}C. ^{1}H NMR (300 MHz, $CDCl_3$) δ 0.88 (t, 6H), 1.3 (m, 4H), 1.6 (m, 12H), 2.6 (t, 4H), 7.1 (s, 4H).[189]

*1,4-di-n-hexyl-2,5-diiodobenzene (**19**)* is known and was prepared by literature procedure.[185] Sodium periodate (6.0 g, 28 mmol, 40% excess) and diiodine (21.3 g, 84 mmol, 40% excess) were stirred into a mixture of glacial acetic acid (100 mL) and acetic anhydride (50 mL) at 5^{o}C. Concentrated sulfuric acid (26.6 mL, 500 mmol) was then added slowly to the stirring suspension. 1,4-Dihexylbenzene (17.3 g, 70 mmol) was added to this solution and stirring was continued for 4 h at room temperature. The

reaction mixture was then poured into an ice-water mixture containing previously dissolved Na_2SO_3 (fume hood). Over about 15 minutes, all precipitate was formed and filtered, washing with cold ethanol. Recrystallization of the product from ethanol resulted in 26 g of pure white, needle-like crystals. Yield 74%. M.p. 47^oC. ^1H NMR (300 MHz, $CDCl_3$) δ 0.88 (t, 6H), 1.35 (m, 12H), 1.55 (m, 4H), 2.6 (t, 4H), 7.6 (s, 2H).[114]

*2,5-Bis-trimethylsilanylethynyl-1,4-dihexylbenzene (**20**).*[113] To a round bottom flask was added 2,5-diiodo-1,4-dihexylbenzene (3.0g, 6.02 mmol), isopropanol (20 mL) and THF (30 mL). The mixture was stirred and degassed with argon for 20 min, then $Pd(PPh_3)Cl_2$ (0.211 g, 0.301 mmol) and CuI (57 mg, 0.301 mmol) were added quickly. The flask was degassed an additional 5 min, then TMS-acetylene (2.13 mL, 15.1 mmol) was added via syringe. The solution was heated to 70^oC and reacted for 12 h under argon gas. The solvents were evaporated, then the crude oil was diluted with ether, washed with water and brine, then dried over $NaSO_{4(s)}$. The filtered solute was dried and run through a short silica plug using 90:10 petroleum ether:CH_2Cl_2 as eluent. The product was collected and the solvent evaporated to give 2.7g of a yellow oil. Yield 100%. ^1H NMR (300 MHz, $CDCl_3$) δ 0.22 (t, 18H), 0.88 (m, 6H), 1.31 (m, 12H), 1.60 (m, 4H), 2.68 (t, 4H), 7.22 (s, 2H). ^{13}C NMR ($CDCl_3$) δ 0.2, 14.4, 22.9, 29.5, 30.9, 32.0, 34.4, 99.0, 104.2, 122.8, 132.7, 142.8. The product was used as is toward further reaction.

*2,5-Diethynyl-1,4-dihexylbenzene (**21**).* Methanol (15 mL), THF (10 mL) and 2,5-bis-trimethylsilanylethynyl-1,4-dihexylbenzene (1.0 g, 2.29 mmol) were degassed with argon for 30 min, then powdered KOH (0.77 g, 13.7 mmol) was added. The reaction was stirred in a dark flask for 2 h at room temperature until a crude aliquot confirmed

the reaction was complete via NMR. The reaction was then quenched with water, diluted with ether, and the organic layer dried over $NaSO_{4(s)}$. After filtration, the solute was evaporated to afford the crude product as 0.62 g of a pure yellow oil. Yield 93%. ^{1}H NMR (300 MHz, $CDCl_3$) δ 0.85 (t, 6H), 1.25 (m, 12H), 1.55 (m, 4H), 2.63 (t, 4H), 3.26 (s, 2H), 7.27 (s, 2H). This crude product was used as is toward further synthesis.

*trans-Bis(tributylphosphine)chloro(2-phenylethynyl)-platinum(II) (**22**)* is a known compound and was prepared by literature methods.[88] Yield 94%. ^{1}H NMR (300 MHz, $CDCl_3$) δ 0.90 (t, 18H), 1.35-1.65 (m, 24H), 2.0 (m, 12H), 7.1-7.3 (m, 5H); ^{31}P NMR ($CDCl_3$) δ 7.94 (J_{Pt-P} = 2373.81 Hz).[88]

Ph_1Pt_2 (23). The crude 2,5-diethynyl-1,4-dihexylbenzene (0.26 g, 0.89 mmol), trans-bis(tributylphosphine)chloro(2-phenylethynyl)-platinum(II) (1.5 g, 2.04 mmol), diethylamine (18 mL) and THF (12 mL) were mixed and degassed with argon for 30 min, followed by the addition of CuI (5 mg, 26.5 μmol). The solution was allowed to react for 1.5 h and then quenched with water. The organics were extracted with CH_2Cl_2 and dried over $NaSO_{4(s)}$. After filtration and evaporation of solvent, the crude yellow oil was loaded onto a column (silica, flash) loaded with 2:1 hexanes/CH_2Cl_2. Fraction 2 (R_f~0.3) was a dark yellow band that exhibited yellow phosphorescence under long wave UV light under argon stream. The solvent was evaporated and this fraction was collected as 1.0 g of solid yellow product. Yield 67%. ^{1}H NMR (300 MHz, $CDCl_3$) δ 0.85 (t, 6H), 1.25 (m, 12H), 1.55 (m, 4H), 2.63 (t, 4H), 3.26 (s, 2H), 7.27 (s, 2H). ^{31}P NMR ($CDCl_3$) δ 4.44 (J_{Pt-P} = 2367.08 Hz). Mass Spec. (APCI-HR) Calc'd for $C_{86}H_{146}P_4Pt_2$ $[M^+ + H]$ 1694.9765; Found $[M^+ + H]$ 1694.9741.

*3-(2,5-Dihexyl-4-iodo-phenyl)-prop-2-yn-1-ol (**24**)* is a known compound and was prepared by the literature method[114] to afford a brown/tan solid. Yield 75%. M.p. 37.5-38.0°C (Lit. 38.4-38.6°C). ^{1}H NMR (300 MHz, $CDCl_3$) δ 0.88 (m, 6H), 1.22-1.42 (m, 12H), 1.47-1.65 (m, 5H), 2.61 (d, 2H), 2.63 (d, 2H), 4.50 (d, 2H), 7.21 (s, 1H), 7.63 (s, 1H).[114]

*3-{2,5-Dihexyl-4-[(triisopropylsilanyl)-ethynyl]-phenyl}-prop-2-yn-1-ol (**25**)* is known and was prepared by the literature method[114] to produce a yellow-orange oil. Yield 84%. ^{1}H NMR (300 MHz, $CDCl_3$) δ 0.88 (m, 6H), 1.15 (s, 21H) 1.22-1.42 (m, 12H), 1.58-1.65 (m, 4H), 2.69 (d, 2H), 2.73 (d, 2H), 4.50 (d, 2H), 7.22 (s, 1H), 7.26 (s, 1H).[114]

*(4-Ethynyl-2,5-dihexyl-phenylethynyl)-triisopropyl-silane (**26**)* is a known compound and was prepared according to literature method[114] to afford an orange oil. Yield 72%. ^{1}H NMR (300 MHz, $CDCl_3$) δ 0.85-0.95 (m, 6H), 1.17 (s, 21H) 1.22-1.42 (m, 12H), 1.59-1.66 (m, 4H), 2.75 (m, 4H), 3.29 (s, 1H), 7.30 (s, 1H), 7.31 (s, 1H).[114]

*3-(4-{2,5-Dihexyl-4-[(triisopropylsilanyl)-ethynyl]-phenylethynyl}-2,5-dihexyl-phenyl)-prop-2-yn-1-ol (**27**)* is a known compound prepared from literature method[114] to afford the product as a yellow oil. Yield 87%. ^{1}H NMR (300 MHz, $CDCl_3$) δ 0.82-0.95 (m, 12H), 1.15 (s, 21H) 1.21-1.45 (m, 24H), 1.55 (s, 1H), 1.58-1.72 (m, 8H), 2.66-2.80 (m, 8H), 4.51 (d, 2H), 7.25 (s, 1H), 7.26 (s, 1H), 7.27 (s, 1H), 7.28 (s, 1H).[114]

*3-[4-(4-Ethynyl-2,5-dihexyl-phenylethynyl)-2,5-dihexyl-phenyl]-prop-2-yn-1-ol (**28**).* To a round bottom flask with a stir bar was added 3-(4-{2,5-Dihexyl-4-[(triisopropylsilanyl)-ethynyl]-phenylethynyl}-2,5-dihexyl-phenyl)-prop-2-yn-1-ol (1.3 g, 1.73 mmol) and THF (20 mL). The mixture was degassed for 30 min with argon followed by the addition of TBAF, 1 M in THF (3.47 mL, 3.47 mmol) via syringe. The

solution was allowed to react at room temperature for 2 h before it was quenched with water. The organic solution was extracted with ether and dried over magnesium sulfate. After filtration of the drying agent and evaporation of solvent, 1.3 g of a yellow/brown oil was collected as the crude product. Yield (crude) 100%. ^{1}H NMR (300 MHz, $CDCl_3$) δ 0.81-0.92 (m, 12H), 1.15 (s, 21H) 1.20-1.42 (m, 24H), 1.55-1.71 (m, 8H), 2.67-2.80 (m, 8H), 3.29 (s, 1H), 4.51 (s, 2H), 7.26-7.27 (m, 2H), 7.30-7.31 (m, 2H). The product was used without further purification toward the next step of the synthesis.

*$Ph_2OH_1Pt_1$ (**29**)*. To a round bottom flask with a stir bar was added **28** (181 mg, 0.252 mmol), **22** (0.40 g, 0.509 mmol), THF (10 mL) and diethylamine (8 mL). The mixture was degassed with argon for 30 min, followed by the addition of CuI (1.7 mg, 9.1 μmol). The solution was reacted for 4 h at room temperature, followed by evaporation of the solvent once TLC confirmed complete disappearance of the free acetylene starting material. The crude product was diluted with CH_2Cl_2, washed with water and brine, and dried over $NaSO_{4(s)}$. The crude material was concentrated into and oil and loaded onto a column (silica, flash) prepped with 3:1 hexanes/CH_2Cl_2. The third fraction was eluted as yellow band, exhibiting orange phosphorescence on TLC with long wave UV light under argon flow. Evaporation of the solvent afforded 200 mg of yellow oil product used as is toward further synthesis. Yield 61%. ^{1}H NMR (300 MHz, $CDCl_3$) δ 0.84-0.96 (t, 30H), 1.25-1.72 (m, 57H), 2.09-2.17 (m, 12H), 2.69-2.82 (m, 8H), 4.54 (d, $^{3}J_{(H,H)}$ = 6Hz, 2H), 7.08-7.31 (m, 9H). ^{31}P NMR ($CDCl_3$) δ 4.45 (J_{Pt-P} = 2360.45 Hz).

*$Ph_2(CCH)_1Pt_1$ (**30**)*. $Ph_2OH_1Pt_1$ (200 mg, 0.155 mmol) and ether (20 mL) were stirred and degassed 30 min under argon flow in a dark flask, followed by a total of 5

sequential additions (at 1 hour intervals) of MnO_2 (0.336g, 3.87 mmol) and powdered KOH (87 mg, 1.55 mmol). The reaction was allowed to go to completion at room temperature overnight, then it was filtered through a silica plug and rinsed with diethyl ether, to collect the crude deprotected product. The solvent of the filtrate was evaporated to afford 140 mg of crude product as a yellow oil. Yield (crude) 72%. The crude product was used as is toward the next step of the synthesis without further purification.

Ph_2Pt_2 (31). $Ph_2(CCH)_1Pt_1$ (140 mg, 0.111 mmol), **22** (204 mg, 0.277 mmol), diethylamine (10 mL) and THF (10 mL) were stirred and degassed with argon for 30 min, followed by the addition of CuI (0.5 mg). The solution was allowed to react at room temperature for 4 h, and then the solvent was evaporated. The crude product mixture was diluted with CH_2Cl_2, washed with water and brine and then dried over $NaSO_{4(s)}$. After filtration and evaporation of solvent, the crude oil was loaded onto a column (silica, flash) prepped and eluted with 1:1 hexanes/CH_2Cl_2. The first fraction eluted was a yellow band whose spot on TLC (long wave UV/argon stream) exhibited orange phosphorescence. The solvent was evaporated to afford 70 mg of yellow solid product. Yield 30%. Elemental Analysis for $C_{106}H_{174}P_4Pt_2$: Calculated C 64.87%, H 8.94%; Found C 64.43%, H 8.67%. ^{1}H NMR (300 MHz, $CDCl_3$) δ 0.83-0.96 (m, 48H), 1.22-1.72 (m, 80H), 1.95-2.28 (m, 24H), 2.68-2.80 (m, 8H), 7.07-7.31 (m, 14H). ^{31}P NMR ($CDCl_3$) δ 4.51 (J_{Pt-P} = 2359.16 Hz).

*3-(2,5-Dihexyl-4-trimethylsilanylethynyl-phenyl)-prop-2-yn-1-ol (**32**)* is a known compound prepared by literature procedure[114] to afford a brown oil product. Yield 79%. ^{1}H NMR (300 MHz, $CDCl_3$) δ 0.19 (s, 9H), 0.74-0.86 (m, 6H), 1.15-1.32 (m, 12H), 1.43-

1.58 (m, 4H), 2.10 (br s, 1H), 2.54-2.62 (m, 4H), 4.43 (s, 2H), 7.13 (s, 1H), 7.17 (s, 1H).[114]

*3-(4-Ethynyl-2,5-dihexyl-phenyl)-prop-2-yn-1-ol (**33**)* is known and was prepared by literature method[114] to produce the product as a red/brown oil. Yield 100%. ^{1}H NMR (300 MHz, $CDCl_3$) δ 0.82-0.92 (m, 6H), 1.18-1.40 (m, 12H), 1.51-1.65 (m, 4H), 2.10 (br s, 1H), 2.62-2.74 (m, 4H), 3.26 (s, 1H), 4.51 (s, 2H), 7.23 (s, 1H), 7.27 (s, 1H).[114]

*3-[4-(2,5-Dihexyl-4-iodo-phenylethynyl)-2,5-dihexyl-phenyl]-prop-2-yn-1-ol (**34**)* is known and was prepared by literature method[114] to afford the product as a yellow solid. Yield 54%. M.p. 58.2-59.0^{o}C (Lit. 62^{o}C). ^{1}H NMR (300 MHz, $CDCl_3$) δ 0.82-1.00 (m, 12H), 1.20-1.51 (m, 24H), 1.51-1.77 (m, 8H), 1.84 (t, 1H), 2.63-2.85 (m, 8H), 4.53 (d, 2H), 7.29-7.34 (3 s, 3H), 7.70 (s, 1H).[114]

*$Ph_2TIPS_1(CCH)_1$ (**35**)* is a known compound and was prepared according to literature method[114] to afford the product as a brown/red oil. Yield 70%. ^{1}H NMR (300 MHz, $CDCl_3$) δ 0.82-0.95 (m, 12H), 1.15 (s, 21H) 1.22-1.48 (m, 24H), 1.56-1.73 (m, 8H), 2.68-2.8 (m, 8H), 3.37 (s, 1H), 7.32-7.34 (4 s, 4H).[114]

*$Ph_4TIPS_1OH_1$ (**36**)* is a known compound prepared similarly to literature methods,[114] only $Pd_2(dba)_3$/CuI/PPh_3 (0.045/0.08/0.15 equiv. vs. starting material, where 1.0 equiv = 1.12 mmol) was used rather than the $Pd(PPh_3)_2Cl_2$/CuI catalyst system, minimizing the amount of acetylene dimer formation drastically. Yield 96%. ^{1}H NMR (300 MHz, $CDCl_3$) δ 0.81-0.98 (m, 24H), 1.16 (s, 21H), 1.35-1.52 (m, 48H), 1.54-1.79 (m, 16H), 2.71-2.88 (m, 16H), 4.52 (s, 2H), 7.31-33 (2 s, 2H), 7.35-7.36 (2 s, 2H), 7.39-7.40 (2 s, 4H).[114]

*$Ph_4OH_1(CCH)_1$ (**37**)* is known and was prepared according to literature method[114], however the product was purified by column chromatography (silica, flash) prepped and eluted with 1:1 petroleum ether/CH_2Cl_2. The product was collected in the first fraction as a yellow solid. Yield 80%. Mp 89-91°C (Lit. 91°C). ^{1}H NMR (300 MHz, $CDCl_3$) δ 0.82-0.98 (m, 24H), 1.24-1.48 (m, 48H), 1.59-1.76 (m, 16H), 2.71-2.87 (m, 16H), 3.30 (s, 1H) 4.54 (d, 2H), 7.29 (s, 1H), 7.34 (m, 3H), 7.37-7.39 (m, 4H).[114]

*$Ph_4OH_1Pt_1$ (**38**)*. To a round bottom flask were added $Ph_4OH_1(CCH)_1$ (0.10 g, 0.089 mmol), **22** (78 mg, 0.106 mmol), THF (7 mL) and diethylamine (10 mL). The solution was degassed under argon flow for 30 min, followed by the addition of CuI (0.5 mg). The solution was allowed to react at room temperature for 1.5 h until TLC revealed completion of reaction. The solution was quenched with water and the organics extracted with CH_2Cl_2 and dried ($NaSO_4$). Filtration of the drying agent and evaporation of the solvent gave a crude yellow/orange oil that was loaded onto a column (silica, flash) prepped with 2:1 petroleum ether/CH_2Cl_2, then switched to 1:1 after elution of fraction 2. The first two fractions that eluted (R_r ~ 0.8 and 0.5) were biproducts. The third fraction eluted was a yellow band (R_f ~ 0.3); the solvent was evaporated to yield 70 mg of a yellow oil that slowly became a solid. Yield 44%. ^{1}H NMR (300 MHz, $CDCl_3$) δ 0.82-1.00 (m, 42H), 1.21-1.81 (m, 88H), 2.02 -2.22 (m, 12H), 2.69-2.88 (m, 16H), 4.56 (s, 2H), 7.09-7.40 (m, 13H). ^{31}P NMR ($CDCl_3$) δ 4.57 (J_{Pt-P} = 2361.37 Hz). Mass Spec. (APCI-HR) Calc'd for $C_{115}H_{174}OP_2Pt$ $[M+Cl]^+$ 1864.2392; Found $[M+Cl]^+$ 1864.2392.

*$Ph_4(CCH)_1Pt_1$ (**39**)*. The starting material $Ph_4OH_1Pt_1$ (0.18 g, 0.098 mmol) and ether (15 mL) were stirred and degassed with argon for 30 min in a dark flask. Hourly

portions (3 total) of MnO_2 (0.214 g, 2.46 mmol) and powdered KOH (55 mg, 0.984 mmol) were then added until the reaction was complete. TLC monitoring showed reaction completion after 4 h. The reaction was filtered through a small plug of silica, washing with ether, then the concentrated filtrate was separated on a column (silica, flash) prepped with 3:1 petroleum ether/CH_2Cl_2. Fraction 1 was a small biproduct of the deprotection, and fraction 2 (eluted as a light yellow band, TLC showing green fluorescence and red phosphorescence under long wave UV light/argon flow) was collected as 110 mg of yellow oil product. Yield 62%. ^{1}H NMR (300 MHz, $CDCl_3$) δ 0.82-0.96 (m, 42H), 1.24-1.51 (m, 60H), 1.52-1.77 (m, 28H), 2.04 -2.20 (m, 12H), 2.71-2.88 (m, 16H), 3.31 (s, 1H) 4.56 (s, 2H), 7.08-7.39 (m, 13H). ^{31}P NMR ($CDCl_3$) δ 4.53 (J_{Pt-P} = 2360.98 Hz). The product was used as is toward further synthesis.

Ph_4Pt_2 (40). Diethylamine (10 mL), $Ph_4(CCH)_1Pt_1$ (110 mg, 0.0611 mmol) and **22** (104 mg, 0.141 mmol) were stirred and degassed with argon for 30 min, followed by the addition of CuI (<1 mg, about 0.04 equiv.). The reaction was allowed to stir at room temperature for 2 h, then quenched with water when TLC revealed that the reaction was complete. The organics were extracted with CH_2Cl_2 and dried ($NaSO_4$); after filtration of the drying agent and evaporation of solvent, the crude oil was loaded onto a column (silica, flash) prepped and eluted with 2:1 hexanes/CH_2Cl_2. The first fraction eluted as a yellow band (R_f ~ 0.25), and TLC revealed the spot as being fluorescent blue/green and phosphorescent red (with argon flow). Collection of the fraction afforded 110 mg of yellow solid product. Yield 72%. ^{1}H NMR (300 MHz, $CDCl_3$) δ 0.82-0.97 (m, 60H), 1.22-1.76 (m, 100H), 2.30-2.25 (m, 24H), 2.71-2.87 (m, 16H), 7.09-7.24 (m, 8H), 7.26-

7.31 (m, 6H), 7.33-7.37 (m, 4H). ^{31}P NMR ($CDCl_3$) δ 4.54 (J_{Pt-P} = 2363.43 Hz). Mass Spec. (APCI-HR) Calc'd for $C_{146}H_{230}P_4Pt_2$ [M^++H] 2499.6346; Found [M^++H] 2499.6371.

*$Ph_4TIPS_1(CCH)_1$ (**41**)* is a known compound prepared by literature method[114] to afford the product as a yellow solid. Yield 79%. M.p. 79°C (Lit 79°C). ^{1}H NMR (300 MHz, $CDCl_3$) δ 0.82-0.95 (m, 24H), 1.16 (s, 21H) 1.26-1.50 (m, 48H), 1.59-1.79 (m, 16H), 2.72-2.87 (m, 16H), 3.31 (s, 1H), 7.31-7.4 (m, 8H).[114]

*$Ph_5I_1OH_1$ (**42**)* is a known compound prepared by literature method[114] to afford a yellow solid. Yield 52%. M.p. 120°C (Lit. 121°C). ^{1}H NMR (300 MHz, $CDCl_3$) δ 0.81-0.99 (m, 30H), 1.25-1.51 (m, 60H), 1.56-1.81 (m, 20H), 2.64-2.90 (m, 20H), 4.58 (s, 2H), 7.31 (s, 1H), 7.34 (s, 1H), 7.36 (s, 1H), 7.40 (br s, 6H), 7.72 (s, 1H).[114]

*$Ph_9TIPS_1OH_1$ (**43**)* is a known compound prepared by literature method[114] to yield the product as a bright yellow solid. Yield 48%. M.p. 184.5-186.0°C (Lit. 187°C). ^{1}H NMR (300 MHz, $CDCl_3$) δ 0.81-0.98 (m, 54H), 1.16 (s, 21H), 1.26-1.79 (m, 144H), 2.71-2.89 (m, 36H), 4.52 (s, 2H), 7.31-33 (2 s, 2H), 7.35-7.36 (2 s, 2H), 7.37-7.45 (m, 14H).[114]

*$Ph_9OH_1(CCH)_1$ (**44**)*. Deprotection of $Ph_9TIPS_1OH_1$ (170 mg, 0.065 mmol) was accomplished by degassing this starting material in THF (15 mL) for 30 min with argon, followed by the addition of 1 M TBAF in THF (0.176 mL, 0.176 mmol) via syringe. The reaction was allowed to stir in a dark flask for 2 h until complete, and then quenched with water. The organic portion was extracted with CH_2Cl_2, dried over $NaSO_{4(s)}$, followed by filtration of the drying agent and evaporation of the solvent to afford a crude oil. This crude mixture was loaded onto a column (silica, flash) prepped and eluted with 1:1 petroleum ether/CH_2Cl_2. The product was eluted as a bright yellow band on the

column (R_f 0.5), exhibiting bright yellow fluorescence on TLC. The collected fractions were evaporated to give the product as 160 mg of a bright yellow solid. Yield 99%. ^{1}H NMR (300 MHz, $CDCl_3$) δ 0.82-0.97 (m, 54H), 1.25-1.51 (m, 108H), 1.59-1.80 (m 36H), 2.69-2.90 (m, 36H), 3.30 (s, 1H), 4.53 (d, $^{3}J_{(H,H)}$ = 6Hz, 2H), 7.28-7.39 (m, 18H). The material was used as is toward further synthesis.

*$Ph_9OH_1Pt_1$ (**45**)*. To a round bottom flask equipped with stir bar was added $Ph_9OH_1(CCH)_1$ (0.150 g, 0.061 mmol), **22** (0.120 g, 0.164 mmol), THF (10 mL) and diethylamine (9 mL). The solution was stirred and degassed under argon flow for 30 min, followed by the addition of CuI (0.4 mg, 2.20 μmol). The reaction was stirred at room temperature for 3 h until TLC confirmed that all of the limiting reagent was consumed, and the reaction was quenched with water. The organic portions were extracted with CH_2Cl_2, washed with saturated $NH_4Cl_{(aq)}$ and brine, and then dried over $NaSO_{4(s)}$. The solvent was evaporated after filtration of the drying agent to give a bright yellow crude solid that was loaded onto a column (silica, flash) prepped with 3:1 petroleum ether/CH_2Cl_2. Fractions 1 and 2 were eluted as either starting materials or side products. The solvent was increased gradually to 2:1 petroleum ether/CH_2Cl_2 and the third fraction (bright yellow band, fluorescent yellow on column) was collected as the product, 160 mg of a bright yellow solid (no phosphorescence was apparent by TLC under $N_{2(g)}$ flow). Yield 83%. ^{1}H NMR (300 MHz, $CDCl_3$) δ 0.82-1.00 (m, 72H), 1.22-1.82 (m, 180H), 2.00-2.22 (m, 12H), 2.66-3.02 (m, 36H), 4.56 (s, 2H), 7.09-7.42 (m, 23H). ^{31}P NMR ($CDCl_3$) δ 4.55 (J_{Pt-P} = 2357.93 Hz). The compound was used as is toward further synthesis.

*$Ph_9(CCH)_1Pt_1$ (**46**)*. A mixture of $Ph_9OH_1Pt_1$ (160 mg, 50.4 μmol) and ether (20 mL) was stirred and degassed under argon flow for 30 min in a dark flask, followed by five hourly addition of portions of MnO_2 (107 mg, 1.23 mmol) and powdered KOH (28 mg, 0.49 mmol) until the reaction was complete. After 5 h, the reaction was almost finished and it was left to run to completion overnight; the solution was filtered through a silica gel plug, washing with CH_2Cl_2, and the filtrate was collected and evaporated. The crude oil was loaded onto a column (silica, flash) prepped with 2:1 petroleum ether/CH_2Cl_2. The first fraction was a small amount of byproduct (fluorescent blue on column). The second fraction to elute was fluorescent yellow on the column. This large fraction was collected and the solvent evaporated to afford 150 mg of yellow oil as product. Yield 94%. ^{1}H NMR (300 MHz, $CDCl_3$) δ 0.72-0.98 (m, 72H), 1.20-1.82 (m, 168H), 2.02-2.24 (m, 12H), 2.66-2.94 (m, 36H), 3.31 (s, 1H), 7.08-7.42 (m, 23H). ^{31}P NMR ($CDCl_3$) δ 4.54 (J_{Pt-P} = 2362.20 Hz). The compound was used as is for further reaction.

Ph_9Pt_2 (47). A round bottom flask was charged with $Ph_9(CCH)_1Pt_1$ (150 mg, 47.7 μmol), **22** (105 mg, 0.143 mmol), THF (10 mL) and diethylamine (15 mL). The solution was degassed for 45 min under argon flow, followed by the addition of a catalytic amount of CuI (0.4 mg, 1.91 μmol). The reaction was stirred at room temperature for 4 h then quenched with water. The organics were extracted with CH_2Cl_2, washed with $NH_4Cl_{(aq)}$ and brine, then dried over $NaSO_{4(s)}$. The drying agent was removed and the solvent evaporated to afford a crude yellow oil. The crude oil was loaded onto a column (silica, flash) prepped with 4:1 petroleum ether/CH_2Cl_2. The first few fractions to elute were organic byproducts and the excess starting material. The third fraction was eluted

as a yellow band (fluorescent yellow on the column). This fraction was collected and the solvent evaporated to yield 80 mg of pure yellow (slowly forming) solid product. (*About 20 mg of product was also collected with the fourth fraction, containing acetylene starting material byproduct.) Yield 43%. Elemental Analysis for $C_{247}H_{374}P_4Pt_2$: Calculated C 76.89%, H 9.78%; Found C 76.81%, H 10.10%. ^{1}H NMR (300 MHz, $CDCl_3$) δ 0.80-0.97 (m, 90H), 1.22-1.79 (m, 192H), 2.04-2.21 (m, 24H), 2.64-2.91 (m, 36H), 7.09-7.24 (m, 8H), 7.26-7.32 (m, 6H), 7.34-7.40 (m, 14H). ^{31}P NMR ($CDCl_3$) δ 4.56 (J_{Pt-P} = 2357.85 Hz).

CHAPTER 5
CONCLUSION

The previous chapters of this dissertation have reviewed both the synthesis and photophysics of various types of π-conjugated oligomers containing platinum. The current studies have focused on further exploration of the fundamental photophysical properties of both charged and excited states of these materials to better understand their potential role in device applications, as well as to further investigate the properties of the triplet excited state that remain relatively elusive in strictly organic materials.

The main challenge in unifying a structure/property relationship in these materials was to synthesize discrete molecules of varying structures for comparison of properties. There has been considerable research focused on the synthesis of mono-disperse, organic π-conjugated oligomers,[90,113-120] however relatively few studies have been reported describing the preparation of oligomers that contain regular repeats of metal centers in the π-conjugated sequence.[88,121] The synthetic work described in Chapter 2 is useful, as the protecting group approach that was developed is general and could be used towards the synthesis of a variety of Pt-acetylide based oligomers and dendrimers. This chapter more specifically reported the synthesis of a series of mono-disperse Pt-acetylide oligomers that were end-capped with naphthalene diimide units, Pt_nNDI_2. In order to more successfully measure the dynamics of exciton and polaron hopping along the chains, relatively long oligomer chains were needed.[58,109-112] The synthetic approach used to construct these oligomers was based on an iterative-convergent method incorporating organometallic synthons with orthogonally protected terminal acetylenes. Oligomers n = 2, 3, 6, and 10 were successfully prepared, both quickly and with ease in separation, via this route. This work was significant as well because it is

the first know report to utilize orthogonal acetylene protecting groups in the synthesis of organometallic oligomers.

After synthesis of the monodisperse Pt_nNDI_2 series had been completed, studies of charge and energy transport in these compounds was investigated and reported in Chapter 3. Charges and triplet excitons created in platinum acetylide chains have been found to be localized to approximately two repeat units. These states are said to be trapped in a part of the chain only by structural relaxation (reorganization), therefore it was predicted that a polaron or exciton may move in random directions to adjacent locations on the chain. While evidence of migration had previously been reported, an in depth investigation of neither the rates of migration nor the mechanism had been reported. This study utilized ultrafast transient absorption and pulse radiolysis techniques to experimentally capture the rates of triplet exciton and negative polaron migration in these chains via spectroscopic evidence of either PET or electron capture at the NDI unit, respectively. To correlate the somewhat complex kinetics of these processes with migration rates, simulated data of a random-walk mechanism was generated and fit to match experimental data. Results conclude that a hopping mechanism is most likely dominate for both exciton and polaron migration along these chains; both processes are fast, and hopping rates for each were estimated to be about 27 ps. This is the first known report of intrachain diffusion rate measurements in these materials.

Another fundamental question that was studied in this dissertation was to further define the extent of delocalization of the triplet exciton in platinum acetylide compounds. As stated previously, in typical Pt-acetylides consisting of an ethynyl-phenyl-ethynyl

spacer between platinum atoms, the exciton had been reported to be highly confined between one to two repeat units based on optical data; calculations alluded to geometric constraints in the confinement the triplet exciton. Other work had studied the extent of triplet delocalization in Pt-capped oligoynes, however in these materials mixing of the metal and ligand orbitals was found to be minimal. Chapter 4 specifically addressed the question of the extent of exciton delocalization in phenylene ethynylene-ligand based platinum-acetylide materials. To study the relationship of increased conjugation length between two platinum moieties, a series of Ph_nPt_2 oligomers were synthesized, where n = 1, 2, 4 and 9. Examination of optical data concluded that the ground state remains highly delocalized throughout the series while quickly approaching its limit in the Ph_9Pt_2 compound. The extent of delocalization in the singlet and triplet excitons seems to have been reached by Ph_4Pt_2, as well as the delocalization in the T_n state. Phosphorescence yields at ambient temperatures decreased with increasing spacer length until emission was almost elusive in the n = 9 oligomer.

There are several avenues of interest that could spawn future work in these areas. One such project may be to examine differences between intrachain negative and positive polaron hopping rates in platinum acetylide compounds. The confinement energies of these states are notably different, therefore it is expected that the diffusional rates may also differ. Design of molecules would be imperative in this study as well, and a suitable hole trap would need to be incorporated into a platinum acetylide, ideally a trap with a distinct spectroscopic fingerprint that absorbs in different regions of the spectrum than the platinum acetylide radical cations.

Another avenue of interest would be to further investigate the properties of the Ph_nPt_2 series in terms of their potential applications in nonlinear absorption. It is well known that platinum acetylides are good candidates in this field, and the higher conjugation lengths between platinum moieties may be of interest toward these applications. Using a variable-wavelength excitation source such as an optically parametric oscillator (OPO), a greater understanding of the multiphoton absorption properties could be investigated. These properties could also be examined on a temporal scale, that is, through excitation by a short (ps) laser pulse. Such information is essential in the development of materials for use as broad-band optical limiters.

APPENDIX
CHARACTERIZATION DATA

APCI-HRMS, $[M+H]^+$ isotope pattern of Ph_1Pt_2

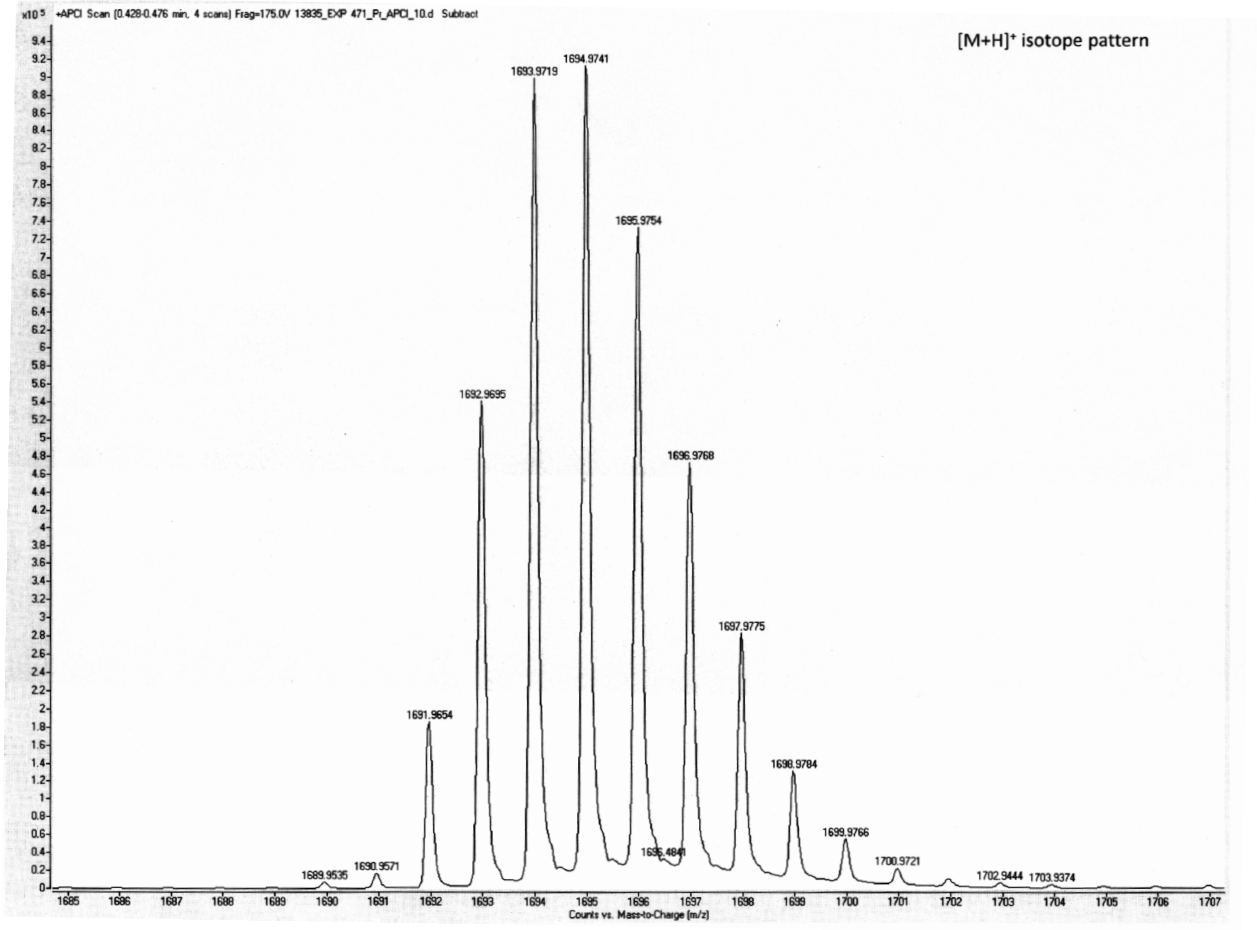

^{1}H NMR of Ph_1Pt_2

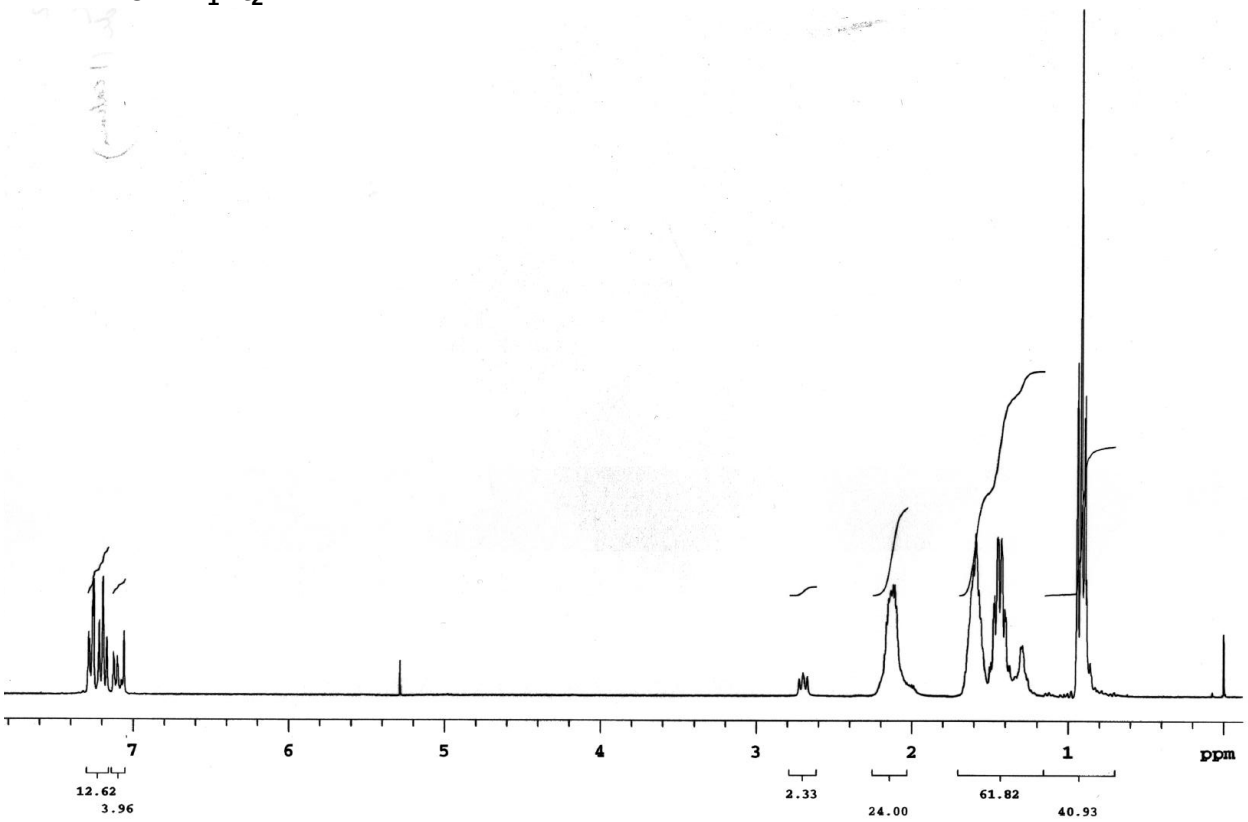

^{31}P NMR of Ph_1Pt_2

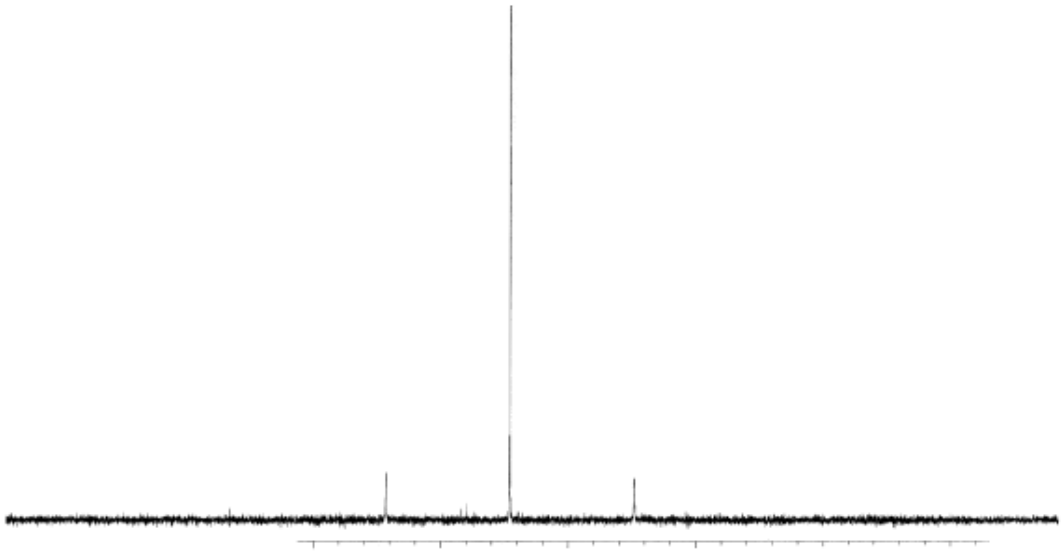

^{1}H NMR of Ph_2Pt_2

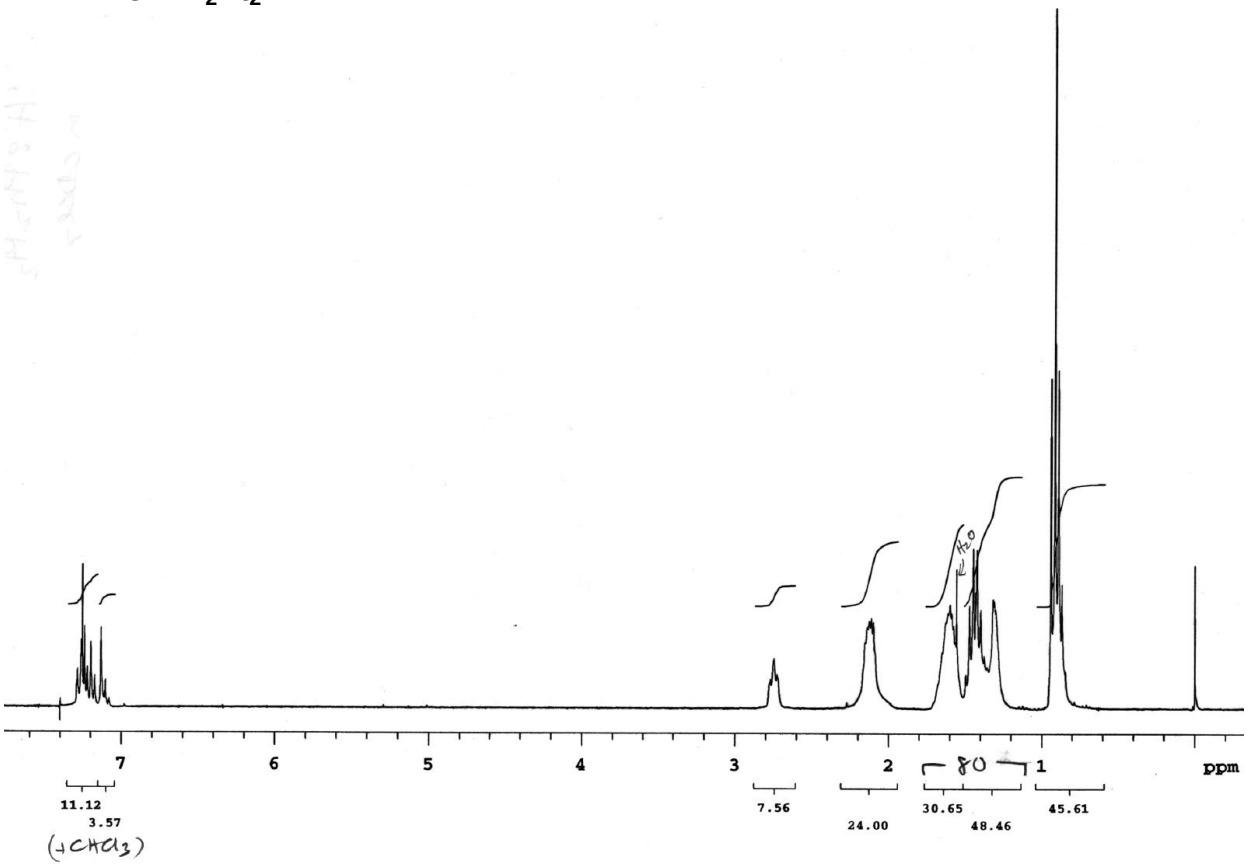

^{31}P NMR of Ph_2Pt_2

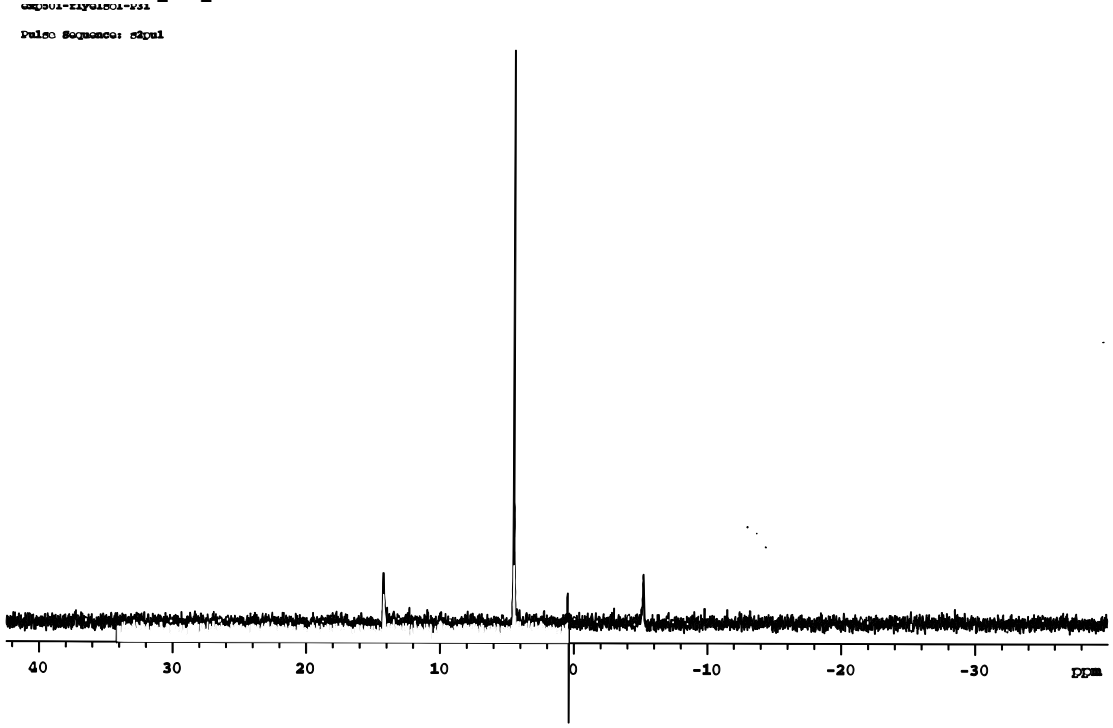

APCI-HRMS, $[M+H]^+$ isotope pattern of Ph_4Pt_2

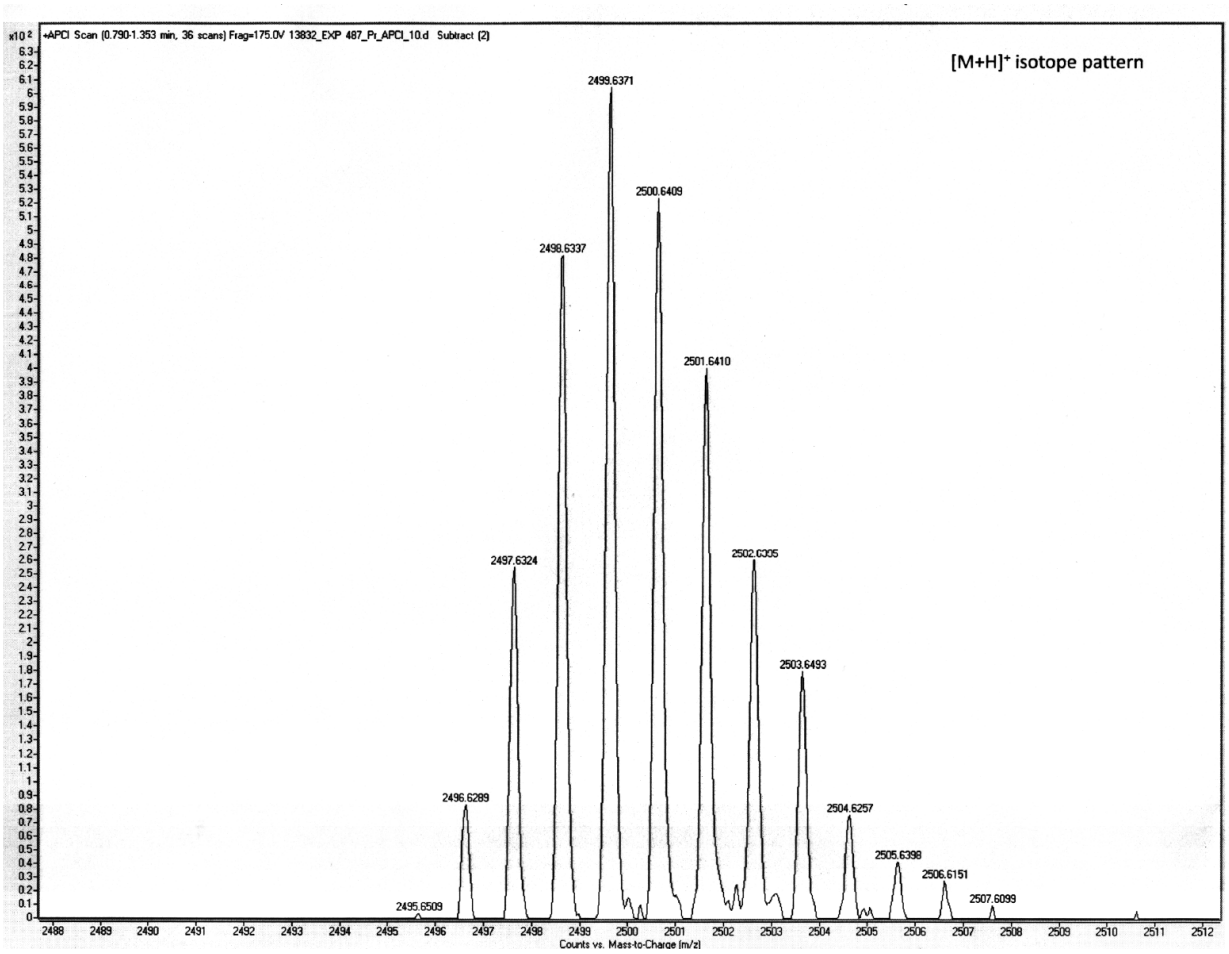

^{1}H NMR of Ph_4Pt_2

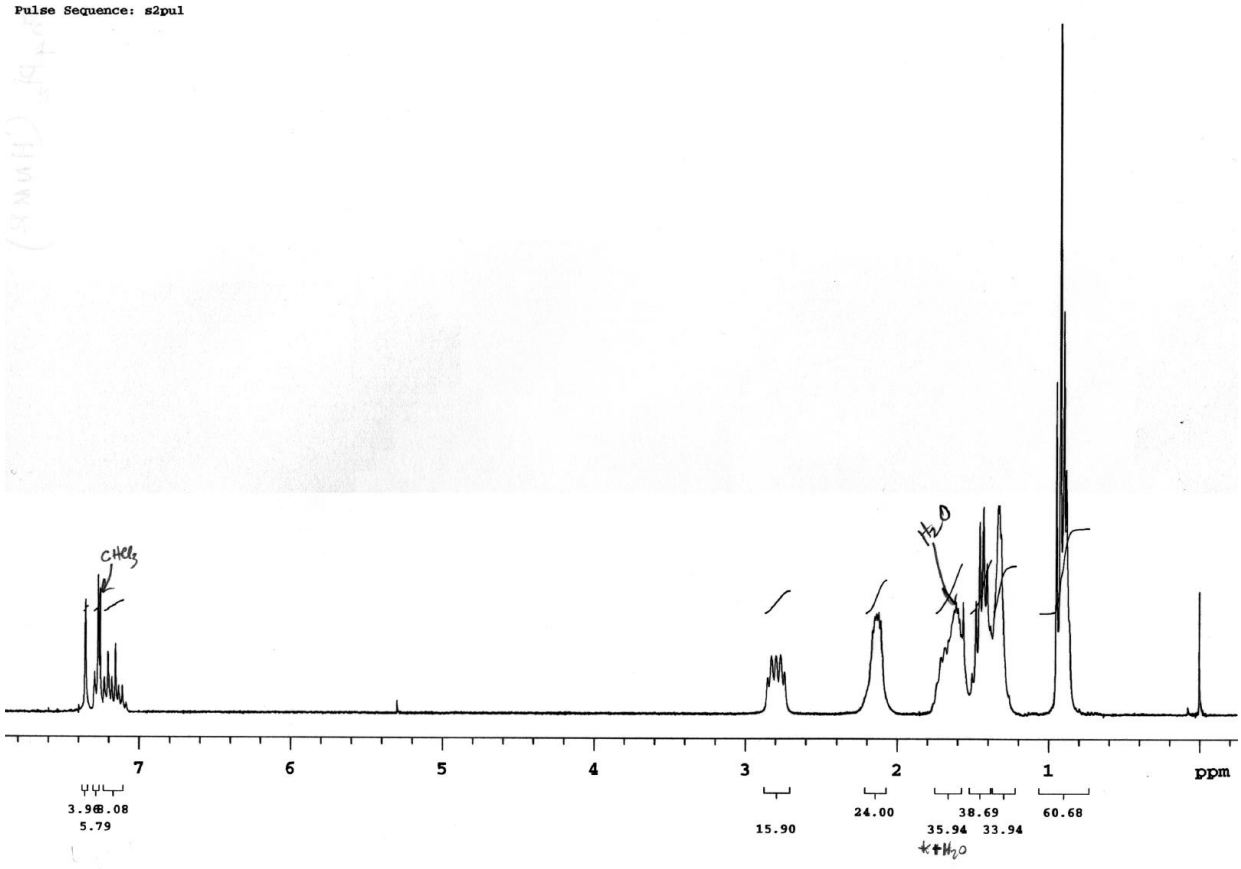

^{31}P NMR of Ph_4Pt_2

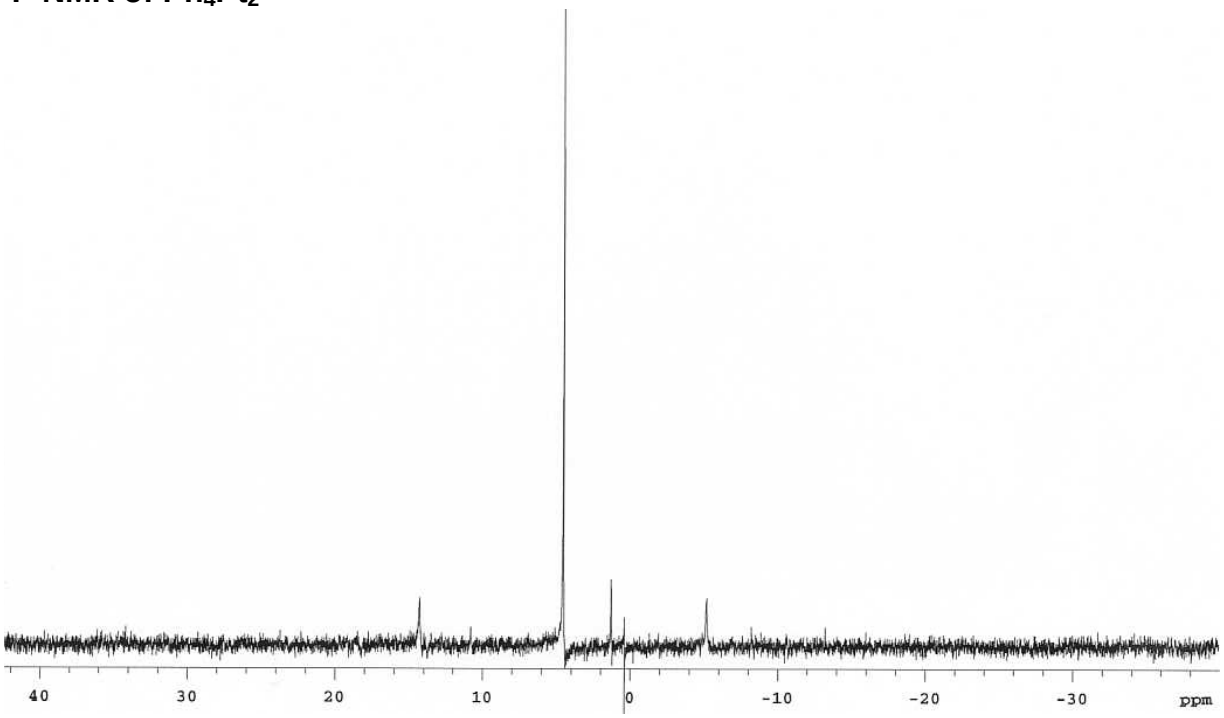

^{1}H NMR of Ph_9Pt_2

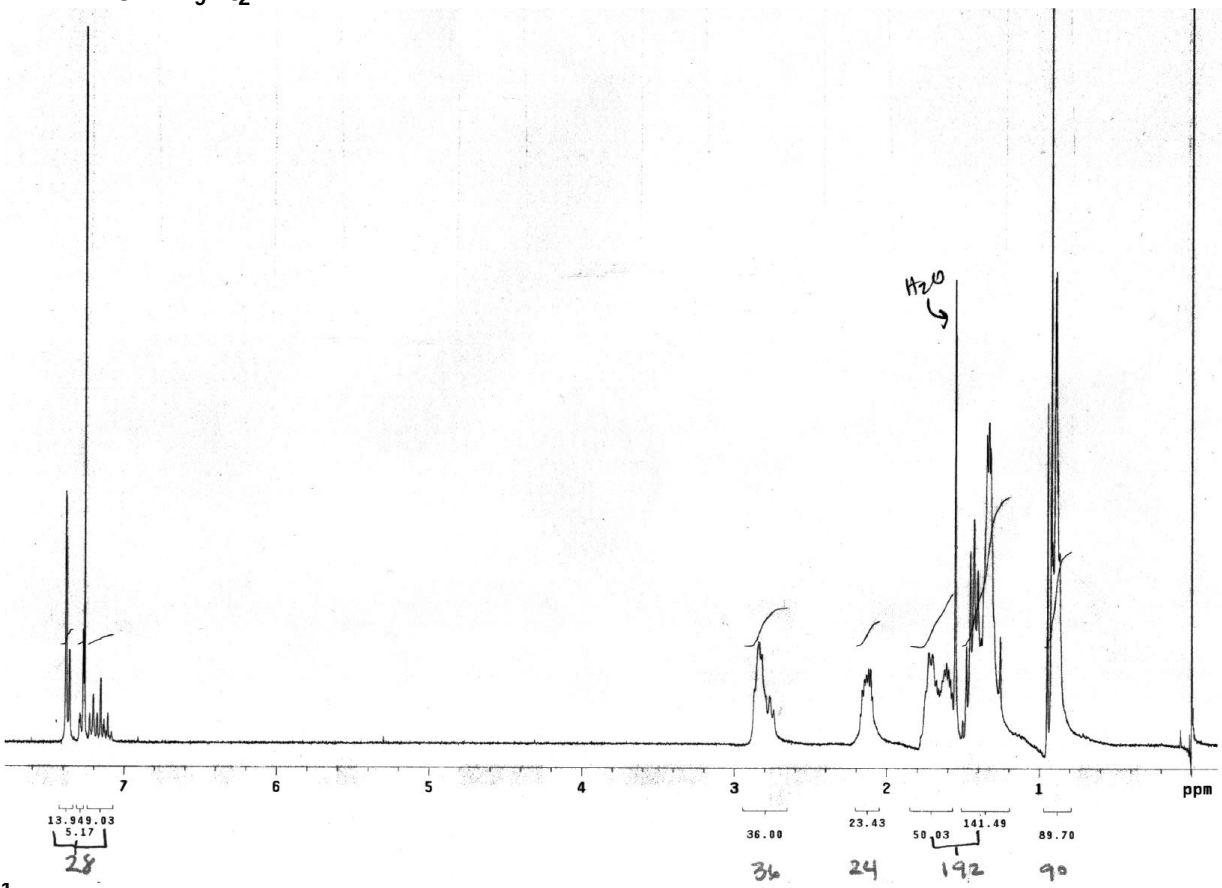

^{31}P NMR of Ph_9Pt_2

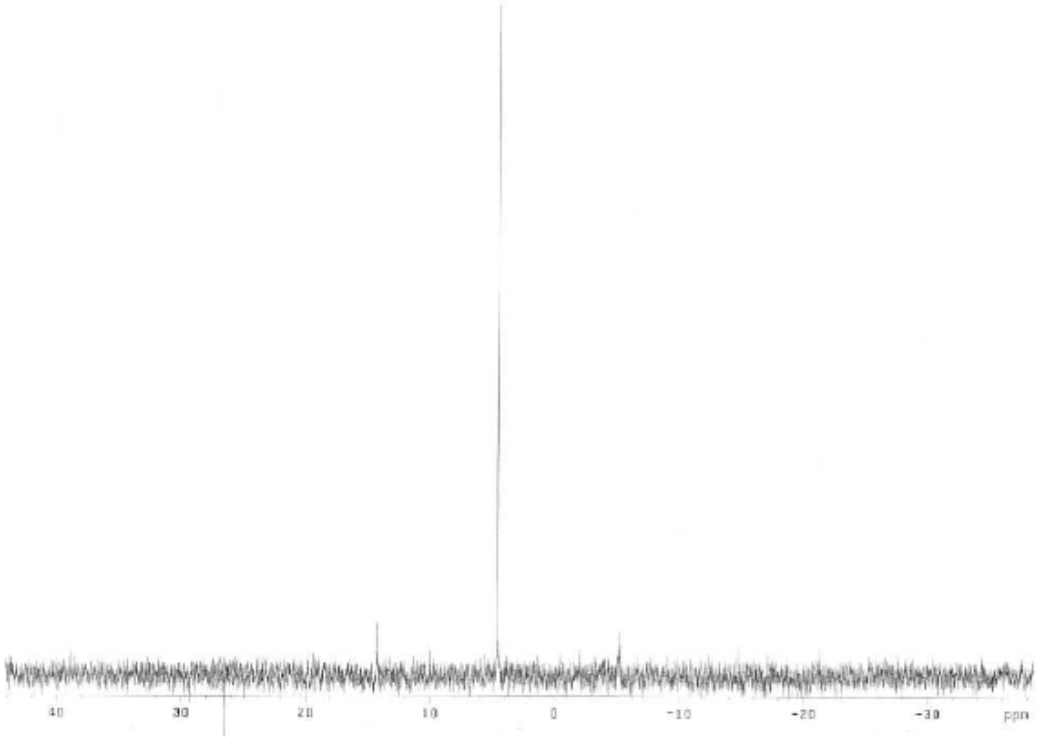

REFERENCES

1. Atkins, P. W., *Physical Chemistry*. W. H. Freeman and Co.: New York, 1940.

2. Tripler, P. A., *Physics for Scientists and Engineers*. Worth Publishers: New York, 1994.

3. Born, N., *Atomic Theory and the Description of Nature*. AMS Press: New York, 1934.

4. Newton, I., *Opticks*. The Warnock Library: London, 1704.

5. Turro, N. J., *Modern Molecular Photochemistry*. University Science Books: Sausalito, 1991.

6. Franck, J. *Trans. Faraday Soc.* **1926,** *21*, 0536-0542.

7. Condon, E. *Phys. Rev.* **1926,** *28*, 1182-1201.

8. McGlynn, S. P.; Smith, F. J.; Cilento, G. *Photochem. Photobiol.* **1964,** *3*, 269-294.

9. Ingle, J. D. J. C., S. R, *In Spectrochemical Analysis*. Prentice-Hall, Inc.: Upper Saddle River, 1988; p 342.

10. Wilson, J. S.; Chawdhury, N.; Al-Mandhary, M. R. A.; Younus, M.; Khan, M. S.; Raithby, P. R.; Kohler, A.; Friend, R. H. *J. Am. Chem. Soc.* **2001,** *123*, 9412-9417.

11. Williams, A. T. R.; Winfield, S. A.; Miller, J. N. *Analyst* **1983,** *108*, 1067-1071.

12. Forster, T. *Discuss. Faraday Soc.* **1959**, 7-17.

13. Dexter, D. L. *J. Chem. Phys.* **1953,** *21*, 836-850.

14. Kim, D.; Osuka, A. *Acc. Chem. Res.* **2004,** *37*, 735-745.

15. Kavarnos, G. J., *Fundamentals of Photoinduced Electron Transfer*. VCH Publisher: New York, 1993.

16. Mattay, J., *Topics in Current Chemistry*. 1990; p 156.

17. Marcus, R. A. *Rev. Mod. Phys.* **1993,** *65*, 599-610.

18. Marcus, R. A. *J. Chem. Phys.* **1956,** *24*, 966-978.

19. Piotrowiak, P. *Chem. Soc. Rev.* **1999,** *28*, 143-150.

20. Closs, G. L.; Calcaterra, L. T.; Green, N. J.; Penfield, K. W.; Miller, J. R. *J. Phys. Chem.* **1986,** *90*, 3673-3683.

21. Gust, D.; Moore, T. A.; Liddell, P. A.; Nemeth, G. A.; Makings, L. R.; Moore, A. L.; Barrett, D.; Pessiki, P. J.; Bensasson, R. V.; Rougee, M.; Chachaty, C.; Deschryver, F. C.; Vanderauweraer, M.; Holzwarth, A. R.; Connolly, J. S. *J. Am. Chem. Soc.* **1987,** *109*, 846-856.

22. Turro, N. J. *Pure Appl. Chem.* **1981,** *53*, 259-286.

23. DeGraziano, J. M.; Macpherson, A. N.; Liddell, P. A.; Noss, L.; Sumida, J. P.; Seely, G. R.; Lewis, J. E.; Moore, A. L.; Moore, T. A.; Gust, D. *New J. Chem.* **1996,** *20*, 839-851.

24. Gust, D.; Moore, T. A.; Moore, A. L. *Acc. Chem. Res.* **2001,** *34*, 40-48.

25. Imahori, H.; Guldi, D. M.; Tamaki, K.; Yoshida, Y.; Luo, C. P.; Sakata, Y.; Fukuzumi, S. *J. Am. Chem. Soc.* **2001,** *123*, 6617-6628.

26. Vehmanen, V.; Tkachenko, N. V.; Tauber, A. Y.; Hynninen, P. H.; Lemmetyinen, H. *Chem. Phys. Lett.* **2001,** *345*, 213-218.

27. Imahori, H.; Fukuzumi, S. *Adv. Funct. Mater.* **2004,** *14*, 525-536.

28. Mataga, N.; Chosrowjan, H.; Taniguchi, S. *J. Photochem. Photobio., C-Photochem. Rev.* **2005,** *6*, 37-79.

29. Shirakawa, H.; Louis, E. J.; Macdiarmid, A. G.; Chiang, C. K.; Heeger, A. J. *J. Chem. Soc.-Chem. Commun.* **1977**, 578-580.

30. Skotheim, T. A.; Reynolds, J. R., *Handbook of Conducting Polymers.* 3rd ed.; CRC press: Boca Raton, 2006.

31. Kokil, A.; Shiyanovskaya, I.; Singer, K. D.; Weder, C. *J. Am. Chem. Soc.* **2002,** *124*, 9978-9979.

32. Babel, A.; Jenekhe, S. A. *J. Phys. Chem. B* **2003,** *107*, 1749-1754.

33. Sirringhaus, H.; Tessler, N.; Friend, R. H. *Science* **1998,** *280*, 1741-1744.

34. Fuchigami, H.; Tsumura, A.; Koezuka, H. *App. Phys. Lett.* **1993,** *63*, 1372-1374.

35. Campbell, I. H.; Smith, D. L.; Neef, C. J.; Ferraris, J. P. *App. Phys. Lett.* **1999,** *74*, 2809-2811.

36. Adams, D. M.; Brus, L.; Chidsey, C. E. D.; Creager, S.; Creutz, C.; Kagan, C. R.; Kamat, P. V.; Lieberman, M.; Lindsay, S.; Marcus, R. A.; Metzger, R. M.; Michel-Beyerle, M. E.; Miller, J. R.; Newton, M. D.; Rolison, D. R.; Sankey, O.; Schanze, K. S.; Yardley, J.; Zhu, X. Y. *J. Phys. Chem. B* **2003,** *107*, 6668-6697.

37. Ashwell, G. J.; Chwialkowska, A. *Chem. Commun.* **2006**, 1404-1406.

38. Ashwell, G. J.; Tyrrell, W. D.; Urasinska, B.; Wang, C. S.; Bryce, M. R. *Chem. Commun.* **2006**, 1640-1642.

39. Aviram, A.; Ratner, M. A. *Chem. Phys. Lett.* **1974,** *29*, 277-283.

40. Reed, M. A.; Zhou, C.; Muller, C. J.; Burgin, T. P.; Tour, J. M. *Science* **1997,** *278*, 252-254.

41. Reed, M. A.; Tour, J. M. *Scientific American* **2000,** *282*, 86-93.

42. Wilbourn, K.; Murray, R. W. *J. Phys. Chem.* **1988,** *92*, 3642-3648.

43. Frommer, J. E. C., R. R., *Encyclopedia of Polymer Science and Engineering*. Wiley: New York, 1986; Vol. 5.

44. Chung, T. C.; Kaufman, J. H.; Heeger, A. J.; Wudl, F. *Phys. Rev. B* **1984,** *30*, 702-710.

45. Bredas, J. L.; Chance, R. R.; Silbey, R. *Phys. Rev. B* **1982,** *26*, 5843-5854.

46. McConnell, H. *J. Chem. Phys.* **1961,** *35*, 508-&.

47. Ratner, M. A., Jortner, J., *Molecular Electronics*. Blackwell: Oxford, UK, 1997; p 73-118.

48. Skotheim, T. A. E., R. L.; Reynolds, J. R., *Handbook of Conducting Polymers*. 2nd ed.; Marcel Dekker: New York, 1998.

49. Bernier, P., Lefrant, S., Bidan, G., *Advances in Synthetic Metals. Twenty Years of Progress in Science and Technology.* Elsevier: Elsevier, 1999.

50. Burroughes, J. H.; Bradley, D. D. C.; Brown, A. R.; Marks, R. N.; Mackay, K.; Friend, R. H.; Burns, P. L.; Holmes, A. B. *Nature* **1990,** *347*, 539-541.

51. Gunder, P., *Nonlinear Optical Effects and Materials*. Springer: New York, 2000.

52. Brabec, C. J.; Sariciftci, N. S.; Hummelen, J. C. *Adv. Funct. Mater.* **2001,** *11*, 15-26.

53. Burrows, H. D.; de Melo, J. S.; Serpa, C.; Arnaut, L. G.; Miguel, M. D.; Monkman, A. P.; Hamblett, I.; Navaratnam, S. *Chem. Phys.* **2002,** *285*, 3-11.

54. Monkman, A.; Burrows, D. *Synth. Met.* **2004,** *141*, 81-86.

55. Candeias, L. P.; Grozema, F. C.; Padmanaban, G.; Ramakrishnan, S.; Siebbeles, L. D. A.; Warman, J. M. *J. Phys. Chem. B* **2003,** *107*, 1554-1558.

56. Swager, T. M.; Gil, C. J.; Wrighton, M. S. *J. Phys. Chem.* **1995,** *99*, 4886-4893.

57. Pschirer, N. G.; Byrd, K.; Bunz, U. H. F. *Macromolecules* **2001,** *34*, 8590-8592.

58. Beljonne, D.; Pourtois, G.; Silva, C.; Hennebicq, E.; Herz, L. M.; Friend, R. H.; Scholes, G. D.; Setayesh, S.; Mullen, K.; Bredas, J. L. *Proc. Natl. Acad. Sci. U. S. A.* **2002,** *99*, 10982-10987.

59. Silverman, E. E.; Cardolaccia, T.; Zhao, X. M.; Kim, K. Y.; Haskins-Glusac, K.; Schanze, K. S. In *The triplet state in Pt-acetylide oligomers, polymers and copolymers*, 2005; pp 1491-1500.

60. Swager, T. M. *Acc. Chem. Res.* **1998,** *31*, 201-207.

61. Zhou, Q.; Swager, T. M. *J. Am. Chem. Soc.* **1995,** *117*, 12593-12602.

62. Wang, B.; Wasielewski, M. R. *J. Am. Chem. Soc.* **1997,** *119*, 12-21.

63. Westlund, R.; Malmstrom, E.; Lopes, C.; Ohgren, J.; Rodgers, T.; Saito, Y.; Kawata, S.; Glimsdal, E.; Lindgren, M. *Adv. Funct. Mater.* **2008,** *18*, 1939-1948.

64. Wilson, J. S.; Dhoot, A. S.; Seeley, A.; Khan, M. S.; Kohler, A.; Friend, R. H. *Nature* **2001,** *413*, 828-831.

65. Sonogashira, K.; Takahashi, S.; Hagihara, N. *Macromolecules* **1977,** *10*, 879-880.

66. Sonogashira, K.; Fujikura, Y.; Yatake, T.; Toyoshima, N.; Takahashi, S.; Hagihara, N. *J. Organomet. Chem.* **1978,** *145*, 101-108.

67. Takahashi, S.; Kariya, M.; Yatake, T.; Sonogashira, K.; Hagihara, N. *Macromolecules* **1978,** *11*, 1063-1066.

68. Johnson, B. F. G.; Kakkar, A. K.; Khan, M. S.; Lewis, J.; Dray, A. E.; Friend, R. H.; Wittmann, F. *J. Mater. Chem.* **1991,** *1*, 485-486.

69. Mather, G. G.; Pidcock, A.; Rapsey, G. J. N. *J. Chem. Soc.-Dalton Trans.* **1973**, 2095-2099.

70. Sonogashira, K.; Kataoka, S.; Takahashi, S.; Hagihara, N. *J. Organomet. Chem.* **1978,** *160*, 319-327.

71. Lewis, J.; Long, N. J.; Raithby, P. R.; Shields, G. P.; Wong, W. Y.; Younus, M. *J. Chem. Soc.-Dalton Trans.* **1997**, 4283-4288.

72. Beljonne, D.; Wittmann, H. F.; Kohler, A.; Graham, S.; Younus, M.; Lewis, J.; Raithby, P. R.; Khan, M. S.; Friend, R. H.; Bredas, J. L. *J. Chem. Phys.* **1996,** *105*, 3868-3877.

73. Kohler, A.; Wilson, J. S.; Friend, R. H.; Al-Suti, M. K.; Khan, M. S.; Gerhard, A.; Bassler, H. *J. Chem. Phys.* **2002,** *116*, 9457-9463.

74. Crabtree, R. H., *The Organometallic Chemistry of the Transition Metals*. John Wiley & Sons, Inc.: Hoboken, 2005.

75. Frapper, G.; Kertesz, M. *Inorg. Chem.* **1993,** *32*, 732-740.

76. Chawdhury, N.; Kohler, A.; Friend, R. H.; Wong, W. Y.; Lewis, J.; Younus, M.; Raithby, P. R.; Corcoran, T. C.; Al-Mandhary, M. R. A.; Khan, M. S. *J. Chem. Phys.* **1999,** *110*, 4963-4970.

77. Cooper, T. M.; Blaudeau, J. P.; Hall, B. C.; Rogers, J. E.; McLean, D. G.; Liu, Y. L.; Toscano, J. P. *Chem. Phys. Lett.* **2004,** *400*, 239-244.

78. Lewis, J.; Khan, M. S.; Kakkar, A. K.; Johnson, B. F. G.; Marder, T. B.; Fyfe, H. B.; Wittmann, F.; Friend, R. H.; Dray, A. E. *J. Organomet. Chem.* **1992,** *425*, 165-176.

79. Younus, M.; Kohler, A.; Cron, S.; Chawdhury, N.; Al-Mandhary, M. R. A.; Khan, M. S.; Lewis, J.; Long, N. J.; Friend, R. H.; Raithby, P. R. *Angew. Chem.-Int. Edit.* **1998,** *37*, 3036-3039.

80. Chawdhury, N.; Younus, M.; Raithby, P. R.; Lewis, J.; Friend, R. H. *Opt. Mat.* **1998,** *9*, 498-501.

81. Chawdhury, N.; Kohler, A.; Friend, R. H.; Younus, M.; Long, N. J.; Raithby, P. R.; Lewis, J. *Macromolecules* **1998,** *31*, 722-727.

82. Wittmann, H. F.; Friend, R. H.; Khan, M. S.; Lewis, J. *J. Chem. Phys.* **1994,** *101*, 2693-2698.

83. Khan, M. S.; Al-Mandhary, M. R. A.; Al-Suti, M. K.; Corcoran, T. C.; Al-Mahrooqi, Y.; Attfield, J. P.; Feeder, N.; David, W. I. F.; Shankland, K.; Friend, R. H.; Kohler, A.; Marseglia, E. A.; Tedesco, E.; Tang, C. C.; Raithby, P. R.; Collings, J. C.; Roscoe, K. P.; Batsanov, A. S.; Stimson, L. M.; Marder, T. B. *New J. Chem.* **2003,** *27*, 140-149.

84. Khan, M. S.; Al-Mandhary, M. R. A.; Al-Suti, M. K.; Feeder, N.; Nahar, S.; Kohler, A.; Friend, R. H.; Wilson, P. J.; Raithby, P. R. *J. Chem. Soc.-Dalton Trans.* **2002**, 2441-2448.

85. Khan, M. S.; Al-Mandhary, M. R. A.; Al-Suti, M. K.; Hisahm, A. K.; Raithby, P. R.; Ahrens, B.; Mahon, M. F.; Male, L.; Marseglia, E. A.; Tedesco, E.; Friend, R. H.; Kohler, A.; Feeder, N.; Teat, S. J. *J. Chem. Soc.-Dalton Trans.* **2002**, 1358-1368.

86. Wilson, J. S.; Kohler, A.; Friend, R. H.; Al-Suti, M. K.; Al-Mandhary, M. R. A.; Khan, M. S.; Raithby, P. R. *J. Chem. Phys.* **2000,** *113*, 7627-7634.

87. Rogers, J. E.; Cooper, T. M.; Fleitz, P. A.; Glass, D. J.; McLean, D. G. *J. Phys. Chem. A* **2002,** *106*, 10108-10115.

88. Liu, Y.; Jiang, S. J.; Glusac, K.; Powell, D. H.; Anderson, D. F.; Schanze, K. S. *J. Am. Chem. Soc.* **2002,** *124*, 12412-12413.

89. Farley, R. T.; Zheng, Q. L.; Gladysz, J. A.; Schanze, K. S. *Inorg. Chem.* **2008,** *47*, 2955-2963.

90. Tour, J. M. *Chem. Rev.* **1996,** *96*, 537-554.

91. Mullen, K.; Wegner, G. *Adv. Mater.* **1998,** *10*, 433-436.

92. Martin, R. E.; Diederich, F. *Angew. Chem. Int. Ed. Engl.* **1999,** *38*, 1351-1377.

93. Tour, J. M. *J. Org. Chem.* **2007,** *72*, 7477-7496.

94. Liu; Y. Li, Y.; Schanze, K. S. *J. Photochem. Photobiol. C: Phtochem. Rev.* **2002,** *3*, 1-23.

95. Ren, T. *Organometallics* **2005,** *24*, 4854-4870.

96. Wong, W. Y.; Ho, C. L. *Coord. Chem. Rev.* **2006,** *250*, 2627-2690.

97. Khan, M. S.; Al-Mandhary, M. R. A.; Al-Suti, M. K.; Al-Battashi, F. R.; Al-Saadi, S.; Ahrens, B.; Bjernemose, J. K.; Mahon, M. F.; Raithby, P. R.; Younus, M.; Chawdhury, N.; Kohler, A.; Marseglia, E. A.; Tedesco, E.; Feeder, N.; Teat, S. J. *Dalt. Trans.* **2004**, 2377-2385.

98. Kohler, A.; Wittmann, H. F.; Friend, R. H.; Khan, M. S.; Lewis, J. *Synth. Met.* **1996,** *77*, 147-150.

99. Guo, F. Q.; Kim, Y. G.; Reynolds, J. R.; Schanze, K. S. *Chem. Commun.* **2006**, 1887-1889.

100. Mei, J.; Ogawa, K.; Kim, Y.-G.; Heston, N. C.; Arenas, D. J.; Nasrollahi, Z.; McCarley, T. D.; Tanner, D. B.; Reynolds, J. R.; Schanze, K. S. *ACS App. Mat. Int.* **2009,** *1*, 150-161.

101. Rogers, J. E.; Slagle, J. E.; Krein, D. M.; Burke, A. R.; Hall, B. C.; Fratini, A.; McLean, D. G.; Fleitz, P. A.; Cooper, T. M.; Drobizhev, M.; Makarov, N. S.; Rebane, A.; Kim, K. Y.; Farley, R.; Schanze, K. S. *Inorg. Chem.* **2007,** *46*, 6483-6494.

102. G.-J. Zhou, W. Y. W. C. Y. Z. L. *Adv. Funct. Mater.* **2007,** *17*, 963-975.

103. Silverman, E. E.; Cardolaccia, T.; Zhao, X. M.; Kim, K. Y.; Haskins-Glusac, K.; Schanze, K. S. *Coord. Chem. Rev.* **2005,** *249*, 1491-1500.

104. Glusac, K.; Kose, M. E.; Jiang, H.; Schanze, K. S. *J. Phys. Chem. B* **2007,** *111*, 929-940.

105. Cardolaccia, T.; Li, Y. J.; Schanze, K. S. *J. Am. Chem. Soc.* **2008,** *130*, 2535-2545.

106. McKay, T. J.; Bolger, J. A.; Staromlynska, J.; Davy, J. R. *J. Chem. Phys.* **1998,** *108*, 5537-5541.

107. Wishart, J. F.; Cook, A. R.; Miller, J. R. *Rev. Sci. Instrum.* **2004,** *75*, 4359-4366.

108. Cardolaccia, T.; Funston, A. M.; Kose, M. E.; Keller, J. M.; Miller, J. R.; Schanze, K. S. *J. Phys. Chem. B* **2007,** *111*, 10871-10880.

109. Hennebicq, E.; Pourtois, G.; Scholes, G. D.; Herz, L. M.; Russell, D. M.; Silva, C.; Setayesh, S.; Grimsdale, A. C.; Mullen, K.; Bredas, J. L.; Beljonne, D. *J. Am. Chem. Soc.* **2005,** *127*, 4744-4762.

110. Funston, A. M.; Silverman, E. E.; Miller, J. R.; Schanze, K. S. *J. Phys. Chem. B* **2004,** *108*, 1544-1555.

111. Funston, A. M.; Silverman, E. E.; Schanze, K. S.; Miller, J. R. *J. Phys. Chem. B* **2006,** *110*, 17736-17742.

112. Asaoka, S.; Takeda, N.; Lyoda, T.; Cook, A. R.; Miller, J. R. *J. Am. Chem. Soc.* **2008,** *130*, 11912-11920.

113. Ziener, U.; Godt, A. *J. Org. Chem.* **1997,** *62*, 6137-6143.

114. Kukula, H.; Veit, S.; Godt, A. *Eur. J. Org. Chem.* **1999**, 277-286.

115. Shortell, D. B.; Palmer, L. C.; Tour, J. M. *Tetrahedron* **2001,** *57*, 9055-9065.

116. Maya, F.; Tour, J. M. *Tetrahedron* **2004,** *60*, 81-92.

117. Flatt, A. K.; Dirk, S. M.; Henderson, J. C.; Shen, D. E.; Su, J.; Reed, M. A.; Tour, J. M. *Tetrahedron* **2003,** *59*, 8555-8570.

118. Flatt, A. K.; Yao, Y. X.; Maya, F.; Tour, J. M. *J. Org. Chem.* **2004,** *69*, 1752-1755.

119. Bauerle, P.; Fischer, T.; Bidlingmeier, B.; Stabel, A.; Rabe, J. P. *Angew. Chem.-Int Edit.* **1995,** *34*, 303-307.

120. Kromer, J.; Rios-Carreras, I.; Fuhrmann, G.; Musch, C.; Wunderlin, M.; Debaerdemaeker, T.; Mena-Osteritz, E.; Bauerle, P. *Angew. Chem.-Int. Edit.* **2000,** *39*, 3481.

121. Onitsuka, K.; Fujimoto, M.; Ohshiro, N.; Takahashi, S. *Angew. Chem.-Int. Edit.* **1999,** *38*, 689-692.

122. Greenfield, S. R.; Svec, W. A.; Gosztola, D.; Wasielewski, M. R. *J. Am. Chem. Soc.* **1996,** *118*, 6767-6777.

123. Lukas, A. S.; Miller, S. E.; Wasielewski, M. R. *J. Phys. Chem. B* **2000,** *104*, 931-940.

124. Schumm, J. S.; Pearson, D. L.; Tour, J. M. *Angew. Chem.-Int Edit.* **1994,** *33*, 1360-1363.

125. Jiang, H.; Lin, W. B. *J. Am. Chem. Soc.* **2004,** *126*, 7426-7427.

126. Shavaleev, N. M.; Adams, H.; Best, J.; Weinstein, J. A. *J. Organomet. Chem.* **2007,** *692*, 921-925.

127. Wilson, J. S.; Wilson, R. J.; Friend, R. H.; Kohler, A.; Al-Suti, M. K.; Al-Mandhary, M. R. A.; Khan, M. S. *Phys. Rev. B* **2003,** *67*.

128. Oevering, H.; Paddonrow, M. N.; Heppener, M.; Oliver, A. M.; Cotsaris, E.; Verhoeven, J. W.; Hush, N. S. *J. Am. Chem. Soc.* **1987,** *109*, 3258-3269.

129. Harriman, A. *Chem. Commun.* **1977**, 777-778.

130. Kauffman, G. B.; Teter, L. A. *Inorganic Syntheses* **1963,** *7*, 9-12.

131. Redmore, N. P.; Rubtsov, I. V.; Therien, M. J. *J. Am. Chem. Soc.* **2003,** *125*, 8769-8778.

132. Cunningham, G. B.; Li, Y. T.; Liu, S. X.; Schanze, K. S. *J. Phys. Chem. B* **2003,** *107*, 12569-12572.

133. Pappenfus, T. M.; Mann, K. R. *Inorg. Chem.* **2001,** *40*, 6301-6307.

134. Jones, N. D.; Wolf, M. O.; Giaquinta, D. M. *Organometallics* **1997,** *16*, 1352-1354.

135. Barbieri, A.; Ventura, B.; Barigelletti, F.; De Nicola, A.; Quesada, M.; Ziessel, R. *Inorg. Chem.* **2004,** *43*, 7359-7368.

136. Clot, O.; Akahori, Y.; Moorlag, C.; Leznoff, D. B.; Wolf, M. O.; Batchelor, R. J.; Patrick, B. O.; Ishii, M. *Inorg. Chem.* **2003,** *42*, 2704-2713.

137. Thomas, K. R. J.; Lin, J. T.; Lin, K. J. *Organometallics* **1999,** *18*, 5285-5291.

138. Encinas, S.; Flamigni, L.; Barigelletti, F.; Constable, E. C.; Housecroft, C. E.; Schofield, E. R.; Figgemeier, E.; Fenske, D.; Neuburger, M.; Vos, J. G.; Zehnder, M. *Chem.-Eur. J.* **2002,** *8*, 137-150.

139. Graf, D. D.; Mann, K. R. *Inorg. Chem.* **1997,** *36*, 150-157.

140. Back, R.; Lennox, R. B. *Langmuir* **1992,** *8*, 959-964.

141. Zhu, Y. B.; Wolf, M. O. *J. Am. Chem. Soc.* **2000,** *122*, 10121-10125.

142. Baldo, M. A.; Thompson, M. E.; Forrest, S. R. *Nature* **2000,** *403*, 750-753.

143. Tang, K. C.; Liu, K. L.; Chen, I. C. *Chem. Phys. Lett.* **2004,** *386*, 437-441.

144. Ikai, M.; Tokito, S.; Sakamoto, Y.; Suzuki, T.; Taga, Y. *App. Phys. Lett.* **2001,** *79*, 156-158.

145. Adachi, C.; Baldo, M. A.; Forrest, S. R.; Thompson, M. E. *App. Phys. Lett.* **2000,** *77*, 904-906.

146. Baldo, M. A.; O'Brien, D. F.; You, Y.; Shoustikov, A.; Sibley, S.; Thompson, M. E.; Forrest, S. R. *Nature* **1998,** *395*, 151-154.

147. Adachi, C.; Baldo, M. A.; Thompson, M. E.; Forrest, S. R. *J. App. Phys.* **2001,** *90*, 5048-5051.

148. Glusac, K. D. S., K. S. *Polymer Preprints* **2002,** *43*, 87-88.

149. Weiss, E. A. W., M. R.; Ratner, M.A., *Molecules as Wires: Molecule-Assisted Movement of Charge and Energy.* Top. Cur. Chem. Springer-Verlag: Berline Heidelberg, 2005.

150. Takeda, N.; Asaoka, S.; Miller, J. R. *J. Am. Chem. Soc.* **2006,** *128*, 16073-16082.

151. Demas, J. N.; Crosby, G. A. *J. Phys. Chem.* **1971,** *75*, 991-&.

152. Wishart, J. F., *Accelerators for Ultrafast Phenomena* in *"Radiation Chemistry: Present Status and Future Trends"*. Elsevier Science: 2001; Vol. *87*, p 21-35.

153. Miller, J. R., Penfield, K., Johnson, M., Closs, G., Green, N. *Adv. Chem. Ser.* **1998,** *254*, 161-176.

154. De Waele, V.; Sorgues, S.; Pernot, P.; Marignier, J. L.; Monard, H.; Larbre, J. P.; Mostafavi, M. *Chem. Phys. Lett.* **2006,** *423*, 30-34.

155. De Waele, V.; Sorgues, S.; Pernot, P.; Marignier, J. L.; Mostafavi, M. *Nucl. Sci. Tech.s* **2007,** *18*, 10-15.

156. Cook, A. R.; Shen, Y. Z. *Rev. Sci. Instrum.* **2009,** *80*.

157. Tranthi, T. H.; Koulkes-Pujo, A. M. *J. Phys. Chem.* **1983,** *87*, 1166-1169.

158. Danilov, E. O.; Pomestchenko, I. E.; Kinayyigit, S.; Gentili, P. L.; Hissler, M.; Ziessel, R.; Castellano, F. N. *J. Phys. Chem. A* **2005,** *109*, 2465-2471.

159. Martin, R. E.; Diederich, F. *Angew. Chem.-Int. Edit.* **1999,** *38*, 1350-1377.

160. Tour, J. M. *Chem. Rev.* **1996,** *96*, 537-553.

161. Moore, J. S. *Acc. Chem. Res.* **1997,** *30*, 402-413.

162. Glusac, K. D.; Jiang, S. J.; Schanze, K. S. *Chem. Commun.* **2002**, 2504-2505.

163. Gosztola, D.; Niemczyk, M. P.; Svec, W.; Lukas, A. S.; Wasielewski, M. R. *J. Phys. Chem. A* **2000,** *104*, 6545-6551.

164. Sreearunothai, P.; Asaoka, S.; Cook, A. R.; Miller, J. R. *J. Phys. Chem. A* **2009,** *113*, 2786-2795.

165. Asaoka, S. T., Norihiko; Iyoda, Tomokazu; Cook, Andrew; Miller, John R. *J. Am. Chem. Soc. submitted*.

166. Grozema, F. C.; Hoofman, R.; Candeias, L. P.; de Haas, M. P.; Warman, J. M.; Siebbeles, L. D. A. *J. Phys. Chem. A* **2003,** *107*, 5976-5986.

167. Schanze, K. S.; Silverman, E. E.; Zhao, X. M. *J. Phys. Chem. B* **2005,** *109*, 18451-18459.

168. Closs, G. L.; Johnson, M. D.; Miller, J. R.; Piotrowiak, P. *J. Am. Chem. Soc.* **1989,** *111*, 3751-3753.

169. Kim, K.; Jordan, K. D.; Paddonrow, M. N. *J. Phys. Chem.* **1994,** *98*, 11053-11058.

170. Sikes, H. D.; Smalley, J. F.; Dudek, S. P.; Cook, A. R.; Newton, M. D.; Chidsey, C. E. D.; Feldberg, S. W. *Science* **2001,** *291*, 1519-1523.

171. Creager, S.; Yu, C. J.; Bamdad, C.; O'Connor, S.; MacLean, T.; Lam, E.; Chong, Y.; Olsen, G. T.; Luo, J. Y.; Gozin, M.; Kayyem, J. F. *J. Am. Chem. Soc.* **1999,** *121*, 1059-1064.

172. Giacalone, F.; Segura, J. L.; Martin, N.; Guldi, D. M. *J. Am. Chem. Soc.* **2004,** *126*, 5340-5341.

173. Atienza, C.; Martin, N.; Wielopolski, M.; Haworth, N.; Clark, T.; Guldi, D. M. *Chem. Commun.* **2006**, 3202-3204.

174. Atienza-Castellanos, C.; Wielopolski, M.; Guldi, D. M.; van der Pol, C.; Bryce, M. R.; Filippone, S.; Martin, N. *Chem. Commun.* **2007**, 5164-5166.

175. Albinsson, B.; Martensson, J. *J. Photochem. Photobio., C-Photochem. Rev.* **2008,** *9*, 138-155.

176. Sachs, S. B.; Dudek, S. P.; Hsung, R. P.; Sita, L. R.; Smalley, J. F.; Newton, M. D.; Feldberg, S. W.; Chidsey, C. E. D. *J. Am. Chem. Soc.* **1997,** *119*, 10563-10564.

177. Warman, J. M.; Smit, K. J.; Jonker, S. A.; Verhoeven, J. W.; Oevering, H.; Kroon, J.; Paddon-Row, M. N.; Oliver, A. M. *Chem. Phys.* **1993,** *170*, 359-80.

178. Cooper, T. M.; McLean, D. G.; Rogers, J. E. *Chem. Phys. Lett.* **2001,** *349*, 31-36.

179. Rogers, J. E.; Hall, B. C.; Hufnagle, D. C.; Slagle, J. E.; Ault, A. P.; McLean, D. G.; Fleitz, P. A.; Cooper, T. M. *J. Chem. Phys.* **2005,** *122*, 214701-214708.

180. Cooper, T. M.; Krein, D. M.; Burke, A. R.; McLean, D. G.; Rogers, J. E.; Slagle, J. E.; Fleitz, P. A. *J. Phys. Chem. A* **2006,** *110*, 4369-4375.

181. Cooper, T. M.; Hall, B. C.; McLean, D. G.; Rogers, J. E.; Burke, A. R.; Turnbull, K.; Weisner, A.; Fratini, A.; Liu, Y.; Schanze, K. S. *J. Phys. Chem. A* **2005,** *109*, 999-1007.

182. Cooper, T. M.; Krein, D. M.; Burke, A. R.; McLean, D. G.; Rogers, J. E.; Slagle, J. E. *J. Phys. Chem. A* **2006,** *110*, 13370-13378.

183. Farley, R. T. *Photophysics of Platinum and Iridium Organometallic Materials: From Molecular Wires to Nonlinear Optics*. Dissertation, University of Florida, Gainesville, 2007.

184. Huang, S. L.; Tour, J. M. *Tet. Lett.* **1999,** *40*, 3347-3350.

185. Lulinski, P.; Skulski, L. *Bull. Chem. Soc. Jpn.* **2000,** *73*, 951-956.

186. Emmert, L. A.; Choi, W.; Marshall, J. A.; Yang, J.; Meyer, L. A.; Brozik, J. A. *J. Phys. Chem. A* **2003,** *107*, 11340-11346.

187. Staromlynska, J.; McKay, T. J.; Bolger, J. A.; Davy, J. R. *J. Opt. Soc. Am. B-Opt. Phys.* **1998,** *15*, 1731-1736.

188. Beljonne, D.; Shuai, Z.; Pourtois, G.; Bredas, J. L. *J. Phys. Chem. A* **2001,** *105*, 3899-3907.

189. Rehahn, H. S. t., A.-D.; Feast, W. J. *Synthesis* **1988,** *5*, 386-388.

BIOGRAPHICAL SKETCH

Julia Marie Keller was born in Owensboro, Kentucky, daughter to Stephen and Rebecca Raymer, along with her identical twin sister, Stephanie. She attended Western Kentucky University in Bowling Green, Kentucky on a music scholarship from 1998-2002, graduating in May 2002 *summa cum laude* and college scholar with a B.S. in chemistry. She then attended graduate school at WKU from 2002-2004, working under Professor Donald W. Slocum in the area of Directed *ortho*-Metalation chemistry. During this time, she was awarded the McNally Graduate Fellowship and attained an M.S. in chemistry. Julia then attended the University of Florida for graduate school, working under Professor Kirk S. Schanze in the area of physical organic chemistry, studying the synthesis and photophysics of Platinum Acetylide materials. During this time, Julia was awarded a Proctor and Gamble Fellowship, both a Departmental and a University Teaching Award, the Jones Award for Creativity, and the Proctor and Gamble Award for Excellence in Graduate Research. She was also one of fifty U.S. delegates selected to attend the Meeting of the Nobel Laureates in Lindau, Germany (funded by ORAU). During this time of studying for her doctoral degree in chemistry, Julia married Jonathan Keller in December of 2005; they had their first son, Joshua, in June 2008 and are expecting the arrival of their daughter Hayleigh in May 2010.